Dissertation

Theoretical Study on the Mechanism of Complex Organic Synthetic Reaction Involving Unexpected Intermediates

(未知の中間体を含む複雑有機合成反応機構の理論的解明)

Ryohei Uematsu

Hokkaido University

2015

Contents

Chapter 1: General Introduction

With the development in quantum chemical methodology, it becomes feasible to follow the change of molecular structure and energy in chemical reaction, and also to predict molecular properties including infrared absorption spectra, by computational chemistry. Furthermore, a target of quantum chemical calculations has extended to a large-scale system (such as protein etc.) with the advance of computational capability in recent years. Nowadays, quantum chemical calculation has become a powerful tool not only to reproduce experimental data but also to predict chemical phenomena.

In the field of organic chemistry, the importance of analysis with computational chemistry has also increased. Many researchers had reported the mechanism of organocatalyst reaction and transition-metal catalyzed reaction with *ab initio* or density functional theory (DFT) calculations.[1, 2] For example, Houk and co-workers examined the mechanism of intramolecular asymmetric aldol reaction (i.e. Hajos-Parrish reaction).[3]

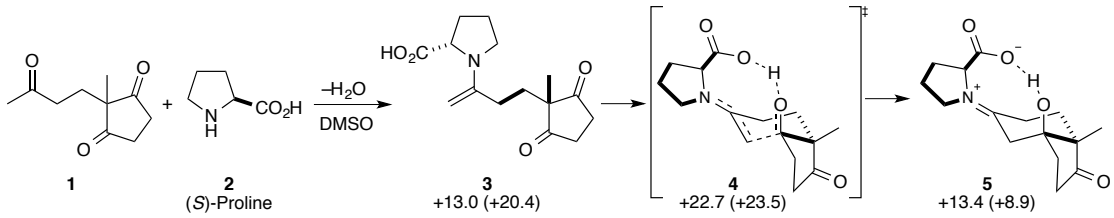

Scheme 1. The proposed rate-limiting step in Hajos-Parrish reaction. Gas-phase energy values based on B3LYP/6-31+G(d,p)//B3LYP/6-31G(d) calculations relative to the reactant (i.e. **1** and **2**) are shown in kcal/mol. Values in parentheses include solvation energies based on HF/6-31+G(d,p) in DMSO (PCM model & UAKS radii)//B3LYP/6-31G(d) calculations.

Dehydration condensation reaction between the methyl ketone part in substrate **1** and (*S*)-proline (**2**) gives enamine **3**, and intramolecular nucleophilic addition proceeds towards the carbonyl group on the five-membered ring. In this transition state (TS) **4**, the proton of carboxylic acid is shared with the carbonyl group via chair-type conformation. Because of this stability of the reactive complex **4**, the TS is ca. 10 kcal/mol more stable than the same conformation system without the catalyst. Moreover, the other proposed TS structures with experimental results are more unfavorable than **4**. Thus, we can achieve the most favorable mechanism, which we can consider, with the discussion about the energetics given by quantum chemistry calculation. Here, it is important to comprehend the approximations applied to

electronic energy calculation and the difference between the real system and the model system for calculation (e.g. the estimation of solvation effect by PCM model[4]).

The important role in considering chemical reaction with computational chemistry is finding equilibrium and transition state (TS) structures on the reaction pathway connecting between reactant and product. Here, an equilibrium structure is located at a local minimum, and a TS structure is located at a first-order saddle point on the potential energy surface (PES).[5] In the traditional approach to analyze reaction mechanism via computational chemistry, it is firstly required to assume the plausible reaction mechanism with careful consideration of experimental results. Then, the equilibrium and TS structures were optimized along this assumed mechanism. This approach has the possibility of overlooking the reaction pathways that cannot be extrapolated from this mechanism.

Secondly, it is necessary to make the initial guess for equilibrium and TS structures along the assumed reaction pathway, and to perform geometry optimization. Usually, optimization of TS structure is more difficult than that of equilibrium structure, because the initial guess must be close to the true TS structure. For example, it is easy to guess the TS structure for an S_N2 reaction[6]; the σ^* orbital of C–X bond in alkyl halide and the lone-pair of nucleophile interact with each other. When the previous study has already reported a TS structure of the similar reaction, the specific initial geometry of TS structure can be confirmed by literature reference[7]. However, if there is little knowledge of TS structures when analyzing unknown reaction mechanism, it is really difficult to determine internal coordinate variables ($3N$–6 degrees of freedom where N is the number of atoms). The initial guess structure for TS is usually built through trial-and-error process. This has been the only one traditional approach to obtain TS structures for unknown chemical reactions.

In 2004, Ohno and Maeda developed the Anharmonic Downward Distortion Following (ADDF) method that can search dissociation / isomerization reaction pathways, starting from equilibrium structures.[8] In general, potential-energy changes from the minimum to TS or dissociation channels (DC) become distorted downward from harmonic potential determined from Hessian matrix at equilibrium structure. It is referred as anharmonic downward distortion (ADD), and it is possible to change the structure uniquely by following ADD towards TSs and DCs.

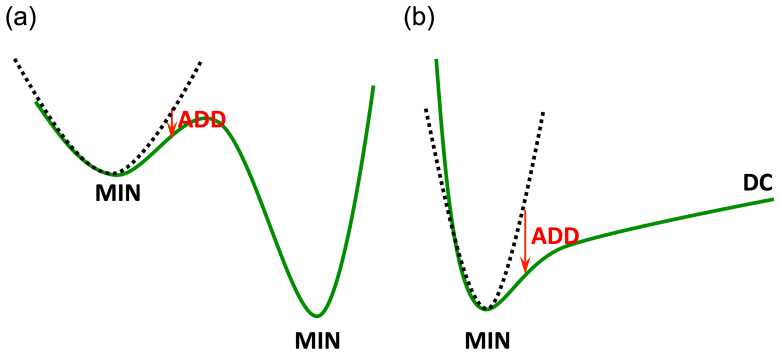

Figure 1. Anharmonic downward distortion from harmonic potential at equilibrium structure (MIN): (a) model potential corresponding to bond rearrangement; (b) model potential connecting to dissociation channel (DC)

Once the ADDF path is determined, the maximum energy point along the ADDF path is a good approximation for TS structure. Starting from this approximate TS, it is easy to find a true TS, and simultaneously one can be determined an intrinsic reaction coordinate (IRC) that is uniquely defined as a minimum energy path connecting minimum, TS, and another minimum. By combining ADDF and IRC calculations, all TS, DC, and equilibrium structures can be determined in a given molecular system.

In 2010, Maeda and Morokuma developed the Artificial Force Induced Reaction (AFIR) method, by which synthetic reaction paths were able to be discovered systematically.[9] In the AFIR method, the special function referred as AFIR function (sum of potential energy and artificial force term) is minimized. For keeping the explanation as simple as possible, we consider the two atoms system (A + B → A–B) where the AFIR function is represented in equation (1).

$$F(r_{AB}) = E(r_{AB}) + \alpha r_{AB} \quad \bullet\bullet\bullet (1)$$

When the atom A and B is put at sufficiently longer distance than the equilibrium bond length, the equilibrium structure corresponding to pre-reaction complex (A•••B) is generally given with minimizing the potential energy $E(r_{AB})$.

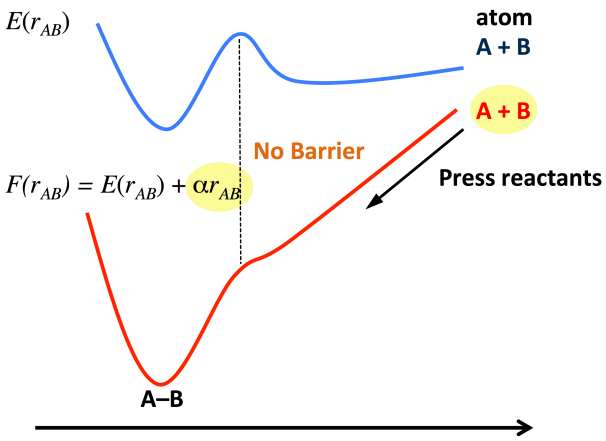

Figure 2. The AFIR method in two atoms system

Here, the artificial force term, which is proportional to the distance between atom A and B, is added to $E(r_{AB})$ for predicting the equilibrium structure (A–B). Minimization of the AFIR function $F(r_{AB})$ gives the approximate equilibrium structure, when proportional constant α is large enough to remove the reaction barrier. By the geometry optimization performed from the approximate structure, the true equilibrium structure is located. Moreover, the structure, which gives the maximum $E(r_{AB})$ in the process of $F(r_{AB})$ minimization, can be a good initial guess of TS structure. By TS optimization from the initial guess and IRC calculation from true TS, reaction pathways can be connected without using any of human-made TS guesses.

For the reaction between the fragment A and B containing of many atoms, the approximate TS and equilibrium structures are found by using equation (2).

$$F(\boldsymbol{Q}) = E(\boldsymbol{Q}) + \alpha \frac{\sum_{i\in A}\sum_{j\in B}\left[(R_i + R_j)r_{ij}^{-1}\right]^p r_{ij}}{\sum_{i\in A}\sum_{j\in B}\left[(R_i + R_j)r_{ij}^{-1}\right]^p} \quad \bullet\bullet\bullet \ (2)$$

In eq. (2), $\boldsymbol{Q}$ is atomic coordinates, R is covalent bond radii, r_{ij} is the distance between j-th atom in the fragment B and i-th atom in the fragment A, and p is the integer (set to 6 in default). In correctly applying the AFIR method, the way to set the fragments is very important: it is necessary to select the fragments carefully by considering (I) the reactivity of functional group around the reactive point and (II) the bond rearrangement from reactant to product. On the other hand, when substitution group, in which bond rearrangement does not occur, is selected in the fragment, unnecessary computational costs increase by simulating the unreal reaction.

In this study, I defined the fragments based on the knowledge of organic chemistry, and

conducted the systematic reaction path sampling from reactant to product for the following reactions. In chapter 2, the AFIR method was applied to the vinylogous Mannich-type reaction activated by a water molecule[10]. It was found that there were five working pathways involving two proposed reaction mechanism by the experimental group and three unexpected mechanisms. This reaction is strongly controlled by not only kinetic stability but also thermodynamic stability. That is, conformation analyses were performed toward products (*anti* and *syn* isomers) by using the ADDF method, and the Boltzmann distribution of obtained rotamers in free energy is well consistent with experimental ratio.

In chapter 3, the AFIR method was applied to the anomalous formal nucleophilic borylation of organic halides with silylborane in the presence of potassium methoxide[11]. The results of this analysis led to the identification of a unique carbanion-mediated mechanism involving the halogenophilic attack of silyl nucleophile on the bromine atom of the substrate. These calculations have therefore provided a mechanistic rationale for this counterintuitive borylation reaction. Furthermore, the good functional group compatibility and high reactivity exhibited by this reaction towards sterically hindered substrates can be understood in terms of the low activation energy required for the reaction of the silyl nucleophile with bromine atom of the substrate, and the subsequent rapid and selective consumption of the carbanion species by the *in situ* generated boron electrophile.

In chapter 4, the AFIR method was applied to the intramolecular C–S cyclization of thiobenzanilide by using $PdCl_2$/CuI catalyst and Bu_4NBr salt in DMSO/NMP solvent[12]. I found that addition of CuI to the $PdCl_2$, Bu_4NBr, DMSO/NMP and substrate mixture: (a) facilitates C–H bond activation by DMSO and C–S bond formation initiated by Bu_4NBr coordination to N–H bond of substrate, and (b) re-oxidizes Pd-center and re-generates the catalyst.

In chapter 5, general conclusion, this study is summarized finally.

References

1. Cheong, P. H.-Y.; Legault, C. Y.; Um, J. M.; Çelebi-Ölçüm, N.; Houk, K. N. *Chem. Rev.* **2011**, *111*, 5042–5137.
2. Koga, N.; Morokuma, K. *Chem. Rev.* **1991**, *91*, 823–842.
3. Clemente, F. R.; Houk, K. N. *Angew. Chem. Int. Ed.* **2004**, *43*, 5766–5768.
4. (a) Mennucci, B.; Cammi, R.; Tomasi, *J. Chem. Phys.* **1999**, *110*, 6858–6870. (b) Cossi, M.; Scalmani, G.; Rega, N.; Barone, V. *J. Chem. Phys.* **2002**, *117*, 43–54.
5. Introduction to Computational Chemistry, 2nd ed.; Jensen, F.; John Wiley & Sons: Chichester, 2006.
6. Organic Chemistry, 2nd ed.; Clayden, J.; Greeves, N.; Warren, S.; Oxford University Press, 2012.
7. Chandrasekhar, J.; Smith, S. F.; Jorgensen, W. L. *J. Am. Chem. Soc.* **1985**, *107*, 154–163.
8. (a) Ohno, K.; Maeda, S. *Chem. Phys. Lett.* **2004**, *384*, 277–282. (b) Ohno, K.; Maeda, S. *Mol. Sci.* **2011**, *5*, A0042. (c) Maeda, S.; Ohno, K.; Morokuma, K. *Phys. Chem. Chem. Phys.* **2013**, *15*, 3683–3701. (d) Maeda, S.; Taketsugu, T.; Morokuma, K. Ohno, K. *Bull. Chem. Soc. Jpn.* **2014**, *87,* 1315–1334.
9. (a) Maeda, S.; Morokuma, K. *J. Chem. Phys.* **2010**, *132*, 241102–241104. (b) Maeda, S.; Morokuma, K. *J. Chem. Theory Comput.* **2011**, *7*, 2335–2345. (c) Maeda, S.; Taketsugu, T.; Morokuma, K. *J. Comput Chem.* **2014**, *35*, 166–173. See also ref. 8(c).
10. Landelle, G.; Claraz, A.; Oudeyer, S.; Levacher, V. *Tetrahedron Lett.* **2012**, *53*, 2414–2416.
11. Yamamoto, E.; Izumi, K.; Horita, Y.; Ito, H. *J. Am. Chem. Soc.* **2012**, *134*, 19997–20000.
12. Inamoto, K.; Hasegawa, C.; Hiroya, K.; Doi, T. *Org. Lett.* **2008**, *10*, 5147–5150.

Chapter 2

Multiple Reaction Pathways Operating in the Mechanism of Vinylogous Mannich-type Reaction Activated by a Water Molecule

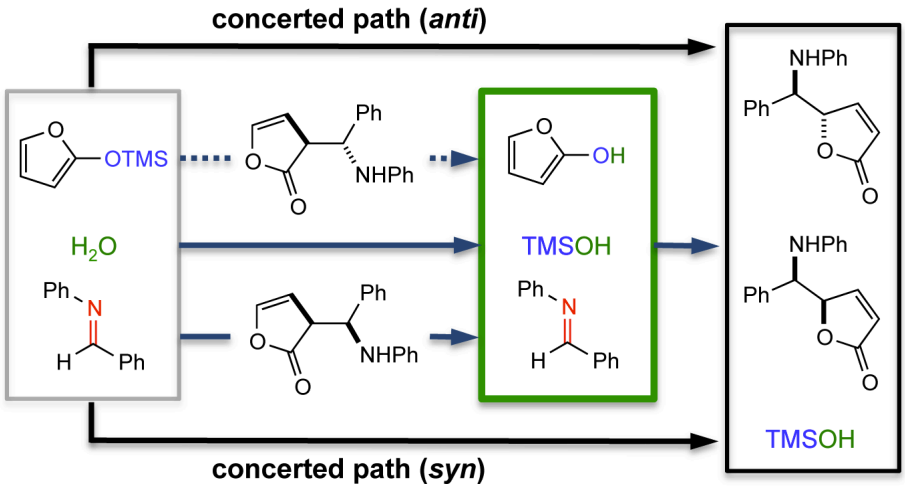

ABSTRACT

A systematic search for reaction pathways in the vinylogous Mannich-type reaction was performed by the artificial force induced reaction method. This reaction affords δ-amino-γ-butenolide in one-pot by mixing 2-trimethylsiloxyfuran (TMSOF), imine, and water, under solvent free conditions. Surprisingly, the search identified five working pathways. Among them, two concertedly produce *anti*- and *syn*-isomers of the product. The other two once give an intermediate, a regioisomer of the main product. This intermediate can undergo retro-Mannich reaction giving a pair of intermediates, imine and 2-furanol. The remaining path directly generates this intermediate pair. These imine and 2-furanol easily react to each other affording the product. Thus, all these stepwise paths finally converge to the main product. The rate-determining step of all these five (two concerted and three stepwise) paths have a common mechanism; concerted Si–O bond formation by a nucleophilic attack of a water molecule to the Si atom followed by a proton transfer from the water molecule to imine. Therefore, these five have comparable barriers and compete with each other.

Introduction

The five-substituted γ-butenolide motif and their derivatives, which are seen in a number of natural products, are useful building blocks of various compounds. Therefore, different methods have been developed for synthesizing this skeleton.[1-13] Recently, Landelle et al. reported efficient synthesis of δ-amino-γ-butenolide in a good yield by only mixing amine, aldehyde, and 2-trimethylsiloxyfuran (TMSOF) at room temperature under solvent free conditions.[14] This synthetic procedure easily affords the product in large quantities with only waste of trimethylsilanol (TMSOH), and thus is very powerful. Such a Mannich reaction which proceeds in nonacidic condition is novel, and a few cases have been found by several groups.[15-17]

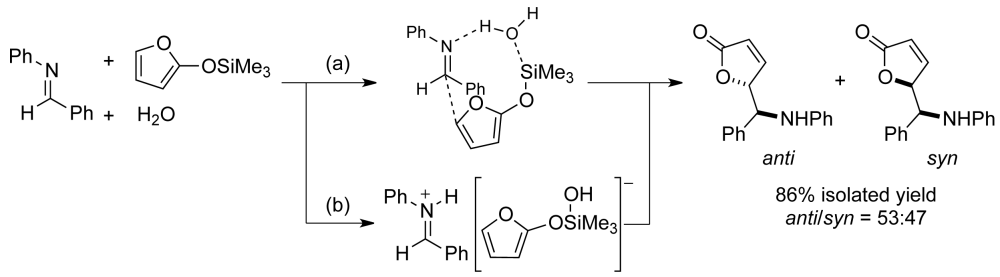

Scheme 1. Palusible Reaction Pathways

In the δ-amino-γ-butenolide synthesis, amine and aldehyde first give imine and water molecules by dehydration condensation reaction. This was confirmed experimentally by mixing prepared imine together with chemically equivalent amounts of water and TMSOF.[14] It was also shown that the reaction between prepared imine and TMSOF does not proceed, implying that participation of water molecule(s) generated in the dehydration condensation is a key. For this reaction, the following two mechanisms involving a water molecule explicitly have been proposed as shown in Scheme 1: (a) a one-step concerted path via a 9-membered ring (neutral) transition state (TS), (b) a stepwise path involving charged ion-pair intermediates, that is, silicate and iminium ions.[14]

In designing better reactions, deep insights into reaction mechanisms are often very helpful. Hence, there have been theoretical studies concerning Mannich reaction.[18-29] However, unlike usual Mannich reaction, the mechanism of the present reaction which proceeds in non-acidic condition without catalyst remains largely unknown. In general, there are many possible pathways in multicomponent reactions depending on approaching directions of multiple reactants. Finding all these by standard geometry optimization techniques using initial guesses

of TS geometries is not very easy. Recently, the artificial force induced reaction (AFIR) method has been developed by Maeda and Morokuma.[30-32] The AFIR method can explore reaction pathways among multiple reactants automatically without needing any guess for TS structures. The AFIR method was successfully applied to Passerini three-component reaction, and elucidated an unexpected four-component mechanism.[33] Since as noted above the mechanism of the present reaction has not been understood well, I studied the mechanism systematically by the AFIR method. It is demonstrated that systematic sampling of various reaction pathways by the AFIR method was essential to correctly describe the mechanism of the present multicomponent reaction.

Results & Discussion

In this study, possible reaction pathways for the imine **1** + TMSOF **2** + H_2O **3** system were explored systematically by using the AFIR method. At first, the AFIR search at the ONIOM(B3LYP/6-31G:PM6) level discovered fourteen independent AFIR paths (see computational methods about the AFIR path) leading to six different species. Among the fourteen, some gave hemiaminal species with a HN–C–OR functional group, which is kinetically and thermodynamically unstable and can easily go back to imine and alcohols. Hence, pathways to hemiaminal species were not studied further. The other paths leading to five different species are illustrated in Figure 1. RT, PD, IM, and TS stand for reactant (separately optimized three molecules), product (separately optimised two molecules), intermediate (separately optimized two or three molucules), and transition state, respectively. Among them, paths (a) and (b) directly produce *anti*/*syn* products **4** with a C–C bond generation at the 5-position, paths (c) and (d) give *anti*/*syn* regioisomers **6** with a C–C bond generation at the 3-position, and path (e) causes decomposition of **2** into **5** and 2-furanol (**7**).

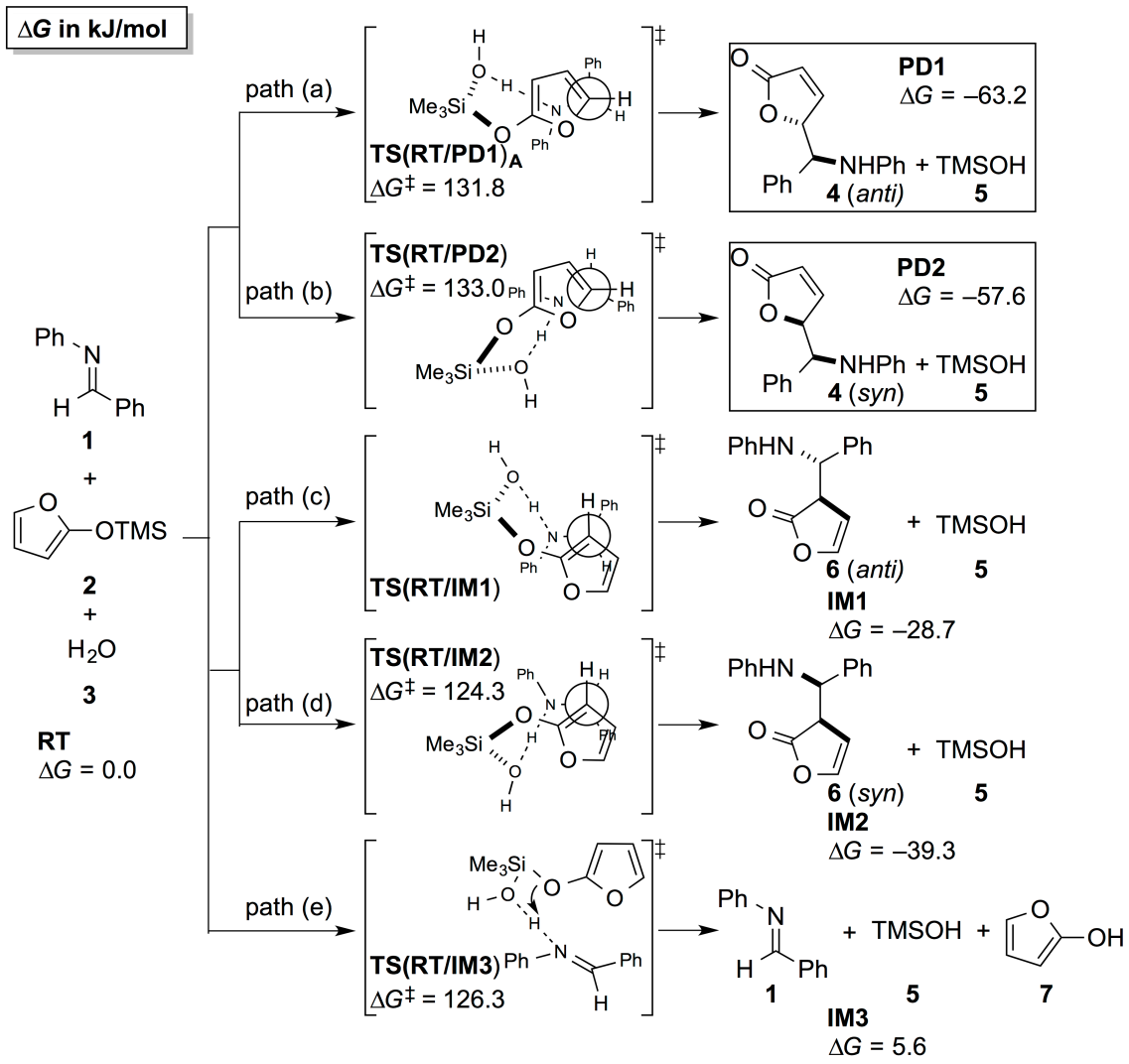

Figure 1. Five pathways obtained by the AFIR search. RT, PD, IM, and TS stand for reactant (separately optimized three molecules), product (separately optimized two molecules), intermediate (separately optimized two or three molecules), and transition state, respectively. Gibbs free energy Δ*G* (298.15 K, 1 atm) based on M06-2X calculations (see text) relative to RT is presented in kJ/mol. TS(RT/IM1), initially obtained at a low computational level, was not located at the final M06-2X calculation due to very flat potential energy surface in the TS region (see text).

These five pathways were further refined at the M06-2X level, where 6-31G(d) basis sets were applied to methyl and phenyl groups while 6-311+G(2d,p) to the remaining reaction-center parts. In this paper, energetics is discussed on the basis of Gibbs free energy in gas-phase, where free energy corrections were estimated assuming the rigid-rotor and the

harmonic approximations. I note that conclusions of this paper conserve even if relative electronic energy values with and without zero-point-energy corrections are used as shown in supporting information S1. Figure 2 presents optimized TS structures at the M06-2X level. Although path (a) has two TSs and one metastable intermediate, in Figure 2 only one TS which exhibits the higher free energy, i.e., $TS(RT/PD1)_A$ ($\Delta G^{\ddagger}$ = 131.8 kJ/mol), is shown and the metastable intermediate and the lower TS, i.e., IM4 (ΔG = 129.6 kJ/mol) and $TS(RT/PD1)_B$ ($\Delta G^{\ddagger}$ = 129.1 kJ/mol), are discussed in the next paragraph. All of these paths including path (a) occur essentially in one step, supporting the concerted mechanism in Scheme 1 (a). Since the free energy barriers are ~130 kJ/mol in all paths, all these may compete as discussed in the section of overall mechanism.

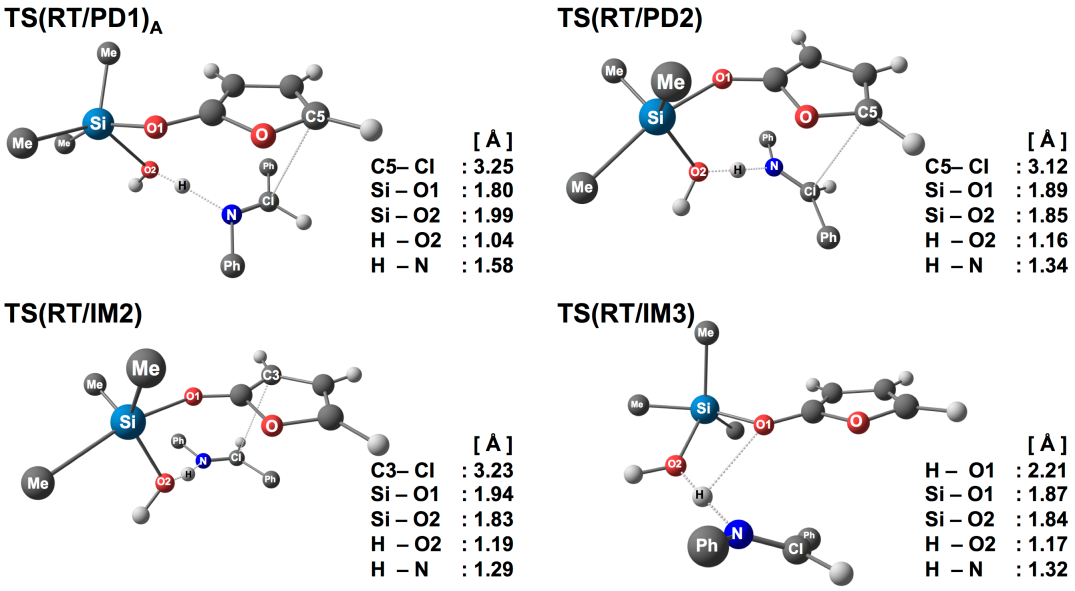

Figure 2. Ball-and-stick illustrations of optimized TS structures for the first step (see Figure 1 for corresponding schematic representations). Important bond distances (in Å) are also shown. Methyl and phenyl groups are simplified and represented by one carbon atom for clarity.

In order to investigate the reaction mechanism in detail, an energy profile along the intrinsic reactions coordinate (IRC) for path (a) is shown in Figure 3. As seen in this figure, in terms of electronic energy ΔE relative to RT (separately optimized three reactant molecules), $TS(RT/PD1)_A$ ($\Delta E^{\ddagger}$ = 12.4 kJ/mol) is slightly lower than $TS(RT/PD1)_B$ ($\Delta E^{\ddagger}$ = 13.1 kJ/mol). At first, the water molecule nucleophilically attacks on the silicon atom of TMSOF, and through $TS(RT/PD1)_A$ an intermediate with a five coordinated Si atom is generated. This intermediate (IM4) is metastable as seen in the IRC profile. Actually, corresponding intermediate does not

exist as explicit local minimum along IRCs for the other paths (b), (d), and (e). After passing through $TS(RT/PD1)_B$, the whole system polarizes significantly. Two extra (non-stationary) points (NSP1 and NSP2) along the IRC profile are shown in Figure 3: NSP1 in a flat region of the energy curve and NSP2 in a region where the energy curve starts to decrease. The total dipole moment varied from 6.2 Debye at IM4 to 8.9 Debye at NSP1. At NSP1, the partial charge on the iminium ion part and the silicate ion part, obtained by taking the summation of natural atomic charge, is +0.79 and –0.79, respectively. In other words, after the proton transfer through $TS(RT/PD1)_B$, the charged ion-pair state as suggested in Scheme 1 (b) appears. This state is not stable enough to give an explicit local minimum along the IRC profile. Instead, there is a flat region ranging from just after $TS(RT/PD1)_B$ to around NSP2. In this region, the iminium and silicate ions seek for the most stable relative orientation and position and finally form a C–C bond at the 5-position giving the product PD1 (**4** (*anti*) + **5**). These features are commonly seen in IRC paths starting from TS(RT/PD2), TS(RT/IM2), and TS(RT/IM3).

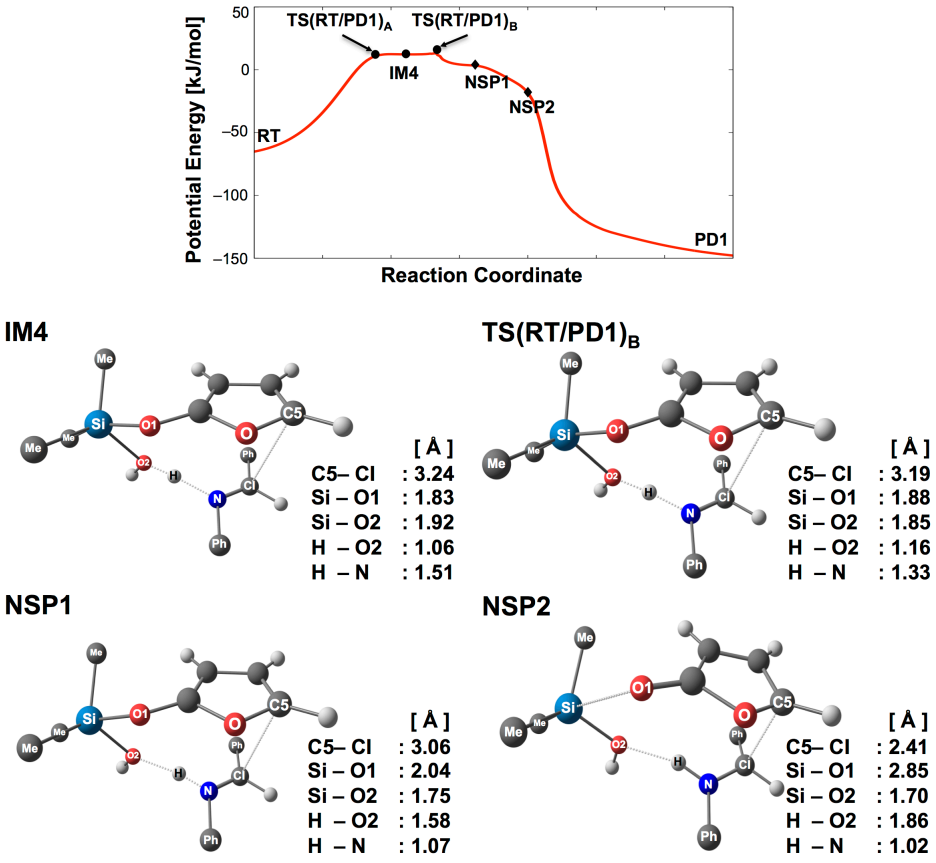

Figure 3. Potential energy (relative to RT) and structural changes along the IRC of path (a). See Figure 2 for the structure of $TS(RT/PD1)_A$.

An approximate TS leading to *anti*-regioisomer obtained in the initial AFIR search for path (c) converged to TS(RT/PD1)$_B$ during the re-optimization procedure at the M06-2X level. This is because the potential energy surface (PES) after the proton transfer from water molecule to nitrogen atom is pretty flat as seen in Figure 3. In this region, the ion-pair character is observed, i.e., the iminium and silicate ions can move and change their relative orientation and position easily in this region. This suggests that the new C–C bond may be generated at either 3-position or 5-position from the ion-pair region on the PES if dynamical fluctuations of these ions are taken into account (cf. bifurcation of the path);[34,35] consideration of the dynamical effects to see bifurcation of the path is beyond the scope of this study and will be a future subject. I suggest that path (c) also has certain contribution in the mechanism of the present reaction.

I checked TS(RT/PD1)$_B$, TS(RT/PD2), and TS(RT/IM3) considering following further points: (1) DFT functional dependence for TS(RT/PD1)$_B$ and TS(RT/PD2), (2) proton transfer medium (imine, H_2O, or TMSOH) dependence for TS(RT/IM3), (3) solvent effects on TS(RT/PD1)$_B$, and (4) participation of one more water molecule in TS(RT/PD1)$_B$. In these checks, TS(RT/PD1)$_B$ is chosen rather than TS(RT/PD1)$_A$ because B is higher than A in terms of electronic energy as noted above. Table 1 shows the functional dependence of structures and energies of TS(RT/PD1)$_B$ and TS(RT/PD2), by four different functionals, M06-2X,[36] B3LYP,[37] and B3LYP with empirical dispersion corrections (B3LYP+D),[38-44] and double-hybrid B2PLYPD.[45] As seen in Table 1, the three modern funtionals, M06-2X, B3LYP+D, and B2PLYPD, gave similar structures and energies, and this suggests that the present results at the M06-2X level are at least qualitatively reliable. This also illustrates significance of weak interactions such as π-π interactions in these TSs, and B3LYP, which is known to significantly underestimate dispersion forces,[40-44] gave very different results.

Table 1. DFT functional dependence of structures and relative energies of TS(RT/PD1)$_B$ and TS(RT/PD2).

	TS(RT/PD1)$_B$ [to **4** (*anti*)] [b]		**TS(RT/PD2)** [to **4** (*syn*)] [c]	
	r(C–C) (Å) [d]	$\Delta E^{\ddagger}$ (kJ/mol) [e]	r(C–C) (Å) [d]	$\Delta E^{\ddagger}$ (kJ/mol) [e]
M06-2X [a]	3.19	13.1	3.12	18.4
B3LYP [a]	3.84	87.8	4.27 [f]	89.1 [f]
B3LYP+D [a]	3.20	8.9	3.07	13.9
B2PLYPD [b, c]	–	9.1	–	16.1

[a] 6-31G(d) for methyl and phenyl groups and 6-311+G(2d,p) for the others. [b] Single point calculation at optimized geometry by M06-2X. [c] cc-pVDZ for methyl and phenyl groups and cc-pVTZ for the others. [d] Distance between two carbons associated with the new C–C bond. [e] Electronic energy relative to the three reactants **1** + **2** + **3**. [f] TS leading to **6** (*syn*) obtained by optimization starting from TS(RT/PD2) at the M06-2X level.

In path (e) through TS(RT/IM3), a proton once attaches to the nitrogen atom and finally transfers to the oxygen atom giving 2-furanol and TMSOH; imine is acting as a proton transfer catalyst. Although other species such as H_2O and TMSOH can be alternative catalysts, imine was found to be the best one as shown in supporting information S2. The present reaction occurred in solvent-free conditions.[14] Thus, I considered water solvent as an example with a large dielectric constant, and TS(RT/PD1)$_B$ was re-optimized at the M06-2X level with the C-PCM method.[46,47] Nevertheless, the shape of the reaction profile as well as the barrier height did not change significantly even in C-PCM-water solvent as shown in supporting information S3. Although I considered participation of one more water molecule in TS(RT/PD1)$_B$, its contribution to the barrier height is also small as shown in supporting information S4.

Second and Third Steps

I performed another AFIR search at the ONIOM(B3LYP/6-31G:PM6) level for **1** + **5** + **7**, because these three were obtained as important intermediates through path (e) via TS(RT/IM3). This AFIR search found four different products, **4** (*anti*), **4** (*syn*), **6** (*anti*), **6** (*syn*), and some hemiaminal species. As noted above, pathways to hemiaminal species were not studied further in this study. Other TSs leading to **4** (*anti*), **4** (*syn*), **6** (*anti*), and **6** (*syn*) were re-optimized at the M06-2X level. As illustrated in Figure 4 and discussed in the next paragraph, these TSs, i.e.,

TS(IM1/IM3), TS(IM2/IM3), TS(IM3/PD1), and TS(IM3/PD2), give the second and third steps of overall mechanisms through paths (c), (d), and (e) in Figure 1. As seen in Figure 5, C–C bond formation/cleavage occurs through these TSs with accompanying a proton transfer from/to 2-furanol (**7**) to/from imine **1** relayed by TMSOH **5**.

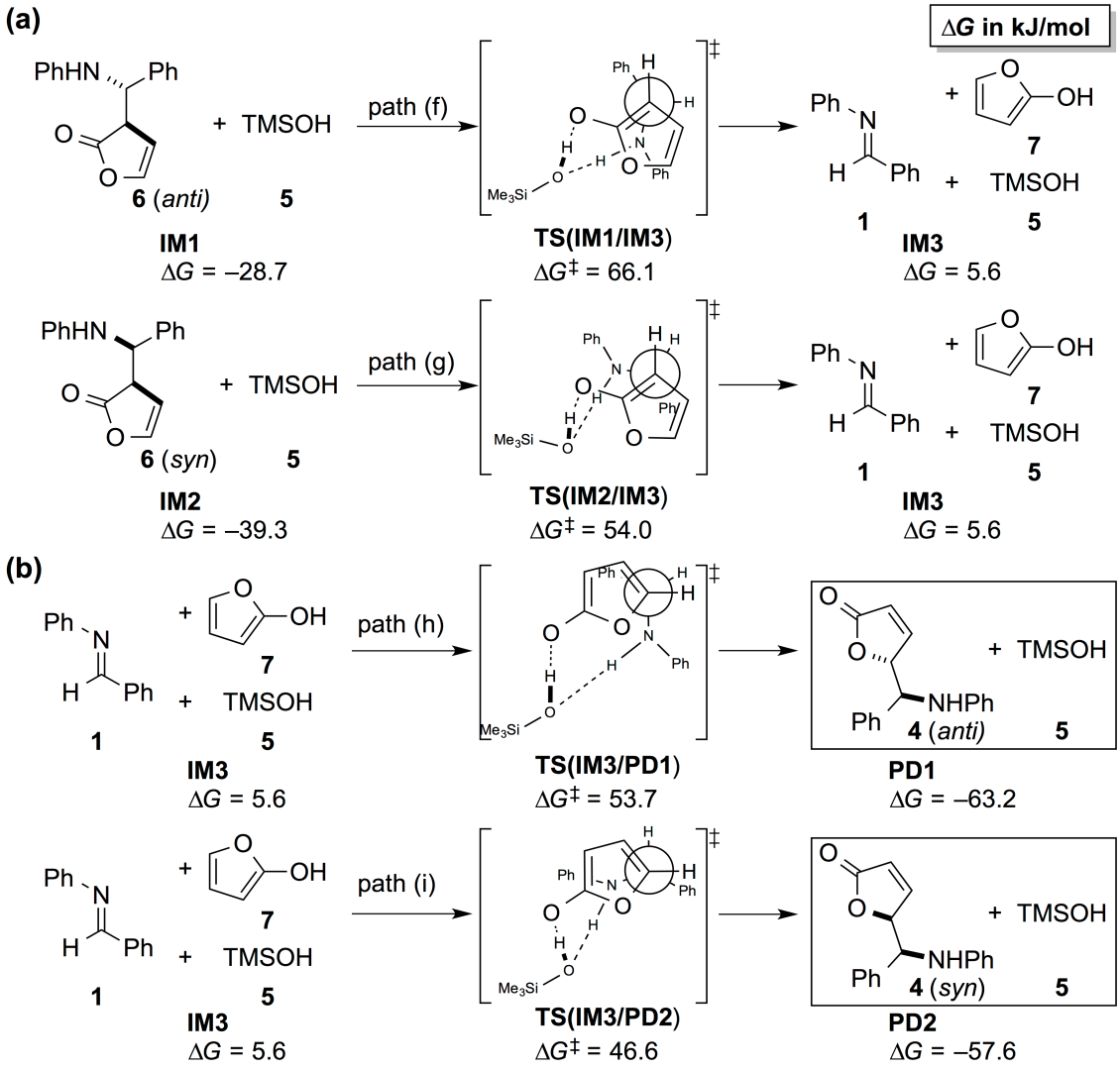

Figure 4. Four pathways obtained by the AFIR search. PD, IM, and TS stand for product (separately optimized two molecules), intermediate (separately optimized two or three molecules), and transition state, respectively. Gibbs free energy Δ*G* (298.15 K, 1 atm) based on M06-2X calculations (see text) relative to RT (separately optimized three reactant molecules) is presented in kJ/mol.

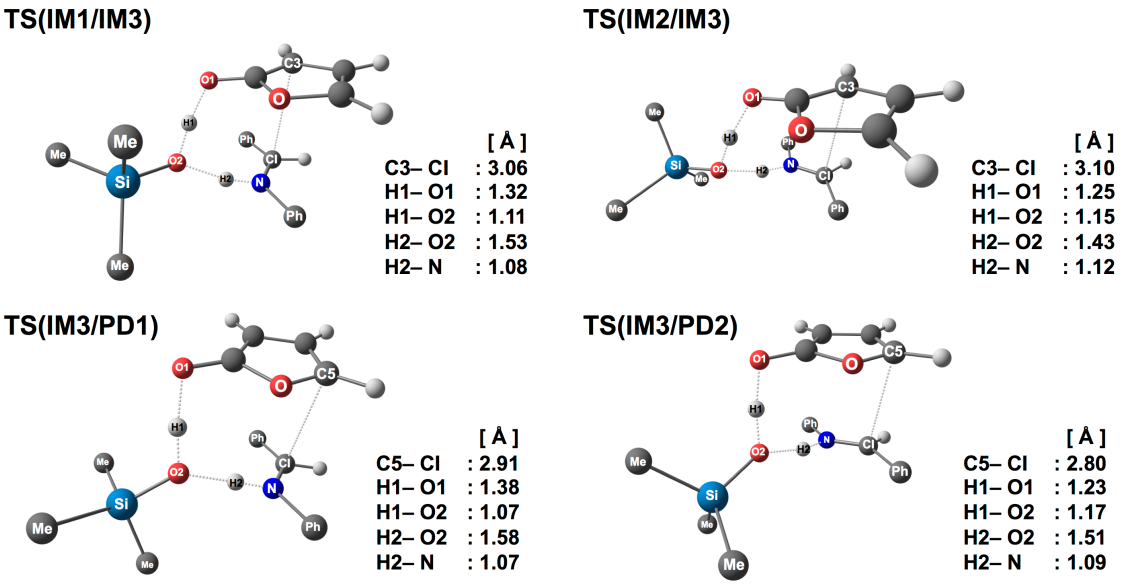

Figure 5. Ball-and-stick illustrations of optimized TS structures for the second and third steps (see Figure 4 for corresponding schematic representations). Important bond distances (in Å) are also shown. Methyl and phenyl groups are simplified and represented by one carbon atom for clarity.

Paths (c) and (d) in Figure 1 give **6** (*anti*) and **6** (*syn*), respectively. **6** (*anti*) and **6** (*syn*) can undergo further reaction steps, because they are thermodynamically unstable compared to **4** (*anti*) and **4** (*syn*). As seen in Figure 4, free energy barriers of retro-Mannich reactions, i.e., IM1 → TS(IM1/IM3) → IM3 and IM2 → TS(IM2/IM3) → IM3, are both around 90 kJ/mol. These are considerably lower than free energy barriers ~130 kJ/mol for their generation. In other words, **6** (*anti*) and **6** (*syn*) decompose into **1** and **7** more rapidly than their production. Once these retro-Mannich reactions take place as the second step, **1** and **7** can undergo the third step giving **4** (*anti*) and **4** (*syn*) through TS(IM3/PD1) and TS(IM3/PD2), respectively. In short, **6** (*anti*) and **6** (*syn*) can be just transient intermediates. Once IM3 is generated through path (e) in Figure 1, **1** and **7** in IM3 can further react to each other through either TS(IM3/PD1) or TS(IM3/PD2) giving **4** (*anti*) and **4** (*syn*); these can be the second step of overall mechanisms through path (e) as well.

Overall Mechanism

Finally, the full reaction mechanism and free energy profiles for *anti*- and *syn*-pathways can be illustrated as Figure 6(a), (b), and (c), respectively, by combining the above elementary steps. At the first step, there are five branches as discussed above and as seen in Figure 6(a). The path leading to IM1 (**6** (*anti*) + **5**) is shown by dashed line in (a) and (b) as the corresponding TS was not found at the M06-2X level as discussed above. The decomposition path of **2** via TS(RT/IM3) is shown both (b) and (c), because this path gives IM3 which can give both PD1 (**4** (*anti*) + **5**) and PD2 (**4** (*syn*) + **5**) through TS(IM3/PD1) and TS(IM3/PD2), respectively. Since the free energy barriers at the first steps are higher than those in any other steps, this is the rate-determining step in this reaction.

Free energy barriers for the first step are commonly around 130 kJ/mol, and the lowest two paths are TS(RT/IM2) to IM2 (**6** (*syn*) + **5**) and TS(RT/IM3) to IM3 (**1** + **5** + **7**). Moreover, **6** (*anti*) can also be generated by the reaction **1** + **5** + **7** through TS(IM1/IM3). It follows that **6** and **7** can be byproducts. The experimental yield of the main product **4** is 86%, and the present automated search predicts that byproducts would be **6** and **7**. Nevertheless, even **6** (*syn*) generated by the lowest path cannot be a major product because its generation through TS(RT/IM2) is slower than the retro-Mannich reaction of **6** (*syn*) decomposing into **1** + **7** via TS(IM2/IM3). Furthermore, **7** can be consumed rapidly by a reaction with **1** through TS(IM3/PD1) or TS(IM3/PD2) giving the main product **4**. In other words, **6** and **7** never gain sufficient population due to existence of faster channels than their generation. Therefore, **6** and **7** can be just short-lived intermediates. In conclusion, all the five paths in Scheme 2 located for the first step can finally converge to the main product **4**.

In the experiment, no *anti*/*syn* selectivity was observed.[14] The lowest paths (in terms of free energy barriers) leading to **4** (*anti*) and **4** (*syn*) are TS(RT/IM3) → TS(IM3/PD1) → PD1 (**4** (*anti*) + **5**)) and TS(RT/IM2) → TS(IM2/IM3) → TS(IM3/PD2) → PD2 (**4** (*syn*) + **5**)), respectively, and these can compete. It is not easy to estimate the relative abundance of *anti*- and *syn*-products, as the number of steps is different and the other paths may also contribute. Moreover, even the products 4 (*anti*) and 4 (*syn*) can undergo the retro-Mannich reactions, PD1 → TS(IM3/PD1) → IM3 and PD2 → TS(IM3/PD2) → IM3. This is because free energy barriers for these reactions are smaller than those for the first step. That is, the *anti*/*syn* selectivity is more or less controlled by the thermodynamic stability of products **4** (*anti*) and **4** (*syn*) as well. Here, I performed conformational analysis toward PD1 and PD2 by using the

anharmonic downward distortion following (ADDF) method[32]. (Details of this analysis are described in Supporting Information S5.) Since the *anti*/*syn* selectivity is well reproduced from the Boltzmann distribution of obtained rotamers in free energy, it is confirmed that this system is controlled by the thermodynamic stability of the products.

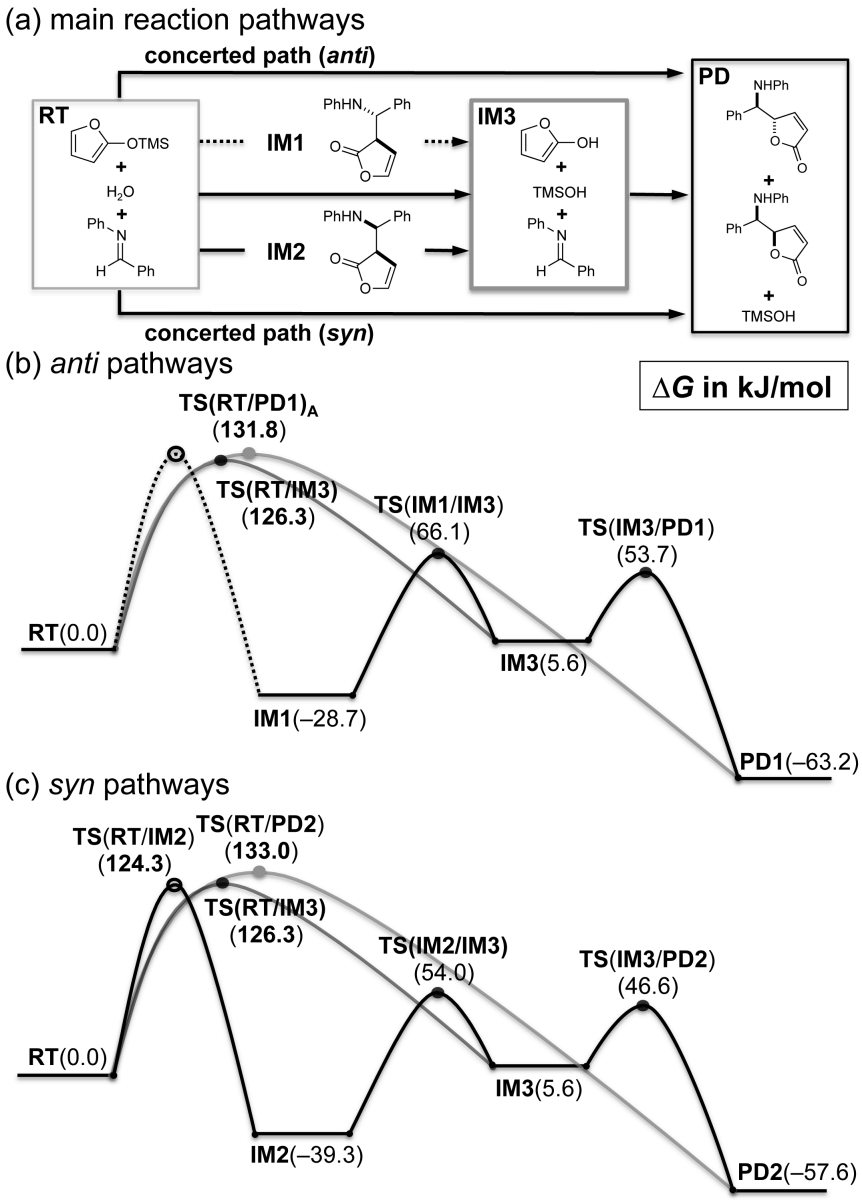

Figure 6. The full reaction mechanism of the present vinylogous Mannich-type reaction. Panel (a) presents main pathways in this reaction. Panaels (b) and (c) represent free energy profiles leading to the *anti*- and *syn*-products, respectively.

The present AFIR search successfully sampled these multiple multistep pathways leading to possible byproducts as well as the main products automatically without using any guess about the reaction mechanism. This search predicted an interesting pathway through an unexpected intermediate 2-furanol (**7**). This suggests a possibility that the γ-butenolide motif and their derivatives may be constructed directly from 2-furanol. In other words, 2-furanol can be generated by any ways. Moreover, TS(IM3/PD2) is substantially lower in free energy than TS(IM3/PD1). It follows that a high *syn*-selectivity can be achieved if a reaction, in which the elemental process **1** + **7** → **4** is the rate-determining step, is developed. In short, a new reaction, which achieves both high stereo-selectivity and reduction of the TMSOH waste, can be designed by considering other ways to generate 2-furanol.

Conclusion

I explored reaction pathways among imine **1**, TMSOF **2**, and a water molecule **3** systematically by using the AFIR method, in order to elucidate the mechanism of a recently found vinylogous Mannich-type reaction. The search located five reaction pathways including unexpected retro-Mannich and decomposition pathways as well as expected concerted ones. These pathways have similar berries and are expected to be working together.

Among these five paths, two lead to the products **4** (*anti*) and **4** (*syn*) directly with concerted mechanisms. The other three also converge to the products **4** (*anti*) and **4** (*syn*) taking stepwise mechanisms. Two of them once give a regio-isomer **6** with different diastereomer, **6** (*anti*) and **6** (*syn*). **6** can undergo the retro-Mannich reaction into **1** and 2-furanol (**7**). The remaining path directly gives **1** and **7**. **1** can react with **7** easily giving the products **4** (*anti*) and **4** (*syn*). Moreover, a certain amount of the products **4** (*anti*) and **4** (*syn*) may go back to **1** and 2-furanol (**7**) with the retro-Mannich reaction. The *anti/syn* selectivity is controlled by thermodynamic stabilities of **4** (*anti*) and **4** (*syn*) from the results of conformational analysis of the products.

The overall mechanism involves multiple pathways including repetition of C–C bond generations and breakings (retro-Mannich reaction) at different (3- or 5-) positions. The final existence ratio of each species, i.e., products and intermediates (byproducts), should be controlled by their thermodynamic stability. In short, multiple pathways are operating in the mechanism of the present reaction. I would conclude that it is essential for correct understanding of the mechanism of multicomponent reactions to make systematic sampling of various reaction pathways.

The unexpected paths through 2-furanol suggest possibilities of better reactions. Since 2-furanol can be generated in the reaction system by any ways, by considering the other ways improvement of the *anti/syn* selectivity and/or reduction of the TMSOH waste may be achieved.

Computational Methods

By the AFIR method, reaction pathways among TMSOF, imine, and water molecules and those among imine, 2-furanol, and TMSOH were searched at the ONIOM(B3LYP/6-31G:PM6) level, where methyl and phenyl groups were treated by PM6 and the other reaction-center parts at the B3LYP/6-31G level. The AFIR method gives many approximate reaction paths called AFIR

paths as minimization paths of a special function called AFIR function.[30-32] The AFIR paths at the ONIOM level were found to be too crude to be compared to the intrinsic reaction coordinate (IRC) path of the final computational level. Hence, AFIR paths were once refined by a conventional path optimization method, the locally updated plane[48] (LUP) method, at the M06-2X level with small basis sets [6-31G(d) for methyl and phenyl groups and 6-31+G(d) for the others]. Since the AFIR path can be a good guess of the minimum energy path, LUP converges quickly and only five LUP iterations were considered. Peaks along the final LUP paths were then optimized to true TSs at the M06-2X level with lager basis sets; 6-31G(d) for methyl and phenyl groups and 6-311+G(2d,p) for the remaining reaction-center parts. Free energy corrections in gas-phase were estimated at optimized structures assuming the rigid-rotor and Harmonic approximations. As discussed in the main text, we examined some important TSs with different functionals B3LYP, B3LYP+D, and B2PLYPD. $TS(RT/PD1)_B$ was considered also with the C-PCM calculations for water solvent.

All DFT calculations were done with Gaussian 09 programs.[49] Using DFT gradients and Hessians, automated searches as well as geometry optimizations were performed by a developmental version of the GRRM program.[50]

References

1. Pansare, S. V.; Paul, E. K. *Chem. Eur. J.* **2011**, *17*, 8770 – 8779.
2. Casiraghi, G.; Battistini, L.; Curti, C.; Rassu, G.; Zanardi, F. *Chem. Rev.* **2011**, *111*, 3076 3154.
3. Casiraghi, G.; Zanardi, F.; Bat- tistini, L.; Rassu, G. *Synlett* **2009**, 1525 – 1542.
4. Brown, S. P.; Goodwin, N. C.; MacMillan, D. W. C. *J. Am. Chem. Soc.* **2003**, *125*, 1192 – 1194.
5. Martin, S. F. *Acc. Chem. Res.* **2002**, *35*, 895 – 905.
6. Cho, C.W.; Krische, M.J.; *Angew. Chem.* **2004**, *116*, 6857–6859; *Angew. Chem. Int. Ed.* **2004**, *43*, 6689 – 6691.
7. Catino, A. J.; Nichols, J. M.; Nettles, B. J.; Doyle, M. P. *J. Am. Chem. Soc.* **2006**, *128*, 5648 – 5649.
8. Jiang, Y. Q.; Shi, Y. L.; Shi, M. *J. Am. Chem. Soc.* **2008**, *130*, 7202 – 7203.
9. Yadav, J. S.; Reddy, B. V. S.; Narasimhulu, G.; Satheesh, G.; *Tetrahedron Lett.* **2008**, *49*, 5683 – 5686.
10. Ube, H.; Shimada, N.; Terada, M. *Angew. Chem.* **2010**, *122*, 1902 – 1905; *Angew. Chem. Int. Ed.* **2010**, *49*, 1858–1861.
11. Palmer, L. I.; Read deAlaniz, J. *Angew. Chem.* **2011**, *123*, 7305 – 7308 ; *Angew. Chem. Int. Ed.* **2011**, *50*, 7167 – 7170.
12. Hou, G.; Yu, J.; Yu, C.; Wu, G.; Miao Z. *Adv. Synth. Catal.* **2013**, *355*, 589 – 593.
13. Ratnikov, M. O.; Doyle, M. P. *J. Am. Chem. Soc.* **2013**, *135*, 1549 – 1557.
14. Landelle, G.; Claraz, A.; Oudeyer, S.; Levacher, V.; *Tetrahedron Lett.* **2012**, *53*, 2414 – 2416.
15. Cheng, L.; Wu, X.; Lu, Y. *Org. Biomol. Chem.* **2007**, *5*, 1018 – 1020.
16. Hayashi, Y.; Urushima, T.; Aratake, S.; Okano, T.; Obi, K. *Org. Lett.* **2008**, *10*, 21 – 24.
17. Sartori, A.; Dell Amico, L.; Curti, C.; Battistini, L.; Pelosi, G.; Rassu, G.; Casiraghi, G.; Zanardi, F. *Adv. Synth. Catal.* **2011**, *353*, 3278 – 3284.
18. Mirabal-Gallardo, Y.; Soriano, M. D. P. C.; Caballero, J.; Alzate-Mo- rales, J.; Simirgiotis, M. J.; Santos, L. S.; *Synthesis* **2012**, 144 – 150.
19. Cheong, P. H.-Y.; Legault, C. Y.; Um, J. M.; Celebi-Ölucüm, N.; Houk, K. N.; *Chem. Rev.* **2011**, *111*, 5042 – 5137.
20. Wong, C. T. *Tetrahedron* **2009**, *65*, 7491 – 7497.

21. Houk, K. N.; Cheong, P. H.-Y. *Nature* **2008**, *455*, 309 – 313.
22. Hayashi, Y.; Okano, T.; Itoh, T.; Urushima, T.; Ishikawa, H.; Uchimaru, T. *Angew. Chem.* **2008**, *120*, 9193 – 9198 ; *Angew. Chem. Int. Ed.* **2008**, *47*, 9053 – 9058.
23. Parasuk, W.; Parasuk, V. *J. Org. Chem.* **2008**, *73*, 9388 – 9392.
24. Yamanaka, M.; Itoh, J.; Fuchibe, K.; Akiyama, T.; *J. Am. Chem. Soc.* **2007**, *129*, 6756 – 6764.
25. Cheong, P. H.-Y.; Zhang, H.; Thayumanavan, R.; Tanaka, F.; Houk, K. N.; Barbas, C. F. *Org. Lett.* **2006**, *8*, 811 – 814.
26. Mitsumori, S.; Zhang, H.; Cheong, P. H.-Y.; Houk, K. N.; Tanaka, F.; Barbas, C. F. *J. Am. Chem. Soc.* **2006**, *128*, 1040 – 1041.
27. Allemann, C.; Gordillo, R.; Clemente, F. R.; Cheong, P. H.-Y.; Houk, K. N. *Acc. Chem. Res.* **2004**, *37*, 558 – 569.
28. Bahmanyar, S.; Houk, K. N. *Org. Lett.* **2003**, *5*, 1249 – 1251.
29. Bur, S. K.; Martin, S. F. *Org. Lett.* **2000**, *2*, 3445 – 3447.
30. Maeda, S.; Morokuma, K. *J. Chem. Phys.* **2010**, *132*, 241102 – 241104.
31. Maeda, S.; Morokuma, K. *J. Chem. Theory Comput.* **2011**, *7*, 2335 – 2345.
32. Maeda, S.; Ohno, K.; Morokuma, K. *Phys. Chem. Chem. Phys*. **2013**, *15*, 3683 – 3701.
33. Maeda, S.; Komagawa, S.; Uchiyama, M.; Morokuma, K. *Angew. Chem*. **2011**, *123*, 670 – 675 ; *Angew. Chem. Int. Ed.* **2011**, *50*, 644 –649.
34. Ess, D. H.; Wheeler, S. E.; Iafe, R. G.; Xu, L.; Celebi-Ölcüm, N.; Houk, K. N. *Angew. Chem.* 2008, 120, 7704 – 7713; *Angew. Chem. Int. Ed.* **2008**, *47*, 7592 – 7601.
35. Harabuchi, Y.; Taketsugu, T. *Theor. Chem. Acc.* **2011**, *130*, 305 – 315.
36. Zhao, Y.; Truhlar, D. G. *Theor. Chem. Acc.* **2008**, *120*, 215 – 241.
37. Becke, A. D. *J. Chem. Phys.* **1993**, *98*, 5648 – 5652.
38. Grimme, S. *J. Comput. Chem.* **2004**, *25*, 1463 – 1473.
39. Grimme, S. *J. Comput. Chem.* **2006**, *27*, 1787 – 1799.
40. Minenkov, Y.; Occhipinti, G.; Jensen, V. R. *J. Phys. Chem. A* **2009**, *113*, 11833 – 11844.
41. Siegbahn, P. E. M.; Blomberg, M. R. A.; Chen, S.-L. *J. Chem. Theory Comput.* **2010**, *6*, 2040 – 2044.
42. Harvey, J. N. *Faraday Discuss*. **2010**, *145*, 487 – 505.
43. Lonsdale, R.; Harvey, J. N.; Mulholland, A. J. *J. Phys. Chem. Lett.* **2010**, *1*, 3232 – 3237.
44. McMullin, C. L.; Jover, J.; Harvey, J. N.; Fey, N. *Dalton Trans.* **2010**, *39*, 10833 – 10836.
45. Schwabe, T.; Grimme, S. *Phys. Chem. Chem. Phys*. **2007**, *9*, 3397– 3406.

46. Barone, V.; Cossi, M. *J. Phys. Chem. A* **1998**, *102*, 1995 – 2001.
47. Cossi, M.; Rega, N.; Scalmani, G.; Barone, V. *J. Comput. Chem.* **2003**, *24*, 669 – 681.
48. Choi, C.; Elber, R. *J. Chem. Phys*. **1991**, *94*, 751 – 760.
49. Gaussian 09, Revision B.01, Frisch, M. J.; Trucks, G. W.; Schlegel, H. B.; Scuseria, G. E.; Robb, M. A.; Cheeseman, J. R.; Scalmani, G.; Barone, V.; Mennucci, B.; Petersson, G. A.; Nakatsuji, H.; Caricato, M.; Li, X.; Hratchian, H. P.; Izmaylov, A. F.; Bloino, J.; Zheng, G.; Sonnenberg, J. L.; Hada, M.; Ehara, M.; Toyota, K.; Fukuda, R.; Hasegawa, J.; Ishida, M.; Nakajima, T.; Honda, Y.; Kitao, O.; Nakai, H.; Vreven, T.; Montgomery, J. A. Jr.; Peralta, J. E.; Ogliaro, F.; Bearpark, M.; Heyd, J. J.; Brothers, E.; Kudin, K. N.; Staroverov, V. N.; Kobayashi, R.; Normand, J.; Raghavachari, K.; Rendell, A.; Burant, J. C.; Iyengar, S. S.; Tomasi, J.; Cossi, M.; Rega, N.; Millam, J. M.; Klene, M.; Knox, J. E.; Cross, J. B.; Bakken, V.; Adamo, C.; Jaramillo, J.; Gomperts, R.; Stratmann, R. E.; Yazyev, O.; Austin, A. J.; Cammi, R.; Pomelli, C.; Ochterski, J. W.; Martin, R. L.; Morokuma, K.; Zakrzewski, V. G.; Voth, G. A.; Salvador, P.; Dannenberg, J. J.; Dapprich, S.; Daniels, A. D.; Farkas, Ö.; Foresman, J. B.; Ortiz, J. V.; Cioslowski, J.; Fox, D. J. Gaussian, Inc. , Wallingford CT, 2009.
50. Maeda, S.; Osada, Y.; Morokuma, K.; Ohno, K. GRRM, a developmental version at Hokkaido University.

Supporting Information

S1. Full representation of stationary points along IRC pathways

S2. Different proton transfer catalysts in the TMSOF decomposition path

S3. Solvent effects on $TS(RT/PD1)_B$

S4. Participation of an additional water molecule in $TS(RT/PD1)_B$

S5. Conformational analysis of PD1 and PD2

S1. Full representation of stationary points along IRC pathways

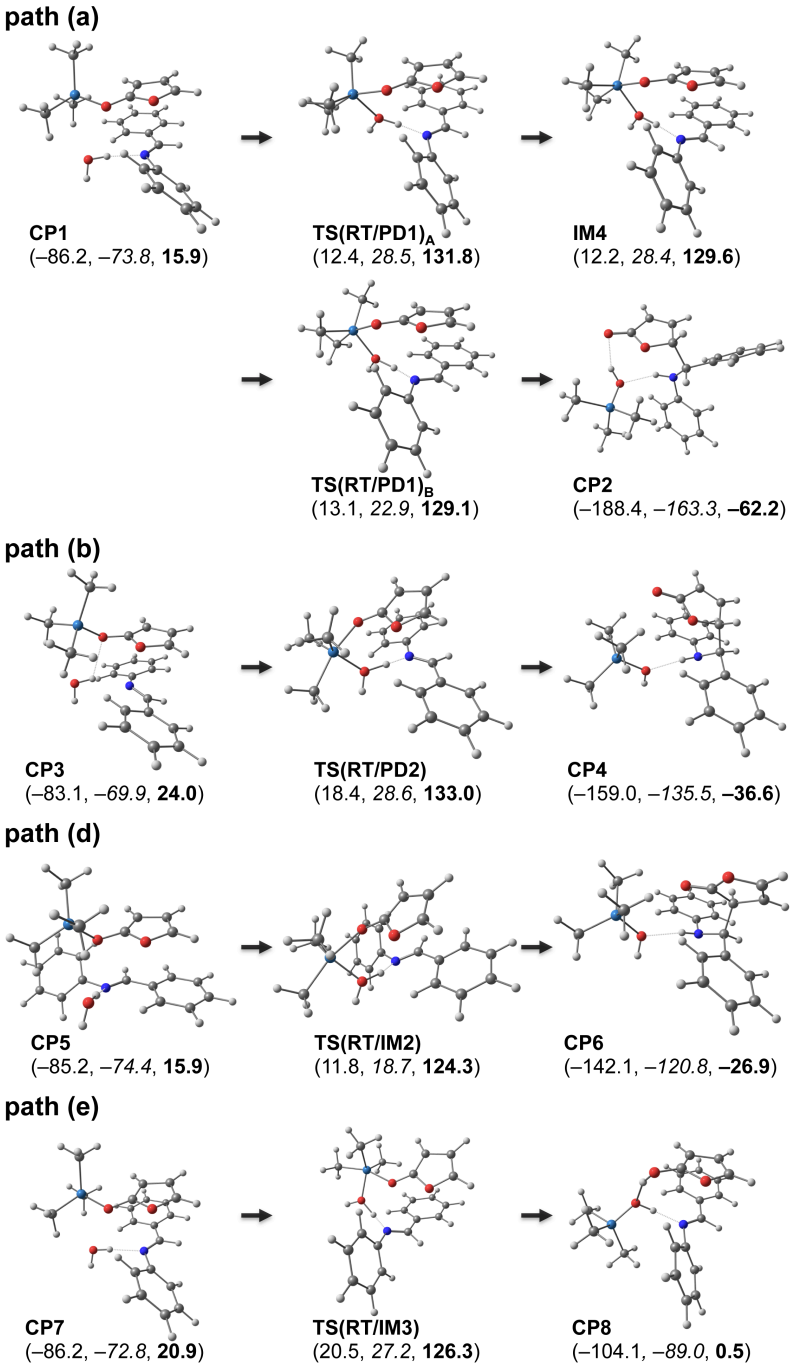

Figure S1-1. Optimized complex (**CP**) and transition state (**TS**) structures for the reaction **1** + **2** + **3**, at the M06-2X level (see main text for basis sets)

In parentheses, three energy values at the M06-2X level are shown; electronic energy *E* (regular), *E* + zero-point-energy (italic), and free energy at 298.15 K (bold), relative to the reactants **1** + **2** + **3**. Unit of these energies is kJ/mol.

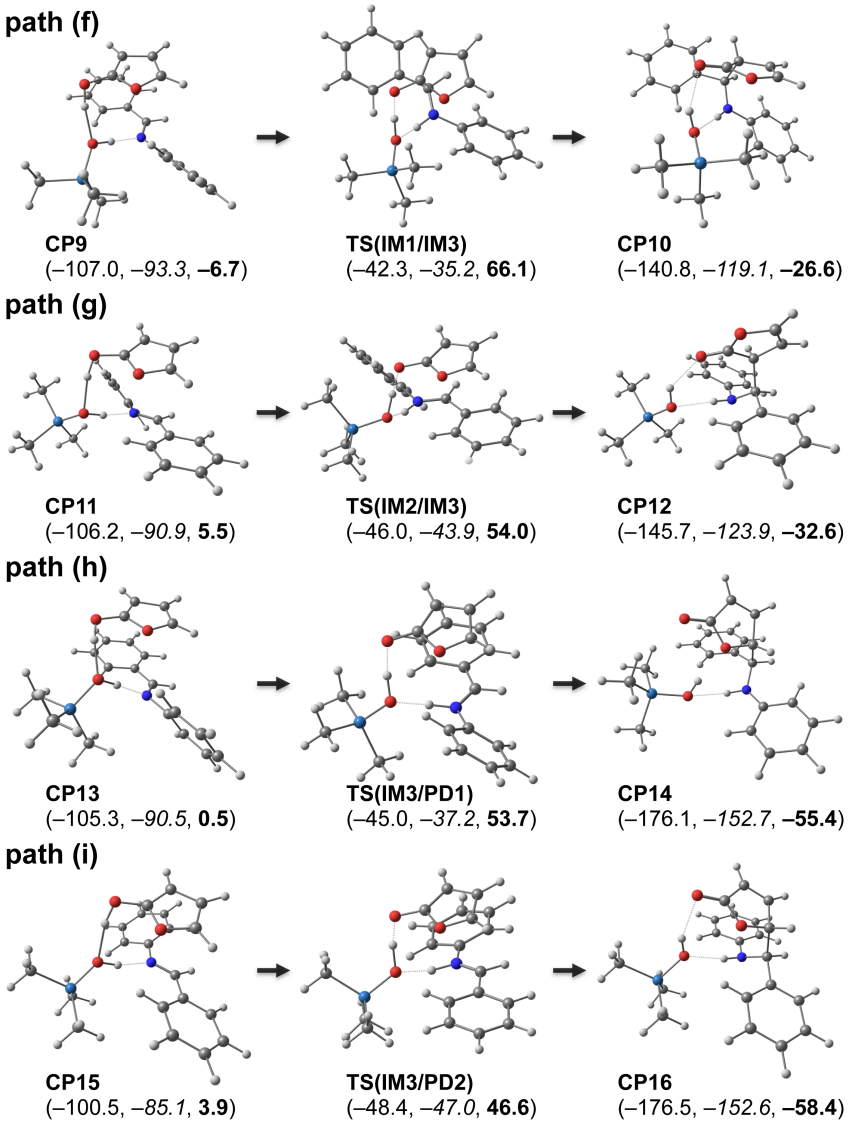

Figure S1-2. Optimized complex (**CP**) and transition state (**TS**) structures for the reaction **1** + **5** + **7**, at the M06-2X level (see main text for basis sets)

In parentheses, three energy values at the M06-2X level are shown; electronic energy *E* (regular), *E* + zero-point-energy (italic), and free energy at 298.15 K (bold), relative to the reactants **1** + **2** + **3**. Unit of these energies is kJ/mol.

S2. Different proton transfer catalysts in the TMSOF decomposition path

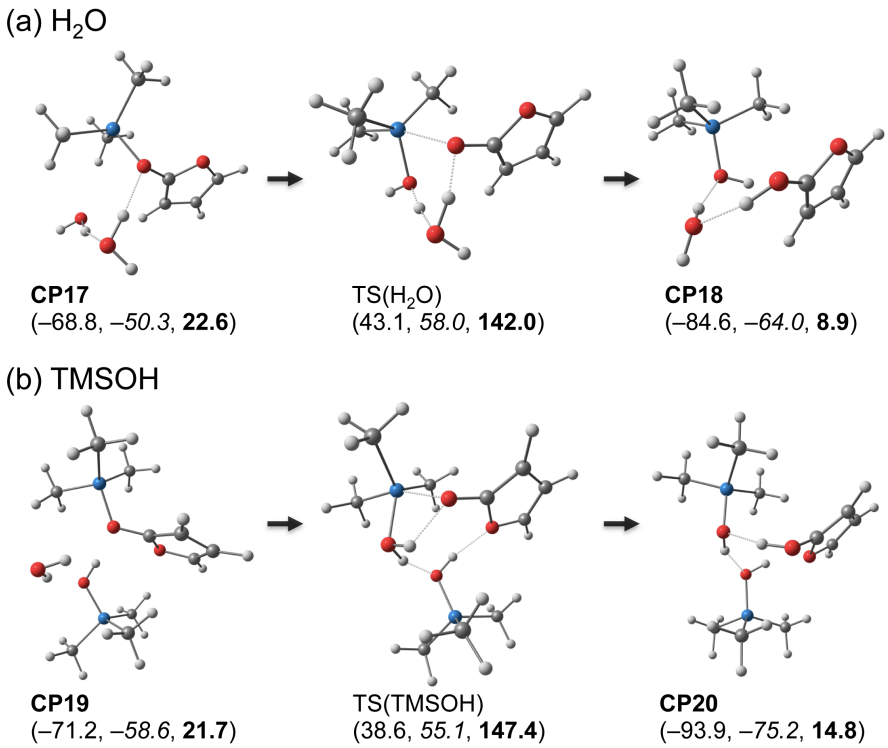

Figure S2. Optimized complex (**CP**) and transition state (**TS**) structures (a) H_2O and (b) TMSOH catalyzed TSs concerning the TMSOF decomposition path, at the M06-2X level (see main text for basis sets)

In parentheses, three energy values at the M06-2X level are shown; electronic energy *E* (regular), *E* + zero-point-energy (italic), and free energy at 298.15 K (bold), relative to the reactants **1** + **2** + **3**. Unit of these energies is kJ/mol. Imine was found to be the best catalyst (see path (e) in Figure 1).

S3. Solvent effects on TS(RT/PD1)$_B$

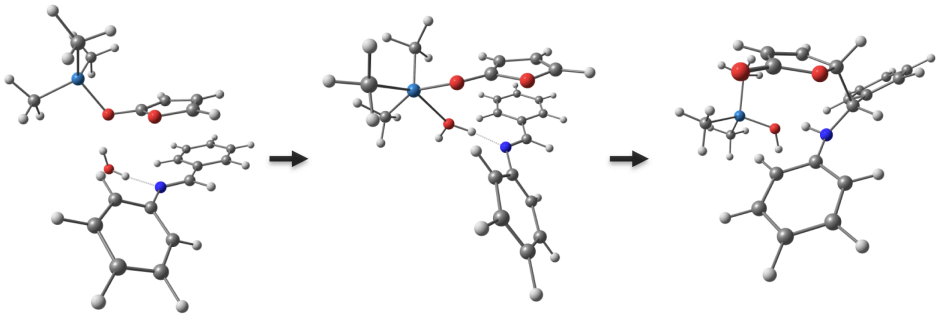

Figure S3. Optimized complex (**CP**) and transition state (**TS**) structures for the concerted path to the **4** (*anti*) in C-PCM-water solvent, at the M06-2X level (see main text for basis sets)

In parentheses, three energy values at the M06-2X level are shown; electronic energy *E* (regular), *E* + zero-point-energy (italic), and free energy at 298.15 K (bold), relative to the reactants **1** + **2** + **3**. Water solvent was considered as an example with a large dielectric constant, and **TS(RT/PD1)$_B$** was re-optimized with C-PCM. As discussed in the main section, there is a metastable intermediate (**IM4**) in gas-phase. On the other hand, in C-PCM-water the IRC path was found to be one step. The barrier (the energy difference between the TS and the pre-reaction complex) in CPCM-water solvent is similar to that in gas-phase (see path (a) in Figure 1).

S4. Participation of an additional water molecule in TS(RT/PD1)$_B$

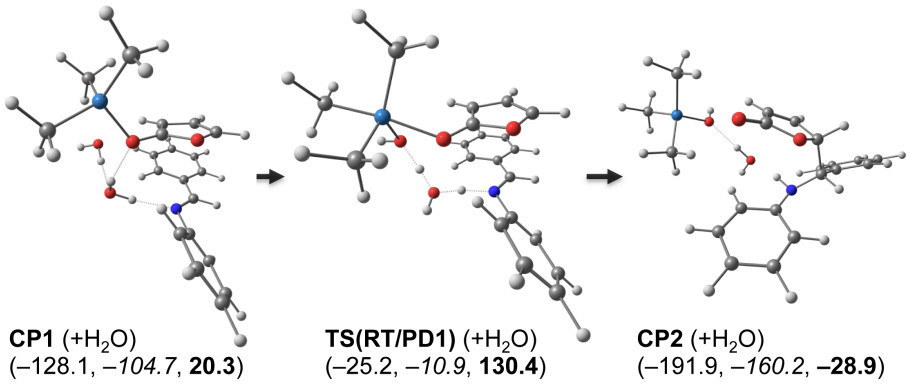

Figure S4. Optimized complex (**CP**) and transition state (**TS**) structures for the concerted path to the **4** (*anti*) with a single water catalyst, at the M06-2X level (see main text for basis sets)

In parentheses, three energy values at the M06-2X level are shown; electronic energy *E* (regular), *E* + zero-point-energy (italic), and free energy at 298.15 K (bold), relative to the reactants **1** + **2** + **3**. The additional H_2O molecule is acting as a proton transfer medium. The barrier (the energy difference between the TS and the pre-reaction complex) is similar to that in the single water case (see path (a) in Figure 1).

S5. Conformational analysis of PD1 and PD2

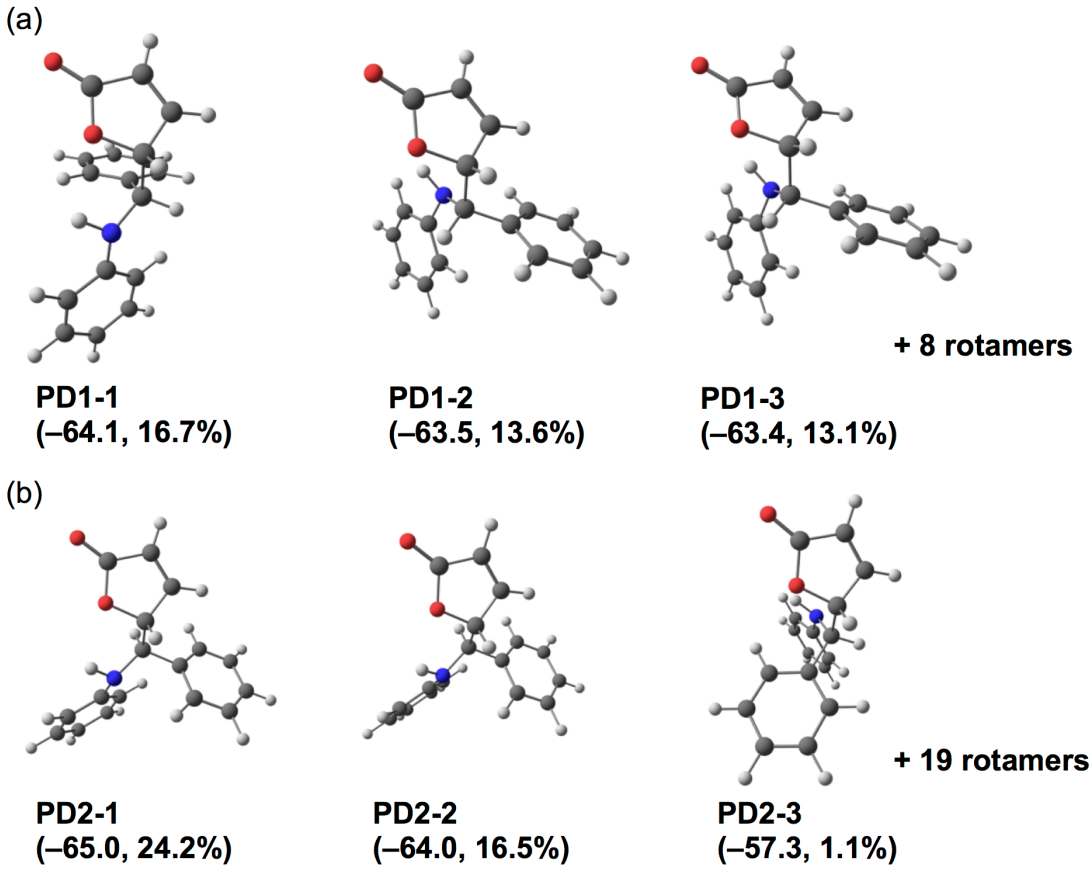

Figure S5. Ball-and-stick illustrations of optimized rotamer structures resulting in the conformation analysis

(a) the top three structures in PD1 (*anti* product); (b) the top three structures in PD2 (*syn* product). The values in parenthesis are the relative Gibbs free energy Δ*G* (298.15 K, 1 atm, and in kJ/mol unit) based on M06-2X calculations (see text) relative to RT (separately optimized three reactant molecules) and the Boltzmann distribution. The eleven *anti* rotamers and twenty-two *syn* rotamers were found in the analysis from the PD1 and PD2, respectively. Here, the Boltzmann distribution was estimated using all these free energy values, and the calculated *anti*/*syn* ratio was 52.6 : 47.4. This result is consistent with the experimental result: *anti*/*syn* = 53 : 47. It is confirmed that this system is controlled by the thermodynamic stability of the products.

Chapter 3

Theoretical Study in Reaction Mechanism of the Anomalous Formal Nucleophilic Borylation of Organic Halides with Silylborane

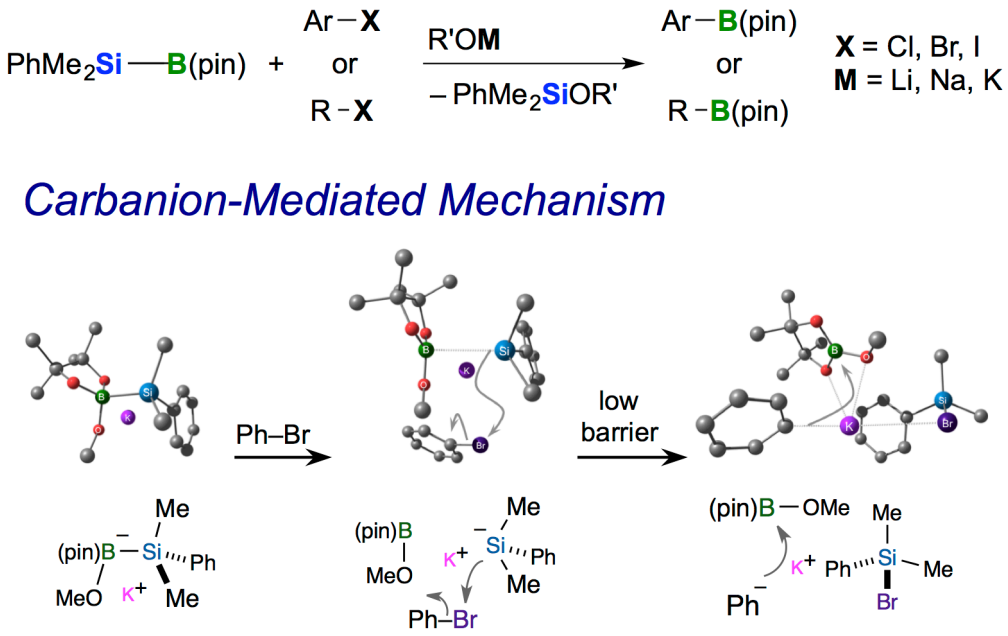

ABSTRACT

Theoretical study has been conducted to elucidate the mechanism of the formal nucleophilic boryl substitution of aryl- and alkyl bromides with silylborane in the presence of potassium methoxide. Density functional theory was used in conjunction with the artificial force induced reaction method in the current study to determine the mechanism of this reaction. The results of this analysis led to the identification of a unique carbanion-mediated mechanism involving the halogenophilic attack of a silyl nucleophile on the bromine atom of the substrate. These calculations have therefore provided a mechanistic rationale for this counterintuitive borylation reaction. Furthermore, the good functional group compatibility and high reactivity exhibited by this reaction towards sterically hindered substrates can be understood in terms of the low activation energy required for the reaction of the silyl nucleophile with the bromine atom of the substrate, and the subsequent rapid and selective consumption of the carbanion species by the *in situ* generated boron electrophile. The anomalous formal nucleophilic borylation mechanism reported in this study could be used to provide new insights in silicon and boron chemistry.

Introduction

Organoboronate esters are important building blocks in organic synthesis and considerable research efforts have been focused on the development of synthetic methods for the construction of compounds containing this boronate ester group.[1] In this regard, Ito et al.[2] recently reported the development of a novel formal nucleophilic boryl substitution reaction, which involved the borylation of aryl-, alkenyl-, and alkyl halides with a silylborane species in the presence of an alkoxy base. This method of borylation is generally referred to as base-mediated borylation with a silylborane (BBS method). The BBS method shows good functional group compatibility and high levels of reactivity toward sterically hindered aryl bromides, and can be conducted at ambient temperature in the absence of a transition metal catalyst. Many organometallic ate complexes (i.e. borate, silicate, cuprate, and zincate etc.) are often applied for transmetalation reaction.[3] However, one of the most interesting features of this reaction is that it appears to exhibit a counterintuitive reaction profile. For example, the reaction of a silylborane reagent with an appropriate base or nucleophile leads to the generation of a silyl nucleophile.[4] In addition, the nucleophilic aromatic substitution of aryl halides does not usually occur under low temperature conditions without a highly electron withdrawing group on the aromatic substrate.[5] The borylation activity described in Ito's work was therefore unexpected, in that it deviated considerably from the reactivity behaviors previously reported in silicon and boron chemistry.[6] Although this reaction is of particular interest with regard to its synthetic utility, very little is known about the mechanism of this reaction, and further work is therefore required to develop a deeper understanding of the mechanism associated with this process.

Significant research efforts have been directed towards the development of borylation reactions for the synthesis of alkyl- and aryl boronate esters,[7-10] and the borylation of organohalides represents one of the most reliable and widely used of these methods for the synthesis of organoboronate esters. Alkyl- and aryl boronate esters can generally be prepared by the reaction of boron electrophiles with organolithium or Grignard reagents, which can be readily prepared from the corresponding organohalides.[7] However, the application of these reactions has been limited by their requirement for strongly basic and highly nucleophilic organometallic reagents, which invariably lead to poor functional group compatibility. The transition metal-catalyzed boryl substitution reaction of aryl- and alkyl halides or pseudo halides has emerged as a useful alternative for the formation of organoboronate esters, showing high levels of functional group compatibility.[8-9] The application of these methods to the synthesis of

pharmaceutical agents or organic materials, however, has been limited because of the costs associated with the use of transition metals on a large scale and the potential for the contamination of the product with residual transition metals.[11]

The BBS method is a newly developed, transition metal-free reaction for the synthesis of organoboronate esters, but the mechanism of this reaction has not yet been elucidated. A tentative mechanism (Scheme 1) has been proposed for this reaction based on several experimental observations,[2] which involves the formation of a carbanion species via a metal-halogen exchange.[9i,12,13] The silyl substitution reaction of aryl halides with a silyllithium reagent was also reported by Strohmann et al.[14] According to this mechanism,[2] $PhMe_2Si–B(pin)$ (**1**) would initially react with potassium methoxide (**2a**) to give the silylborane/alkoxy base complex A. Subsequent nucleophilic attack of the silyl moiety of complex **A** on the bromine atom of the alkyl- or aryl bromide **3** would lead to the formation of complex **B** or **C**, which would contain a nucleophilic carbon moiety or carbanion species, respectively. The carbon nucleophile would then attack the boron electrophile rather than the silyl bromide (**4**) to give the corresponding organoborate intermediate $[RB(pin)OMe]^-K^+$, which would provide the organoboronate ester **5** through the reaction of $[RB(pin)OMe]^-K^+$ with the in situ generated silyl bromide **4**, with silyl ether **6** and potassium bromide (**7**) being formed as by-products. There are, however, several issues with this mechanism. For example, this mechanism assumes that a thermodynamically and kinetically unstable organopotassium intermediate can be generated from a relatively unreactive, silyl borate species. Furthermore, the proposed generation of a highly reactive organopotassium intermediate is not consistent with the high level of functional group compatibility observed for this method. Based on these inconsistencies, it is clear that further comprehensive theoretical studies are required to provide a deeper understanding of this reaction mechanism. Extensive reaction path screening could be also used to exclude other possible reaction pathways.

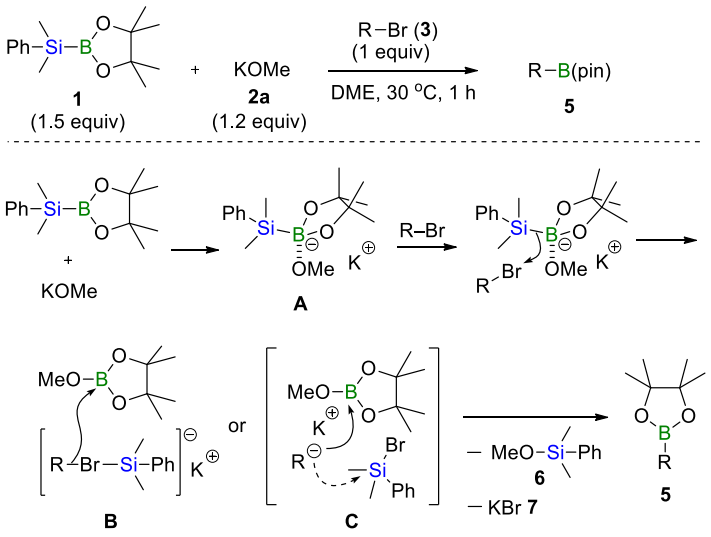

Scheme 1. Proposed Reaction Mechanism of Formal Boryl Substitution of Organic Bromine Compounds (R = Aryl or Alkyl) with Silylborane and Alkoxy Base

Given that it is not easy to explain the products resulting from the BBS method according to our current understanding of silicon and boron chemistry, it may not be possible to apply our existing theoretical understanding of the borylation of C–X and C–H bonds by transition metals[15] to this reaction. With this in mind, further studies are necessary to enhance our theoretical understanding to the extent that we can adequately explain this transformation. Nevertheless it can be difficult to apply conventional calculation methods to mechanistic studies involving novel or poorly defined reaction mechanisms because it may be necessary to consider multiple reaction pathways. Furthermore, this approach requires a large number of trial-and-error calculations to allow for the sequential identification of the intermediates and transition states (TSs) involved in the assumed mechanism. The artificial force induced reaction (AFIR) method is an automated reaction path search method[16, 17] that can be used as a powerful tool in theoretical studies towards the elucidation of reaction mechanisms. The AFIR method pushes given chemical species, such as substrates, catalysts, bases, etc., together by applying an artificial force. In practice, a model function called AFIR function is used, where this function is given as the sum of the potential energy function of the reacting system and a force term. The force term eliminates potential barriers along a reaction coordinate, and allows for efficient identification of product's geometry by minimization of this function. Moreover, along the minimization path of the model function (AFIR path), approximate TS geometries can be obtained. These approximate TSs are further optimized without the force in order to obtain real

TSs. I note that in the following all TSs as well as minimum energy structures discussed are real TSs and local minima which were reoptimized without the force term. By systematic applications, the AFIR method allows for the identification of working reaction pathways including unexpected ones from the many different possibilities without the need to estimate any of the TS structures.

Herein, I present the results of a detailed density functional theory (DFT) study on the BBS method using the AFIR method. The results of this comprehensive theoretical investigation have allowed for the construction of a complete reaction pathway. This new pathway shows several similarities to the carbanion-mediated mechanism in Scheme 1. The results of this study can also be used to rationalize the selectivity of the borylation/silylation process, as well as the good functional group compatibility and the high reactivity exhibited by the reactions towards sterically hindered substrates. The results of this study have also eliminated the possibility of a neutral radical or radical anion-mediated mechanism being involved in the reaction using CIS- and TDDFT-based electronic excitation energy calculations.

Results

My initial efforts focused on systematically exploring the pathways potentially involved in the reaction of (dimethylphenylsilyl)boronic acid pinacol ester [$PhMe_2Si$–B(pin), **1**] with (2-bromoethyl)benzene (**3a**) in the presence of potassium methoxide using the AFIR method. Further details of this process have been provided below in the Computational Details section. Based on the intermediates and TSs obtained for this set of substrates, the reaction pathways for the reaction of compound **1** with bromobenzene (**3b**) in the presence of potassium methoxide were computed using standard geometry optimization calculations. These reactions are described in Scheme 2 [case-A (eq 1) and case-B (eq 2), respectively].

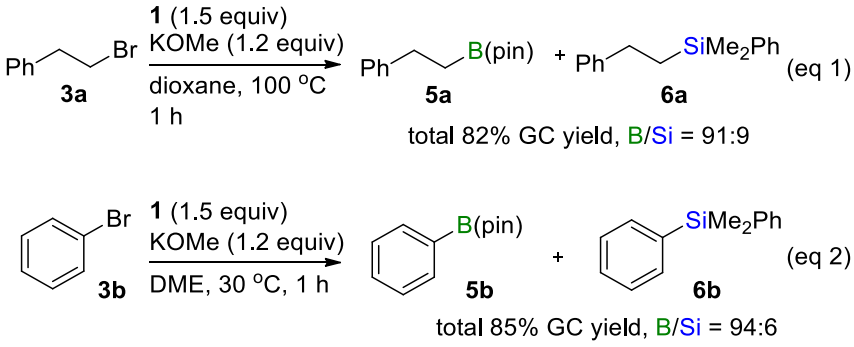

Scheme 2. Boron Substitution Reactions of Compounds **3a** and **3b** Using the BBS Method

All of the structures described in this paper were optimized at the M06-L[18a]/6-311+G(2d,p) level. It is important to mention that the energy profiles described in the current study have been discussed in terms of the Gibbs free energy in the gas phase. Furthermore, the free energy corrections used in the current study were estimated using ideal gas, rigid-rotor and harmonic approximations. Single-point calculations were made at the M06[18b]/6-311+G(3df,2p) level for all of the structures identified in the current study, and solvent effects were taken into account using the C-PCM[19] method. The main features of the energy profiles discussed below do not change between these two computational levels, and information pertaining to the latter is shown in the Supporting Information.

Case-A (R = $PhCH_2CH_2$). The current mechanism was obtained by the application of a systematic reaction path search to the case-A reaction using the AFIR method.[17] The range used in the current reaction path search is described below. An approximate upper energy barrier threshold can be specified in AFIR calculations, and the value used in the current study was set to 47.8 kcal/mol (= 200 kJ/mol). All of the atoms in the methyl and phenyl groups of the compound **1**-**3a**, as well as the potassium atom and all the atoms in the pinacolate portion of the B(pin) moiety, were set as being inactive (i.e., reactions involving bond rearrangements in these areas of the substrates were ignored). A systematic search was then conducted at a low computational level (see Computational Details), which led to the identification of numerous reaction pathways. Reaction involving E2 elimination and α-proton elimination mechanisms with compound **3a** were found but excluded without further consideration. These reactions were not seen in the experiment,[2] and were therefore considered to be unimportant to the main mechanism of the BBS method. All of the other pathways were considered at a reliable computational level, and the results are discussed below. It is important to mention that pathways for conformational changes in the inactive parts were not examined systematically.[20] Although exhaustive sampling of the conformations present in the TS is required to quantitatively predict the selectivity of a given process,[17b] this work was considered to be well beyond the scope of this study, and was therefore not conducted.

Figure 1 shows the free energy diagram (373.15 K, 1.0 atm) obtained for the case-A reaction, which involved the borylation of an sp^3 carbon. Five elementary reactions were identified during this process, including (I) the coordination of the methoxide ion (**2a'**) to the boron atom of compound **1** to give complex $[PhMe_2Si–B(pin)OMe]^-K^+$ (A2 of Figure 1); (II-a) adsorption of $PhCH_2CH_2Br$ (**3a**) to A2 giving A2'; (II-b) generation of $PhMe_2Si^-$ (**8**) and MeOB(pin) (**9**) via the cleavage of the B–Si bond (A3 of Figure 1); (III) formation of

$PhCH_2CH_2^-$ (**10a**) and $PhMe_2SiBr$ (**4**) by the reaction of **8** with $PhCH_2CH_2Br$ (**3a**), which allowed for the initial anion charge to be transferred from the silicon atom to the carbon atom (A4 of Figure 1); (IV) production of $[PhCH_2CH_2B(pin)OMe]^-K^+$ (**11a**) via the reaction of **9** with **10a** (A5 of Figure 1); and (V) removal of the methoxy group in **11a** by a nucleophilic substitution reaction to give the desired product **5a** (A6 of Figure 1). I computed both paths with and without **3a** for the reaction steps (I) and (II), and Figure 1 only shows the most feasible path in which **3a** adsorbs at the step (II-a). In the steps from A3 to A5 or A7, there are also species that do not explicitly participate in the reaction, e.g., MeOB(pin) in TS(A3/A4). However, the barriers in all these reaction steps are tiny. These steps thus proceed rapidly without waiting for dissociation of such species. On this point, a detailed discussion is made for the case B reaction in Supporting Information.

Silyl and alkyl anions bearing alkali metals as their counterions generally exhibit high levels of nucleophilicity and basicity, which can lead to the occurrence of various side reactions. However, the theoretical energy profile suggested that this was not the case in the current reaction. The silyl anion **8** in A3 was rapidly consumed by the subsequent halogenophilic attack process, which proceeded via TS(A3/A4') with a very low energy barrier of only 0.4 kcal/mol. Furthermore, significant cation-π interactions existed between the potassium cation and the phenyl group of the $PhCH_2CH_2$ moiety in the metastable intermediate A4',[21] which proceeds directly to the borylation reaction through TS(A4'/A5). The carbanion **10a** reacted with MeOB(pin) (**9**) in A4' through TS(A4'/A5), which had a very low energy barrier of only 1.2 kcal/mol. These results therefore indicated that the reactive carbanion species were short-lived intermediates that had very little chance of reacting with the other functional groups.

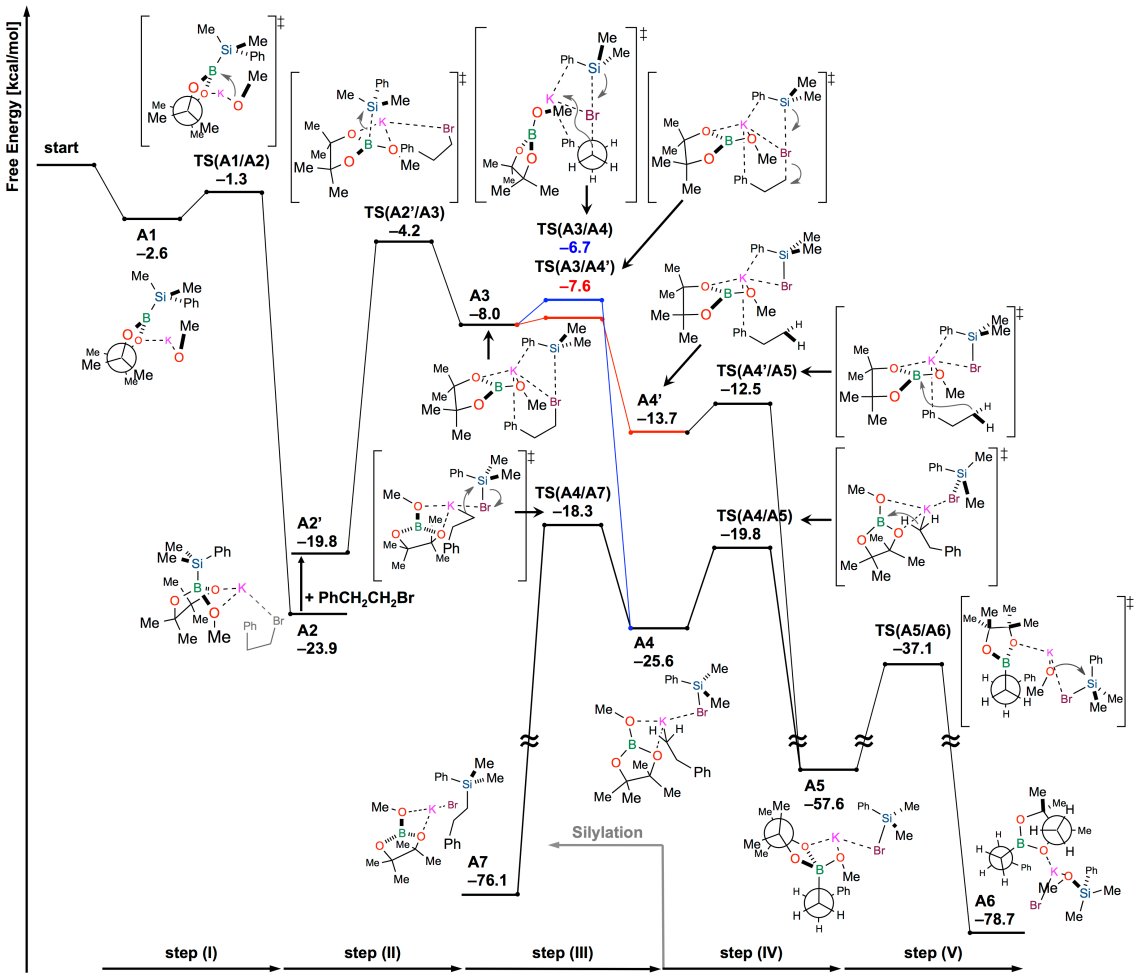

Figure 1. Reaction Pathways Leading to the Boron Product. The use of "**start**" corresponds to the reactant (i.e., **1**, **2a** and **3a**, which were separately optimized), A*n* to an intermediate complex (local minimum),[20] and TS(A*n*/A*m*) to the transition state connecting A*n* and A*m*. Gibbs free energy values (373.15 K, 1.0 atm) based on M06-L/6-311+G(2d,p) calculations relative to the "**start**" position are shown in kcal/mol. Schematic representations of the optimized structures corresponding to A*n* or TS(A*n*/A*m*) are shown in the current reaction. For steps from the "**start**" position to A2, profiles without **3a** are presented as the most reasonable path.

Although A4 can undergo both borylation and silylation reactions, the ratio for the generation of A4 and A4' from A3 was determined to be 23:77, based on the free energy gap of 0.9 kcal/mol between TS(A3/A4) and TS(A3/A4'), as well as the Boltzmann distribution at 373.15 K. The Boltzmann distribution revealed that the reaction path through TS(A3/A4) was the minor component and that A3 was mainly consumed by the borylation reaction, which

proceeded through TS(A3/A4') and TS(A4'/A5). The energy difference between TS(A4/A5) and TS(A4/A7) was determined to be 1.5 kcal/mol, and this value was used to predict the ratio for the generation of A5 and A7 from A4, which was 88:12. The borylation/silylation ratio was then calculated by combining the two ratios described above for the two different branches of the reaction, and was found to be 97:3. This ratio was therefore consistent with the experimental borylation/silylation selectivity of 91:9.[2]

In the final step, $[PhCH_2CH_2B(pin)OMe]^-K^+$ (**11a**) would react with $PhMe_2SiBr$ (**4**) in A5. Although there was a substantial energy barrier to this step, there is no need to discuss this step in greater detail because the desired product was obtained from both A5 and A6 following an aqueous quench of the reaction. Of the five different reaction steps, step (II), which involved a heterolytic B–Si bond cleavage reaction, had the highest energy barrier and was therefore considered to be the rate-determining step in this reaction.

The possibility of the silyl substitution via an S_N2 mechanism in the case-A reaction system was investigated. The combination of a silylborane species with a strong base can lead to the *in situ* production of nucleophilic silyl species.[4] With this in mind, it was envisaged that $PhMe_2Si^-$ (**8**) could react with compound **3a** via an S_N2 pathway.[2] The AFIR search identified a reaction path corresponding to this S_N2 mechanism. Two alternative S_N2 pathways leading to the formation of C–O bonds were also identified during the AFIR search and TSs for all three of these S_N2 pathways are described in Figure 2. The free energies ($\Delta G^‡$) relative to the individually optimized reactants ("**start**" in Figure 1) are shown below each TS structure together with the activation free energies ($\Delta\Delta G^‡$). The nucleophilic attack of the methoxide group through the TSs shown in Figure 2a and 2b, would require the formation of unstable TSs with high $\Delta G^‡$ values of 15.6 and 22.4 kcal/mol, respectively. The TS for the silylation, which would involve the nucleophilic attack of $PhMe_2Si^-$ (**8**) in Figure 2c was also found to be unfavorable with a $\Delta G^‡$ value of −0.1 kcal/mol, which was higher than that of the TSs shown in Figure 1. Furthermore, the activation barriers ($\Delta\Delta G^‡$) for these pathways were also high. Based on these results, the S_N2 pathways were dismissed as having a negligible impact on the outcome of the current reactions.

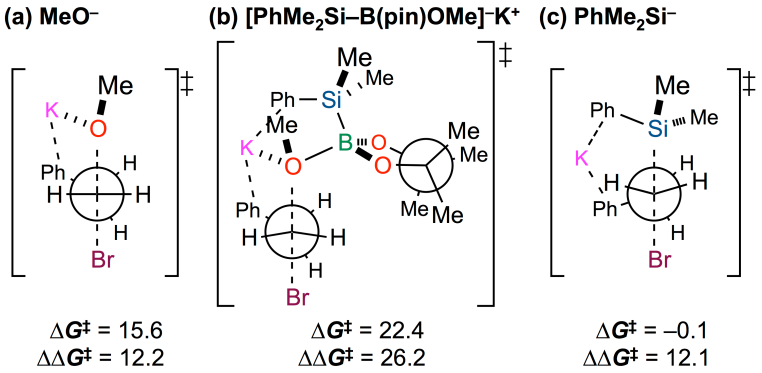

Figure 2. TS Structures, Free Energies ($\Delta G^{\ddagger}$) Relative to the Reactants (i.e., **1**, **2a** and **3a**), and Activation Free Energies ($\Delta\Delta G^{\ddagger}$) of the S_N2 Reaction Pathways. Free energy values (373.15 K, 1.0 atm) based on M06-L/6-311+G(2d,p) calculations have been given in kcal/mol. It was assumed that the molecule that did not participate in the reactions in (a) and (c) existed at an infinity distance.

Case-B (R = Ph). The free energy diagram (303.15 K, 1.0 atm) for the borylation and silylation reactions of the sp^2 carbon in the case-B reaction is shown in Figure 3. It is noteworthy that different temperatures of 373.15 and 303.15 K were used to evaluate the free-energy profiles for the case-A and case-B reactions, respectively, to allow for the results to be compared with experimental results that were obtained at the same temperatures. Figure 3 looks very similar to the diagram shown in Figure 1, in that the overall reaction is composed of five steps (i.e., steps I–V), which were discussed above for the case-A reaction. Given that the final step was considered to have very little impact on the outcome of the overall reaction, and the rate-determining step was therefore determined to be the step corresponding to the cleavage of the B–Si bond through TS(B2'/B3).

Detachment/attachment of PhBr (**3b**) at B3 is slower than the forward and backward steps. This was confirmed by evaluation of the free energy along their reaction coordinates. That is, I performed a constrained optimization fixing the distance between Br in **3b** and K in the remaining part at $R_{K–Br}$ = 6 Å and the normal-mode analysis for the projected Hessian. This gave an estimate of the free energy –3.4 kcal/mol at $R_{K–Br}$ = 6 Å. This is higher than both TS(B3/B4) and TS(B2'/B3). On the other hand, the free energy at $R_{K–Br}$ = 6 Å along the detachment/attachment coordinate of **3b** at B2' was –20.9 kcal/mol. This is much lower than TS(B2'/B3). The profile shown in Figure 2 thus is the best path concerning existence or non-existence of **3b**. Details of this analysis are described in Supporting Information, Figure S4, S6-1, and S6-2.

Decomposition of reaction complexes with dissociation of species that do not directly participate in the reaction can be a favored process. However, this is not the case in the reaction steps from B3 to B5 and B7 of the present reaction. This is because activation free energies required in these steps are all very low. In other words, these steps proceed rapidly before dissociation of such species. In order to confirm this, I calculated free energy values along dissociation coordinates of these species. For example, for the reaction complex B4, the distance $R_{K–B}$ between the K atom and the B atom in (pin)B–OMe was chosen as the dissociation coordinate of (pin)B–OMe. Then, I performed a constrained optimization fixing the distance at $R_{K–B}$ = 8 Å and the normal-mode analysis for the projected Hessian. This gave an estimate of the free energy –27.0 kcal/mol at $R_{K–B}$ = 8 Å. This is much higher than the TSs for the forward reactions, –35.3 kcal/mol for borylation and –33.9 kcal/mol for silylation. Thus, the reaction proceeds before dissociation of (pin)B–OMe. In this way, I confirmed that the reaction proceeds with the path from B3 to B5 and B7 shown in Figure 3 without dissociation of any species. Details of this analysis are described in Supporting Information, Figure S6-1.

The possibility of radical reaction pathways was checked using several calculations. Strohmann et al.[14a] suggested the existence of a radical-mediated pathway in the reaction of silyl anions with organic halides, which is mechanistically related to the BBS method,[14a] and TS(B3/B4), which involves the halogenophilic attack step, could possess some radical characters. The results of a CIS-based MO-stability-check[22] at the UM06-L/6-311+G(2d,p) level, however, indicated that TS(B3/B4) was closed-shell at the electronic ground state. Furthermore, TDDFT-based electronic excitation energy calculations for the complex composed B2 and PhBr revealed that the closed-shell electronic ground state was well separated from the first electronic excited state by 103.6 and 122.2 kcal/mol at the CAM-B3LYP[23]/6-311+G(2d,p) and LC-BLYP[24]/6-311+G(2d,p) levels, respectively. These results therefore excluded the possibility of an open-shell radical species being involved in this reaction.

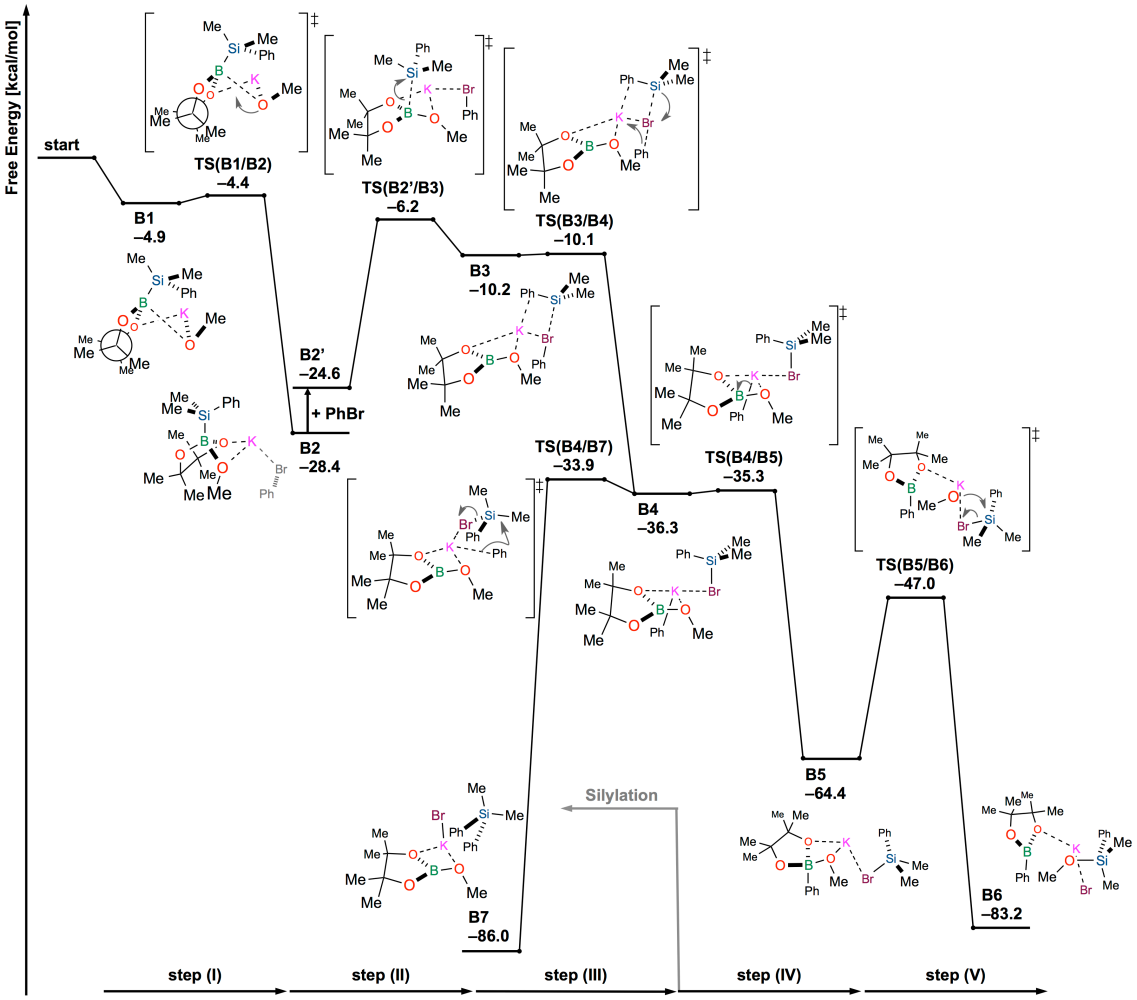

Figure 3. Reaction Pathways Leading to the B/Si Products. The use of "**start**" corresponds to the different reactants (i.e., **1**, **2a** and **3b**, which were optimized separately). B*n* refers to an intermediate complex (local minimum),[20] and TS(B*n*/B*m*) to a transition state connecting B*n* and B*m*. Gibbs free energy values (303.15 K, 1.0 atm) based on M06-L/6-311+G(2d,p) calculations relative to the "**start**" position have been presented in kcal/mol. Schematic representations of the optimized B*n* and TS(B*n*/B*m*) structures in the current reaction. For steps from the "**start**" position to B2, profiles without **3b** are presented as the most reasonable path.

A significant difference was found between the case-A and case-B pathways in terms of the complexes containing the anionic intermediates $PhCH_2CH_2^-$ and Ph^- (A4' and B4). In the case-B reaction, cleavage of the C–Br bond resulted in the formation of the stable intermediate B4 bearing a K–C bond. The interaction between the terminal C atom of the $PhCH_2CH_2^-$ anion and the potassium cation in A4' was weakened, however, by the strong interaction between the potassium cation and the Ph group, which separated the potassium cation from the terminal C

atom. The relatively strong interaction between the potassium cation and the Ph group of the $PhCH_2CH_2^-$ anion could explain why the metastable intermediate A4' was identified as a local potential energy minimum in the case-A reaction.

In a similar manner to the case-A reaction, the case-B reaction also involved two reaction pathways at B4 (i.e., borylation and silylation reactions). Experimental results showed that the borylation reaction occurred in preference to the silylation reaction. This preference can be understood in terms of the difference in the free energy values of TS(B4/B5) and TS(B4/B7), with the former being 1.4 kcal/mol lower in energy than the latter. This energy difference was very similar to the corresponding energy gap of 1.5 kcal/mol in the case-A reaction. Taken together, these results indicated that the borylation reaction was kinetically favored over the silylation reaction. Based on this free energy gap and the Boltzmann distribution, the B/Si branching ratio of the case-B reaction was estimated to be 92:8, and this ratio was consistent with the experimental borylation/silylation ratio of 94:6 from the BBS method.

Substrate and Base Dependence. I now have the major reaction path for the BBS method. Thus, it would be interesting to look energy profiles of this path for different substrates and bases. In practice, five aryl halides **3c**-**3g** and four bases **2b**-**2e** listed in Scheme 4 were considered. In the Supporting Information, all computed energy profiles are compared in Figure 3. Some trends seen in these energy profiles provided several points that can be beneficial for further optimization of the BBS method.

Ar–X	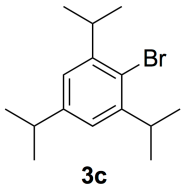 **3c**	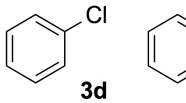 **3d**	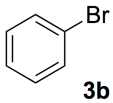 **3b**	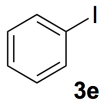 **3e**	
		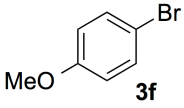 **3f**	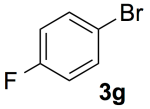 **3g**		
Base	KOMe **2a**	LiOMe **2b**	NaOMe **2c**	K(O-*t*-Bu) **2d**	Li(O-*t*-Bu) **2e**

Scheme 4. Aryl Halides and Bases Used in Discussions on the Reactivity of the BBS Method

At first, the activation energy in the halogenophilic attack on sterically hindered 2,4,6-triisopropylbromobenzene (**3c**) was investigated and found to be reasonably low ($\Delta\Delta G^{\ddagger}$ = 1.9 kcal/mol, Figure 4). TS(B2'/B3) was slightly lower than TS(B3/B4) for **3c** as shown in Figure S5-1, and the reaction thus is expected to proceed smoothly with **3c**. This is consistent

with the high reactivity of the BBS method toward sterically hindered substrates.[2]

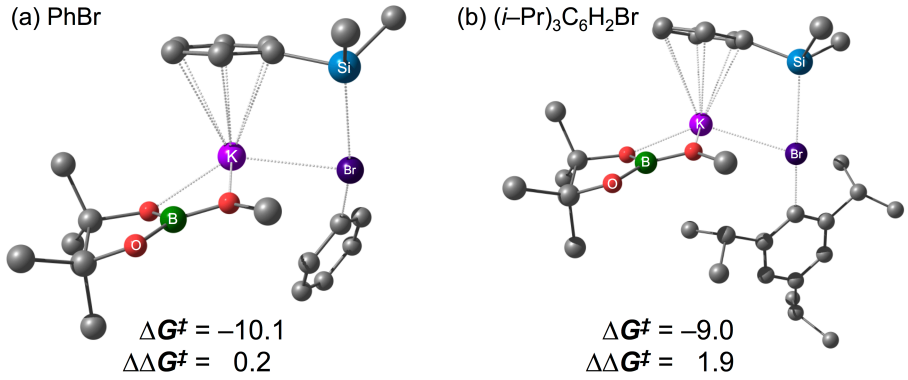

Figure 4. TS Structures, Free Energies ($\Delta G^{\ddagger}$) Relative to the Reactants (**1**, **2a** and **3b**/**3c**), and Activation Free Energies ($\Delta\Delta G^{\ddagger}$) for the Halogenophilic Attack Reaction Steps. Free energy values (303.15 K, 1.0 atm) based on M06-L/6-311+G(2d,p) calculations are given in kcal/mol.

Second, the halide effect [PhBr (**3b**) vs. PhCl (**3d**) vs. PhI (**3e**)] and substitution effect of *para*-position [PhBr (**3b**) vs. *p*-MeO–C_6H_4Br (**3f**) vs. *p*-F–C_6H_4Br (**3g**)] were investigated theoretically (See Supporting Information: Figures S5-2, S5-4, S6-2, and S6-3 for energy profiles.) Experimentally, it was shown that the reactivity increases as **3e** > **3b** > **3d** and **3g** > **3b** > **3f**.[26] These experiments also showed that reactions of different substrates are in competition when two substrates are combined together.[26] Consistently, $\Delta G^{\ddagger}$ at the rate determining TS(B2'/B3) are very close to each other for these substrates; $\Delta G^{\ddagger}$ at TS(B2'/B3) are 7.5, 8.7, 7.3, 6.9, and 7.2 kcal/mol for **3b**, **3d**, **3e**, **3f**, and **3g**, respectively, in our best estimate with inclusion of the solvent effect by C-PCM. These values reproduce the experimental reactivity trends qualitatively; only the $\Delta G^{\ddagger}$ for **3f** showed deviation from the experimental trend. Nevertheless, these <1 kcal/mol energy differences are too small to be discussed with the present computational level. Moreover, the computational trend changed by inclusion of the solvent effect with C-PCM (See Supporting Information). The more accurate treatment with the more accurate *ab initio* theory and explicit consideration of movements of surrounding solvent molecules is required for further quantitative predictions.

Thirdly, the impact of the base is investigated. It was reported that KOMe (**2a**) gave the borylation and minor silylation products of *p*-MeO–C_6H_4Br (**3f**) in 92% yield with high B/Si ratio (95:5). The reaction with NaOMe (**2c**) resulted in 81% yield (**5b**+**6b**) with a B/Si ratio of 80:20. It was also found that the borylation of PhBr (**3b**) with K(O-*t*-Bu) (**2d**), and Li(O-*t*-Bu)

(**2e**) as the base gave moderate to high yield and B/Si selectivity [66% yield (**5b**+**6b**), B/Si = 73:27, 94% yield (**5b**+**6b**), B/Si = 85:15, respectively] under previously reported reaction conditions.[2, 26] Theoretical results showed that all the bases shown in Scheme 4 provide low $\Delta\Delta G^{\ddagger}$ values enough to promote the borylation reaction. However, it is difficult to fully elucidate the reactivity and selectivity trends of the experimental results. This is probably because of the solubility difference of the bases.[26] KOMe (**2a**), LiOMe (**2b**), and NaOMe (**2c**) are only partially soluble in dimethoxyethane, whereas K(O-*t*-Bu) (**2d**) and Li(O-*t*-Bu) (**2e**) are fairly soluble in the solvent. It is noted that the reaction of LiOMe (**2b**) afforded no borylation/silylation products in the experiment, although the theoretical results for LiOMe indicate its moderate reactivity. This inconsistency is attributable to the very slow Si–B bond cleavage in the real LiOMe reaction system because of the extremely low solubility of LiOMe in the reaction medium and relatively higher $\Delta\Delta G^{\ddagger}$ value at the Si–B bond cleavage step (B2' → B3) (For details, see Supporting Information). Furthermore, in this study, I just optimized TSs obtained for the reaction with **2a** after substituting the corresponding metal atom without further conformational analysis. The B/Si selectivity would be determined by a subtle energy gap between the silylation TS and the borylation TS, and its quantitative prediction further requires an extensive conformational sampling. Such an analysis for quantitative discussions of the B/Si selectivity will be a future subject.

Discussion

The pathways computed in the current study for the case-A and case-B reactions provide adequate explanations of many of the characteristic features of the BBS method. The BBS method was initially highlighted for its good functional group compatibility and high reactivity toward sterically hindered substrates.[2] In the reaction profiles shown in Figures 1 and 3, the step involving the cleavage of the Si–B bond through TS($A_{or}B2'/A_{or}B3$) was identified as the rate-determining step. The reaction proceeded rapidly beyond this point, with unstable intermediates such as the silyl anion and carbanion species being immediately consumed with very low energy barriers (see the steps from $A_{or}B3$ to $A_{or}B5$ in Figures 1 and 3). This result indicated that all of these intermediates almost exclusively underwent the borylation reaction, even when they contained other reactive functional groups. Furthermore, the structures of the TSs involved in these steps provide some rationale for the high borylation reactivity observed in the BBS method towards sterically hindered aryl bromides. The TS(B3/B4) structure shows that the steric hindrance provided by the substrate would be too far removed from the reactive σ*(C–Br) orbital to have a noticeable impact on the reactivity whereas catalysts usually interacts the carbon and bromo atoms in the C–Br bond directly in the transition-metal-catalyzed boryl substitution of aryl bromides. Actually, a bulky substrate **3c** showed a reasonable potential profile with low barriers.

The BBS method proceeded to give a product with counterintuitive borylation reaction, as well as a small amount of the silylation product (5–10%).[2] This distribution of products suggests that these two channels are competing with each other, and that the energy barrier for the borylation reaction must be slightly lower than that of the silylation reaction by a few kcal/mol. This feature of the BBS method was effectively reproduced in the current reaction profiles. Furthermore, the results of simple thermodynamic analyses on the basis of their free energy barriers and Boltzmann distributions predicted that the borylation/silylation ratios of the case-A and case-B reactions to be 97:3 and 92:8, respectively. These ratios were qualitatively consistent with the experimental ratios of 91:9 and 94:6. The energy profiles for these reactions showed that all of the borylation/silylation TSs existed along favorable pathways [i.e., TS(A4'/A5), TS(A4/A5), TS(A4/A7), TS(B4/B5), and TS(B4/B7)], with energy barriers in the range of 1–7 kcal/mol. These low energy barriers were attributed to the carbanion species, $PhCH_2CH_2^-$ and Ph^-, which are highly reactive intermediates that can react spontaneously with B or Si. The B/Si selectivities observed in these reactions can therefore be understood in terms of the

effectiveness of their inter-orbital attraction between the Ph^- and B/Si species. The selectivity of an organic transformation can be understood and controlled in terms of the hard and soft acids and bases principle. With this in mind, the sp^3/sp^2 hybrid orbital of $PhCH_2CH_2^-/Ph^-$ would better overlap much more effectively with the empty 2p orbital of the MeOB(pin) moiety than the σ*(Si–Br) orbital of the $PhMe_2SiBr$ moiety. This would explain why carbanions prefer to react with B rather than Si.

These findings provide strong support for the proposed mechanism shown in Scheme 1.[2] Furthermore, the application of the current AFIR search to the case-A reaction allowed for the contributions from many other possible pathways to be eliminated in a systematic way, which provided further evidence in support of the validity of this mechanism. Although the mechanism shown in Scheme 1 may look unusual, in the sense that it involves highly reactive intermediates derived from silyl anion and carbanion species, it is important to realize that all of the theoretical and experimental results of the current study are consistent with this mechanism.

.

Conclusion

A theoretical investigation of the BBS reaction has been conducted using the AFIR method. The resulting complete reaction pathway for the BBS method was shown to involve the halogenophilic attack of a silyl anion on the bromine atom of the substrate and the rapid and selective consumption of a resulting carbanion species by a boron electrophile. These calculations provided a rational explanation for the counterintuitive borylation reactivity, as well as accounting for the good functional group compatibility of the reaction and its high reactivity toward sterically hindered substrates. The use of the AFIR method in the current study not only provided a complete reaction pathway but also demonstrated the validity of the proposed reaction mechanism by comprehensively accounting for the other reaction mechanisms. It is hoped that this novel mechanism will allow us to expand our knowledge and understanding of silicon and boron chemistry.

Computational Details

For the case-A reaction, reaction pathways involving the conversion of the reactants (i.e., **1**, **2a** and **3a**) to the major products and byproducts were searched systematically at the B3LYP[27] level with small basis sets (STO-3G for all of the methyl and phenyl groups, and 6-31G for all

of the other groups) using the AFIR method. It is necessary to determine an upper threshold for the energy barrier when the AFIR method is being used to conduct a systematic reaction pathway search. The upper threshold used in the current study was set to 47.8 kcal/mol (= 200 kJ/mol) for the initial searches. These searches can be performed efficiently by choosing the reactive sites appropriately. Three reactive sites were defined in reactants for the case-A reaction, including (i) the ethylene moiety and Br atom in $PhCH_2CH_2Br$; (ii) the B and Si atoms in $PhMe_2Si$–B(pin); and (iii) the O atom in potassium methoxide. These settings were employed consistently in all of the reaction steps. The AFIR method gives many approximate reaction pathways called AFIR paths as minimization pathways of the AFIR function.[16] The AFIR paths at the low computational level were subsequently optimized using a conventional path optimization method known as the locally updated planes[28] (LUP) method at the M06-L/6-311+G(d) level. Because the AFIR path can provide a good estimate of the minimum energy path, LUP calculations converge quickly and only five LUP iterations were considered. Peaks along the LUP paths were then optimized to the true TSs at the M06-L/6-311+G(d) level. Important pathways were further optimized at the M06-L/6-311+G(2d,p) level, and free energy corrections in the gas phase were estimated by assuming ideal gas, rigid-rotor and harmonic approximations. The natural population analysis was performed at the M06-L/6-311+G(2d,p) level. TSs for the case-B reaction were optimized using important TSs obtained from the case-A reaction by substituting the $PhCH_2CH_2$ group for a Ph group. Moreover, for discussions of the substrate and base dependences, these TSs were further optimized at the same computational level with different substrates and bases, where, only for I atom, the Stuttgard ECP46MDF[29] effective core potential and corresponding basis set were applied. All of the DFT calculations were performed with the Gaussian 09 programs.[30] Automated searches as well as geometry optimizations were performed using a developmental version of the GRRM program with the DFT gradients and Hessians.[31]

Single point calculations were performed at the M06/6-311+G(3df,2p) level for all of the local minima and TSs shown in Figures 1 and 3, and TS(B2'/B3) shown in Figure S5-2 and S5-4. These solvent effects were considered using the C-PCM method.[19] 1,4-Dioxane was selected in the C-PCM calculations because it was the experimentally optimized solvent in the case-A reaction. THF was selected as the solvent for the case-B reaction in the C-PCM calculations because the C-PCM parameters for THF were available in Gaussian 09. Furthermore, experimental results have demonstrated that THF exhibits similar reactivity and

selectivity properties to dimethoxyethane, which was employed as the optimized solvent in the experiment. Gas-phase free energy corrections were conducted at the M06-L/6-311+G(2d,p) level and added to the C-PCM single-point energies at the M06/6-311+G(3df,2p) level to allow for the free energy values to be estimated. In the case-A and case-B reactions, the free energy profiles from $A_{or}B2$ to $A_{or}B5$ in the C-PCM-solvents did not differ significantly from those in the gas-phase calculations. Most notably, the reaction steps following TS($A_{or}B2$/$A_{or}B3$) to $A_{or}B5$ possessed negligible barriers, which remained unchanged regardless of any solvent effects. The free energy profiles in the C-PCM-solvents are shown in the Supporting Information.

References

1. (a) Miyaura, N.; Suzuki, A. *Chem. Rev*. **1995**, *95*, 2457-2483. (b) Boronic Acids: Preparation and Applications in Organic Synthesis, Medicine and Materials, 2nd ed.; Hall, D. G., Ed.; Wiley-VCH: Weinheim, Germany, 2011.
2. Yamamoto, E.; Izumi, K.; Horita, Y.; Ito, H. *J. Am. Chem. Soc.* **2012**, *134*, 19997-20000.
3. (a) Nishikata, T.; Yamamoto, Y.; Miyaura, N. *Organometalics* **2004**, *23*, 4317–4324. (b) Nakao, Y.; Hiyama, T. *Chem. Soc. Rev.* **2011**, *40*, 4893–4901. (c) Wilf, P. *Synthesis* **1993**, *6*, 527–557.
4. (a) O'Brien, J. M.; Hoveyda, A. H. *J. Am. Chem. Soc.* **2011**, *133*, 7712-7715. (b) Ito, H.; Horita, Y.; Yamamoto, E. *Chem. Commun.* **2012**, *48*, 8006-8008. (c) Kawachi, A.; Minamimoto, T.; Tamao, K. *Chem. Lett.* **2001**, 1216-1217. (d) Hata, T.; Kitagawa, H.; Masai, H.; Kurahashi, T.; Shimizu, M.; Hiyama, T. *Angew. Chem., Int. Ed.* **2001**, 40, 790-792. (e) Borner, C.; Kleeberg, C. *Eur. J. Inorg. Chem.* **2014**, 2486-2489.
5. Organic Chemistry, 2nd ed.; Clayden, J.; Greeves, N.; Warren, S.; Oxford University Press, 2012.
6. Oestreich, M.; Hartmann, E.; Mewald, M. *Chem. Rev.* **2013**, *113*, 402-441.
7. (a) Brown, H. C.; Cole, T. E. *Organometallics* **1983**, *2*, 1316-1319. (b) Brown, H. C.; Srebnik, M.; Cole, T. E. *Organometallics* **1986**, *5*, 2300-2303. (c) Baron, O.; Knochel, P. *Angew. Chem., Int. Ed.* **2005**, *44*, 3133-3135. (d) Clary, J. W.; Rettenmaier, T. J.; Snelling, R.; Bryks, W.; Banwell, J.; Wipke, W. T.; Singaram, B. *J. Org. Chem.* **2011**, *76*, 9602-9610. (e) Pintaric, C.; Olivero, S.; Gimbert, Y.; Chavant, P. Y.; Duñach, E. *J. Am. Chem. Soc.* **2010**, *132*, 11825-11827.

8. For recent reviews of transition-metal-catalyzed borylation of aryl halides, see: (a) Chow, W. K.; Yuen, O. Y.; Choy, P. Y.; So, C. M.; Lau, C. P.; Wong, W. T.; Kwong, F. Y. *RSC Adv.* **2013**, *3*, 12518-12539. (b) Primas, N.; Bouillon, A.; Rault, S. *Tetrahedron*, **2010**, *66*, 8121-8136. (c) Ishiyama, T.; Miyaura, N. *Chem. Rec.* **2004**, *3*, 271-280.

9. For selected recent papers of transition-metal-catalyzed borylation of aryl halides, see: (a) Ishiyama, T.; Murata, M.; Miyaura, N. *J. Org. Chem.* **1995**, *60*, 7508-7510. (b) Ito, H.; Kubota, K. *Org. Lett.* **2012**, *14*, 890-893. (c) Kubota, K.; Yamamoto, E.; Ito, H. *J. Am. Chem. Soc.* **2013**, *135*, 2635-2640. (d) Bose, S. K.; Fucke, K.; Liu, L.; Steel, P. G.; Marder, T. B. *Angew. Chem., Int. Ed.* **2014**, *53*, 1799-1803. (e) Dudnik, A. S.; Fu, G. C. *J. Am. Chem. Soc.* **2012**, *134*, 10693-10697. (f) Yi, J.; Liu, J.-H.; Dai, J.-J.; Yang, C.-T.; Fu, Y.; Liu, L. *Adv. Synth. Catal.* **2012**, *354*, 1685-1691. (g) Murata, M.; Watanabe, S.; Masuda, Y. *Tetrahedron Lett*. **2000**, *41*, 5877-5880. (h) Zhang, P.; Roundtree, I, A.; Morken, J. P. *Org. Lett.* **2012**, *14*, 1416-1419. (i) Nagashima, Y.; Takita, R.; Yoshida, K.; Hirano, K.; Uchiyama, M. *J. Am. Chem. Soc.* **2013**, *135*, 18730-18733. (j) Kleeberg, C.; Dang, L.; Lin, Z.; Marder, T. B. *Angew. Chem., Int. Ed.* **2009**, *48*, 5350-5354.

10. For recent reviews of transition-metal-catalyzed C–H borylation, see: (a) Hartwig, J. F. *Acc. Chem. Res.* **2012**, *45*, 864-873. (b) Mkhalid, I. A. I.; Barnard, J. H.; Marder, T. B.; Murphy, J. M.; Hartwig, J. F. *Chem. Rev.* **2010**, *110*, 890-931.

11. Rosso, V. W.; Lust, D. A.; Bernot, P. J.; Grosso, J. A.; Modi, S. P.; Rusowics, A.; Sedergran, T. C.; Simpson, J. H.; Srivastava, S. K.; Humora, M. J.; Anderson, N. G. *Org. Process Res. Dev.* **1997**, *1*, 311-314.

12. Studies on metal-halogen exchange mechanism concerning halogenophilic attack of boryl nucleophiles, see: Cheung, M. S.; Marder, T. B.; Lin, Z. *Organometallics* **2011**, *30*, 3018-3028.

13. Related halogen-metal exchange reactions, see; (a) Mori, M.; Kaneta, N.; Isono,N.; Shibasaki, M. *Tetrahedron Lett.* **1991**, *32*, 6139-6142. (b) Ando, K. *J. Org. Chem.* **2006**, *71*, 1837-1850. (c) Beak, P.; Allen, D. J. *J. Am. Chem. Soc.* **1992**, *114*, 3420-3425. (d) Harada, T.; Katsuhira, T.; Oku, A. *J. Org. Chem.* **1992**, *57*, 5805-5807. (e) Farnham, W. B.; Calabrese, J. C. *J. Am. Chem. Soc.* **1986**, *108*, 2449-2451. (f) Rogers, H. R.; Houk, J. *J. Am. Chem. Soc.* **1982**, *104*, 522-525. (g) Winkler, H. J. S.; Winkler, H. *J. Am. Chem. Soc.* **1966**, *88*, 969-974. (h) Winkler, H. J. S.; Winkler, H. *J. Am. Chem. Soc.* **1966**, *88*, 964-969.

14. (a) Däschlein, C.; Bauer, S. O.; Strohmann, C. *Eur. J. Inorg. Chem.* **2011**, 1454-1465. (b)

Strohmann. C.; Bindl, M.; Fraaß, V. C.; Hörnig, J. *Angew., Chem., Int. Ed.* 2004, 43, 1011-1014.

15. For recent examples of computational study of transition-metal-catalyzed boryl substitution of haloarenes and arene C–H borylation, see: (a) Liu, B.; Gao, M.; Dang, L.; Zhao, H.; Marder, T. B.; Lin, Z. *Organometallics* **2012**, *31*, 3410-3425. (b) Dang, L.; Lin, Z.; Marder, T. B. *Organometallics* **2010**, *29*, 917-927. (c) Zhao, H.; Dang, L.; Marder, T. B.; Lin, Z. *J. Am. Chem. Soc.* **2008**, *130*, 5586-5594. (d) Abe, Y.; Kuramoto, K.; Ehara, M.; Nakatsuji, H.; Suginome, M.; Murakami, M.; Ito, Y. *Organometallics* **2008**, *27*, 1736-1742. (e) Dang, L.; Lin, Z.; Marder, T. B. *Organometallics* **2008**, *27*, 4443-4454. (f) Dang, L.; Zhao, H.; Lin, Z. *Organometallics* **2008**, *27*, 1178-1186. (g) Dang, L.; Zhao, H.; Lin, Z.; Marder, T. D. *Organometallics* **2007**, *26*, 2824-2832. (h) Lam, K. C.; Lin, Z.; Marder, T. B. *Organometallics* **2007**, *26*, 3149-3156. (i) Zhao, H.; Lin, Z.; Marder, T. B. *J. Am. Chem. Soc.* **2006**, *128*, 15637-15643. (j) Hartwig, J. F.; Cock, K. S.; Hapke, M.; Incarvito, C. D.; Fan, Y.; Webster, C. E.; Hall, M. B. *J. Am. Chem. Soc.* **2005**, *127*, 2538-2552. (k) Lam, W. H.; Lam, K. C.; Lin, Z.; Shimada, S.; Perutz, R. N.; Marder, T. B. *Dalton Trans*. **2004**, 1556-1562. (l) Sumimoto, M.; Iwane, N.; Takahama, T.; Sakaki, S. *J. Am. Chem. Soc.* **2004**, *126*, 10457-10471. (m) Webster, C. E.; Fan, Y.; Hall, M. B.; Kunz, D.; Hartwig, J. F. *J. Am. Chem. Soc.* **2003**, *125*, 858-859. (n) Tamura, H.; Yamazaki, H.; Sato, H.; Sakaki, S. *J. Am. Chem. Soc.* **2003**, *125*, 16114-16126. (o) Lam, W. L.; Lin, Z. *Organometallics* **2003**, *22*, 473-480. (p) Wan, X.; Wang, X.; Luo, Y.; Takami, S.; Kubo, M.; Miyamoto, A. *Organometallics* **2002**, *21*, 3703-3708. (q) Green, A. G.; Liu, P.; Merlic, C. A.; Houk, K. N. *J. Am. Chem. Soc.* **2014**, *136*, 4575-4583. (r) Vanchura, II, B. A.; Preshlock, S. M.; Roosen, P. C.; Kallepalli, V. A.; Staples, R. J.; Maleczka, Jr., R. E.; Singleton, D. A.; Smith, III, M. R. *Chem. Commun.* **2010**, *46*, 7724-7726. and reference 8j.

16. (a) Maeda, S.; Morokuma, K. *J. Chem. Phys.* **2010**, *132*, 241102-241104. (b) Maeda, S.; Morokuma, K. *J. Chem. Theory Comput.* **2011**, *7*, 2335-2345. (c) Maeda, S.; Ohno, K.; Morokuma, K. *Phys. Chem. Chem. Phys*. **2013**, *15*, 3683-3701. (d) Maeda, S.; Taketsugu, T.; Morokuma, K. *J. Comput. Chem.* **2014**, *35*, 166-173.

17. For recent examples of computational study of unknown organic synthesis reaction mechanisms by the AFIR method, see: (a) Maeda, S.; Komagawa, S.; Uchiyama, M.; Morokuma, K. *Angew. Chem.,* **2011**, *123*, 670-675; *Angew. Chem., Int. Ed.* **2011**, *50*, 644-649. (b) Hatanaka, M.; Maeda, S.; Morokuma, K. *J. Chem. Theory Comput.* **2013**, *9*,

2882-2886. (c) Hatanaka, M.; Morokuma, K. *J. Am. Chem. Soc.* **2013**, *135*, 13972-13979. (d) Uematsu, R.; Maeda, S.; Taketsugu, T. *Chem. Asian J.* **2014**, *9*, 305-312.

18. (a) Zhao, Y.; Truhlar, D. G. *J. Chem. Phys.* **2008**, *125*, 194101-194118. (b) Zhao, Y.; Truhlar, D. G. *Theor. Chem. Acc.* **2008**, *120*, 215-241.
19. (a) Cossi, M.; Rega, N.; Scalmani, G.; Barone, V. *J. Comp. Chem*. **2003**, *24*, 669-681. (b) Barone, V.; Cossi, M. *J. Phys. Chem. A*, **1998**, *102*, 1995-2001.
20. In this study, TSs for conformational rearrangements at local minimums were not searched. In case a conformation in a local minimum obtained by the IRC calculation in the last step differs from the one for the starting point of the next step, relative free energy for the lower energy conformation is shown in the free energy profiles. This treatment assumes that such a conformational rearrangement in local minimums occurs easily. In many cases, for qualitative discussions this assumption is not inappropriate. Actually, the present free energy profiles explains experimental findings well.
21. About cation-π interaction, see: (a) Kumpf, R. A.; Dougherty, D. A. *Science*, **1993**, *261*, 1708-1710. (b) Dougherty, D. A. *Science*, **1996**, *271*, 163-168. (c) Cabarcos, O. M.; Weinheimer, C. J.; Lisy, J. M. *J. Chem. Phys.* **1999**, *110*, 8429-8435. (d) De Wall, S. L.; Barbour, L. J.; Gokel, G. W. *J. Am. Chem. Soc.* **1999**, *121*, 8405-8406. (e) Fukin, G. K.; Lindeman, S. V.; Kochi, J. K. *J. Am. Chem. Soc.* **2002**, *124*, 8329-8336. (f) Forbes, G. C.; Kennedy, A. R.; Mulvey, R. E.; Roberts, B. A.; Rowlings, R. B. *Organometallics* **2002**, *21*, 5115-5121. (g) Lau, J. K-C.; Wong, C. H. S.; Ng, P. S.; Siu, F. M.; Ma, N. L.; Tsang, C. W. *Chem. Eur. J.* **2003**, *9*, 3383-3396. (h) Siu, F. M.; Ma, N. L.; Tsung, C. W. *Chem. Eur. J.* **2004**, *10*, 1966-1976. (i) Ruan, C.; Rodgers, M. T. *J. Am. Chem. Soc.* **2004**, *126*, 14600-14610. (j) Ilkhechi, A. H.; Mercero, J. M.; Silanes, I.; Bolte, M.; Scheibitz, M.; Lerner, H-W.; Ugalde, J. M.; Wargner, M. *J. Am. Chem. Soc.* **2005**, *127*, 10656-10666. (k) Åhman, A.; Nissinen, M. *Chem. Commum.* **2006**, 1209-1211. (l) Davidson, M. G.; Garcia-Vivo, D.; Kennedy, A. R.; Mulvey, R. E.; Robertson, S. D. *Chem. Eur. J.* **2011**, *17*, 3364-3369. (m) Armstrong, D. R.; Brammer, E.; Cadenbach, T.; Hevia, E.; Kennedy, A. R. *Organometallics* **2013**, *32*, 480-489.
22. (a) Seeger, R.; Pople, J. A. *J. Chem. Phys.* **1977**, *66*, 3045-3050. (b) Bauernschmitt, R.; Ahlrichs, R. *J. Chem. Phys.* **1996**, *104*, 9047-9052.
23. Yanai, T.; Tew, D.; Handy, N. *Chem. Phys. Lett.* **2004**, *393*, 51-57.
24. Iikura, H.; Tsuneda, T.; Yanai, T.; Hirao, K. *J. Chem. Phys.* **2001**, *115*, 3540-3544.
25. Hudrlik, P. F.; Hudrlik, A. M.; Jeilani, Y. a. *Tetrahedron* **2011**, *67*, 10089-10096.

26. Yamamoto, E; Ito, H. private communication.
27. Becke, A. D. *J. Chem. Phys.* **1993**, *107*, 8554-8560.
28. Choi, C.; Elber, R. *J. Chem. Phys*. **1991**, *94*, 751-760.
29. Stoll, H.; Metz, B.; Dolg, M. *J. Comput. Chem.* **2002**, *23*, 767–778.
30. Frisch, M. J.; Trucks, G. W.; Schlegel, H. B. et al. Gaussian 09, Revision B. 01; Gaussian, Inc.; Wallingford, CT, 2009.
31. Maeda, S.; Osada, Y.; Morokuma, K.; Ohno, K. GRRM, a developmental version at Hokkaido University.

Supporting Information

S1. Full References for Gaussian 09

Frisch, M. J.; Trucks, G. W.; Schlegel, H. B.; Scuseria, G. E.; Robb, M. A.; Cheeseman, J. R.; Scalmani, G.; Barone, V.; Mennucci,B.; Petersson, G. A.; Nakatsuji, H.; Caricato, M.; Li, X.; Hratchian, H. P.; Izmaylov, A. F.; Bloino, J.; Zheng, G.; Sonnenberg, J. L.; Hada, M.; Ehara, M.; Toyota, K.; Fukuda, R.; Hasegawa, J.; Ishida, M.; Nakajima, T.; Honda, Y.; Kitao, O.; Nakai, H.; Vreven, T.; Montgomery, J. A., Jr.; Peralta, J. E.; Ogliaro, F.; Bearpark, M.; Heyd, J. J.; Brothers, E.; Kudin, K. N.; Staroverov, V. N.; Kobayashi, R.; Normand, J.; Raghavachari, K.; Rendell, A.; Burant, J. C.; Iyengar, S. S.; Tomasi, J.; Cossi, M.; Rega, N.; Millam, N. J.; Klene, M.; Knox, J. E.; Cross, J. B.; Bakken, V.; Adamo, C.; Jaramillo, J.; Gomperts, R.; Stratmann, R. E.; Yazyev, O.; Austin, A. J.; Cammi, R.; Pomelli, C.; Ochterski, J. W.; Martin, R. L.; Morokuma, K.; Zakrzewski, V. G.; Voth, G. A.; Salvador, P.; Dannenberg, J. J.; Dapprich, S.; Daniels, A. D.; Farkas, Ö.; Foresman, J. B.; Ortiz, J. V.; Cioslowski, J.; Fox, D. J. Gaussian 09, Revision B.01; Gaussian, Inc.: Wallingford, CT, 2009.

S2. Energy Profiles Including Solvent Effects Estimated by C-PCM

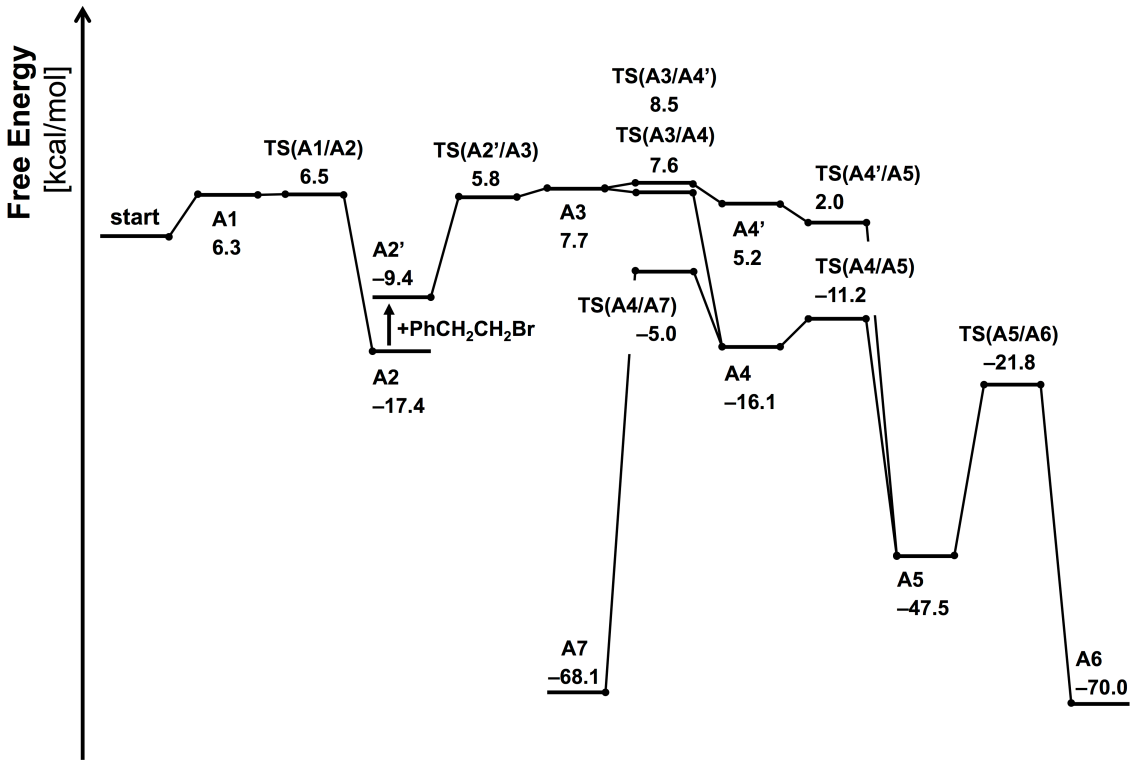

Figure S2-1. Reaction Pathways Leading to the B/Si Products for **3a**

The use of "**start**" corresponds to the reactant (i.e., **1**, **2a** and **3a**, which were separately optimized), A*n* to an intermediate complex (local minimum), and TS(A*n*/A*m*) to the transition state connecting A*n* and A*m*. Single-point energies based on M06/6-311+G(3df,2p) calculations with the C-PCM-dioxane solvent plus Gibbs free energy corrections in gas phase (373.15 K, 1.0 atm) at the M06-L/6-311+G(2d,p) level relative to the "**start**" position are shown in kcal/mol. From the "**start**" position to A2, $PhCH_2CH_2Br$ (**3a**) does not explicitly participate the reaction (see Figure S4-1).

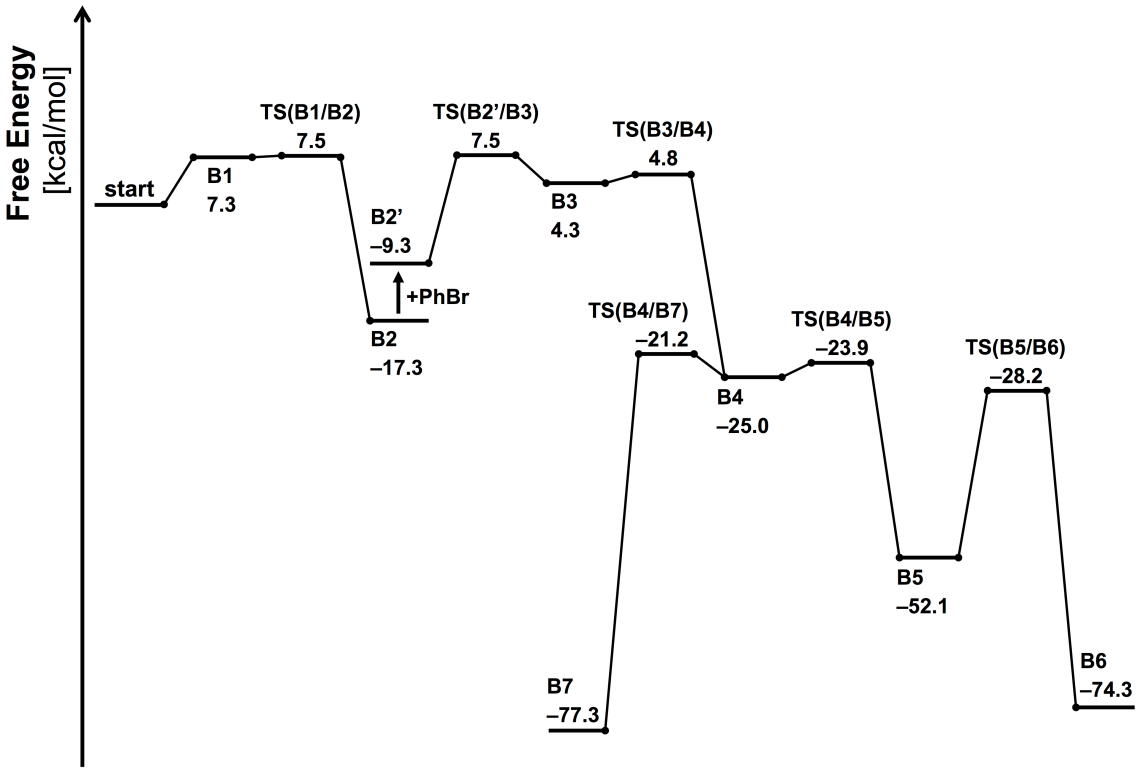

Figure S2-2. Reaction Pathways Leading to the B/Si Products for **3b**

The use of "**start**" corresponds to the reactant (**1**, **2a** and **3b**, which were separately optimized), B*n* to an intermediate complex (local minimum), and TS(B*n*/B*m*) to the transition state connecting B*n* and B*m*. Single-point energies based on M06/6-311+G(3df,2p) calculations with the C-PCM-THF solvent plus Gibbs free energy corrections in gas phase (303.15 K, 1.0 atm) at the M06-L/6-311+G(2d,p) level relative to the "**start**" position are shown in kcal/mol. From the "**start**" position to B2, PhBr (**3b**) does not explicitly participate the reaction (see Figure S4-2).

S3. Energy Profiles in terms of Electronic Energy + Zero Point Vibration Energy

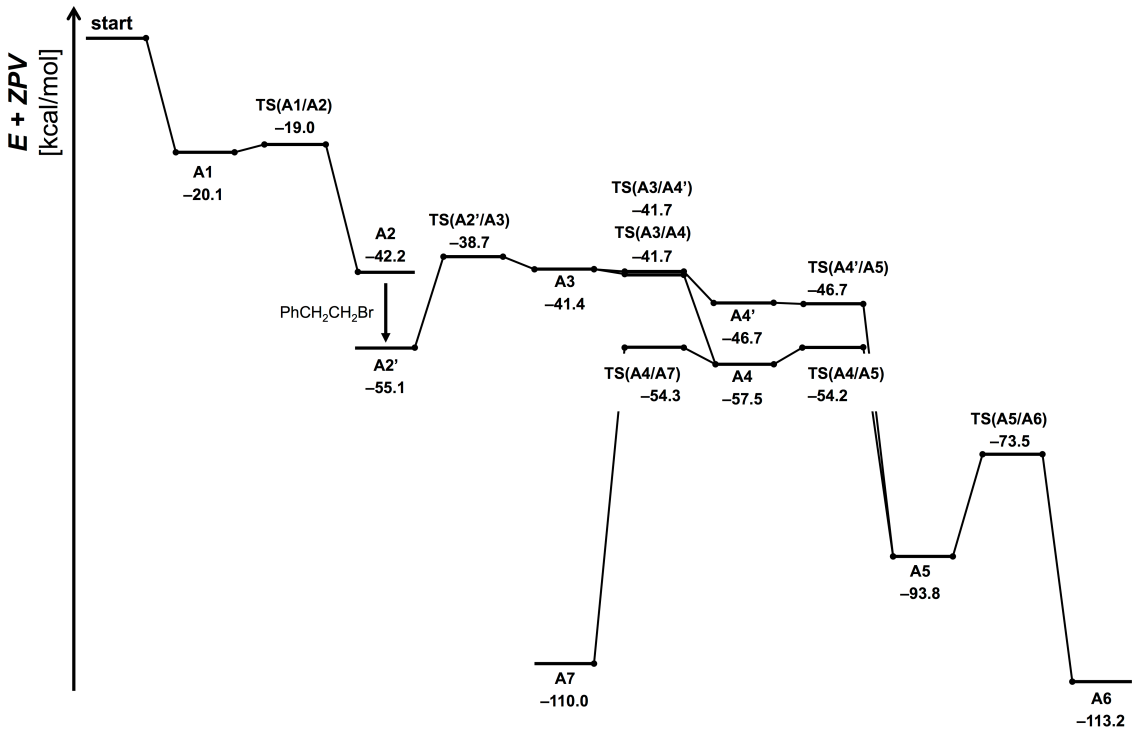

Figure S3-1. Reaction Pathways Leading to the B/Si Products for **3a**

The use of "**start**" corresponds to the reactant (**1**, **2a** and **3a**, which were separately optimized), A*n* to an intermediate complex (local minimum), and TS(A*n*/A*m*) to the transition state connecting A*n* and A*m*. Electronic energies plus zero-point vibration energy values based on M06-L/6-311+G(2d,p) calculations relative to the "**start**" position are shown in kcal/mol. From the "**start**" position to A2, $PhCH_2CH_2Br$ (**3a**) does not explicitly participate the reaction (see Figure S4-1).

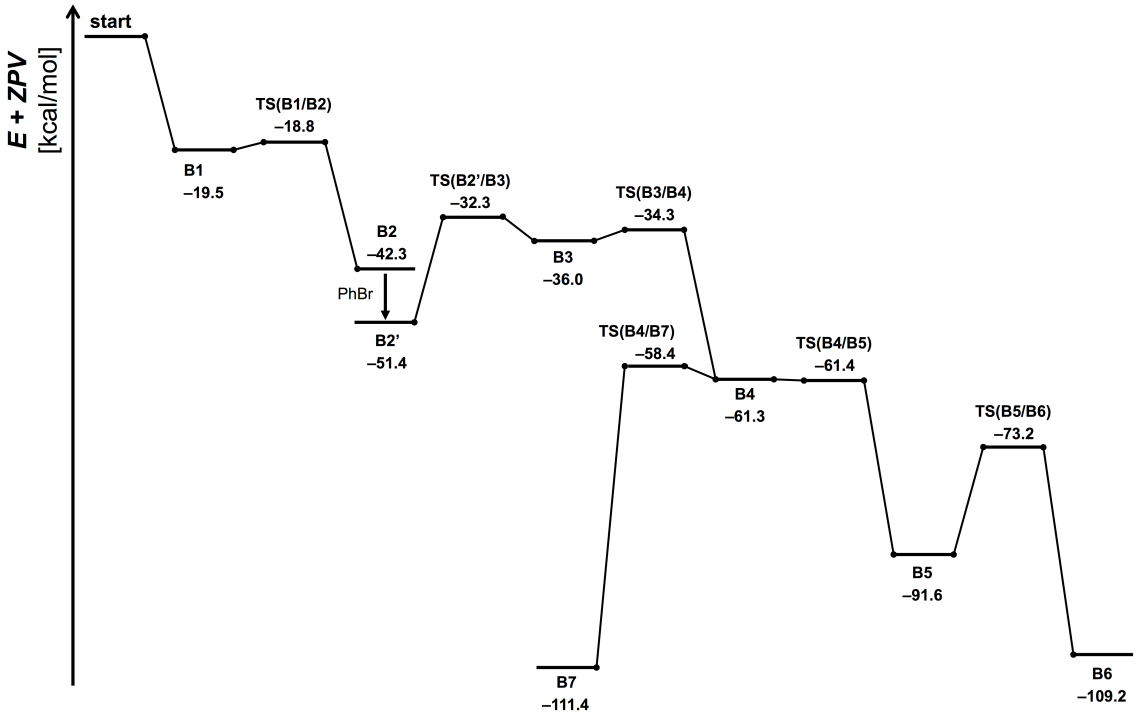

Figure S3-2. Reaction Pathways Leading to the B/Si Products for **3b**

The use of "**start**" corresponds to the reactant (**1**, **2a** and **3b**, which were separately optimized), B*n* to an intermediate complex (local minimum), and TS(B*n*/B*m*) to the transition state connecting B*n* and B*m*. Electronic energies plus zero-point vibration energy values based on M06-L/6-311+G(2d,p) calculations relative to the "**start**" position are presented in kcal/mol. From the "**start**" position to B3, PhBr (**3b**) does not explicitly participate the reaction (see Figure S4-2).

S4. Pathways from "start" to Silyl Potassium Intermediate with Explicit Participation of 3a/3b

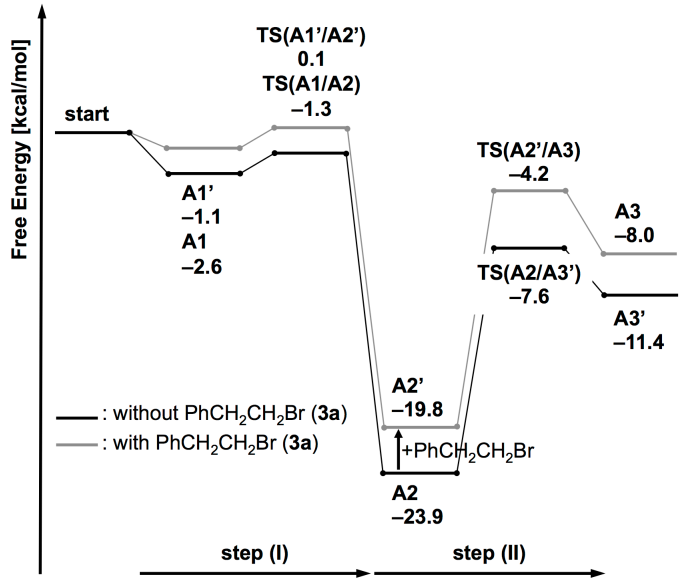

Figure S4-1 Reaction Pathways Leading to the Silyl Potassium Intermediate with and without $PhCH_2CH_2Br$ (**3a**)

The use of "**start**" corresponds to the reactant (**1**, **2a** and **3a**, which were separately optimized), A*n* to an intermediate complex (local minimum), and TS(A*n*/A*m*) to the transition state connecting A*n* and A*m*. Gibbs free energy values (373.15 K, 1.0 atm) at the M06-L/6-311+G(2d,p) level relative to the "**start**" position are shown in kcal/mol. Intermediates, A1', A2' and A3, and TSs, TS(A1'/A2') and TS(A2'/A3), with **3a** are indicted by the gray line. Compared to the path without **3a**, the path with **3a** seems not to be favorable because of entropic effects. However, **3a** is expected to participate in the reaction from the step (II) as shown in the case B reaction (see Figure S4-2).

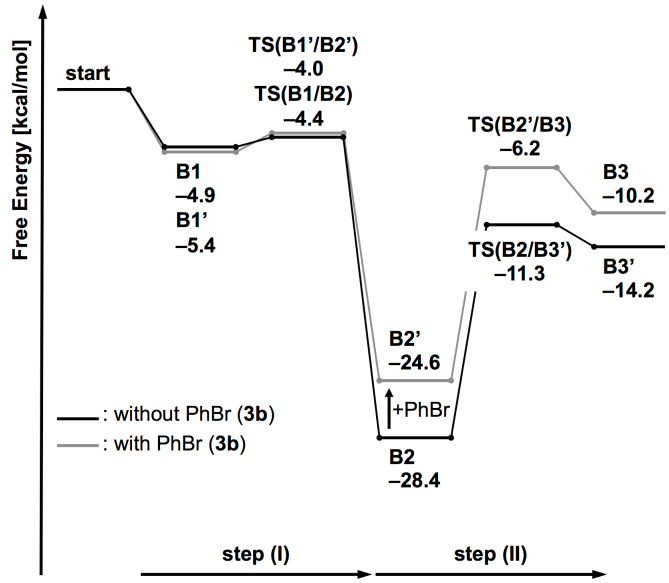

Figure S4-2 Reaction Pathways Leading to the Silyl Potassium Intermediate with and without PhBr (**3b**)

The use of "**start**" corresponds to the reactant (**1**, **2a** and **3b**, which were separately optimized), B*n* to an intermediate complex (local minimum), and TS(B*n*/B*m*) to the transition state connecting B*n* and B*m*. Gibbs free energy values (303.15 K, 1.0 atm) at the M06-L/6-311+G(2d,p) level relative to the "**start**" position are shown in kcal/mol. Intermediates, B1', B2' and B3, and TSs, TS(B1'/B2') and TS(B2'/B3), with **3b** are indicted by the gray line. Compared to the path without **3b**, the path with **3b** seams not to be favorable because of entropic effects. However, it was found that the free energy barrier for detachment / attachment of **3b** at B3' is higher than TS(B2'/B3) as shown in Figure S6-2 and S6-3. Thus, **3b** will participate in the reaction from the step (II).

S5. Substrate and Base Dependence

S5-1. Steric Effect (R = $^{i}Pr_3C_6H_2$–)

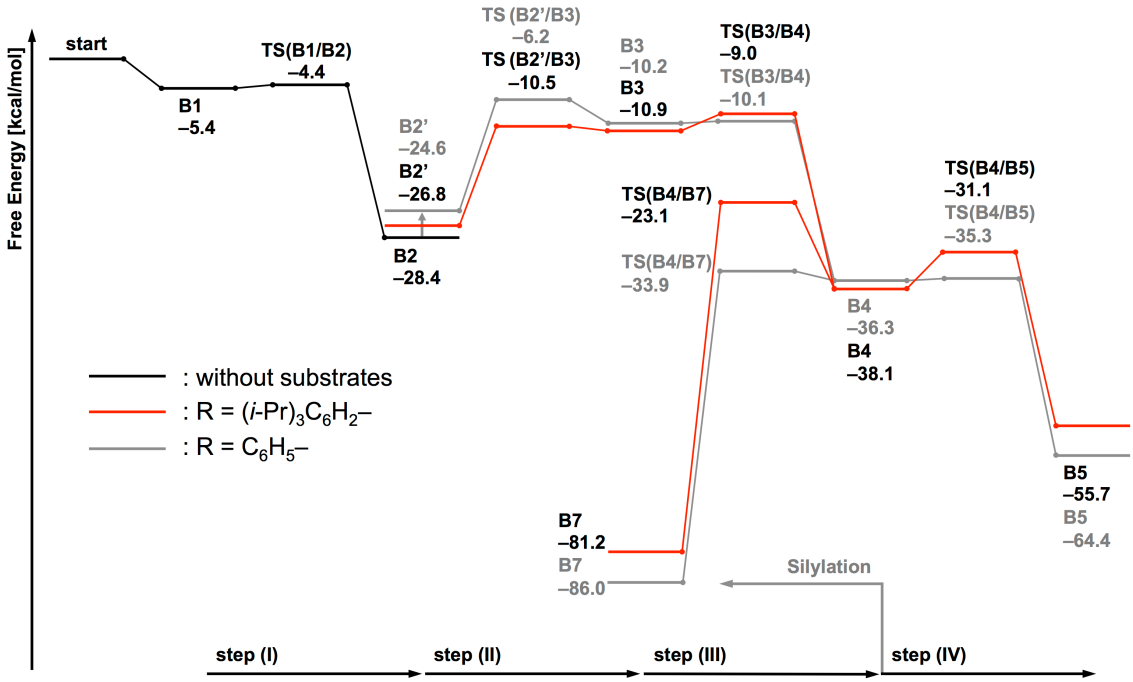

Figure S5-1. Reaction Pathways Leading to the B/Si Products with R = $^{i}Pr_3C_6H_2$

The use of "**start**" corresponds to the reactant (i.e., **1**, **2a**, **3b**, and **3c** which were separately optimized), B*n* to an intermediate complex (local minimum), and TS(B*n*/B*m*) to the transition state connecting B*n* and B*m*. Gibbs free energy values (303.15 K, 1.0 atm) at the M06-L/6-311+G(2d,p) level relative to the "**start**" position are shown in kcal/mol. From the "**start**" position to B2, PhBr (**3b**) and $^{i}Pr_3C_6H_2Br$ (**3c**) do not explicitly participate the reaction. From B2' to B5/B7, the red line shows that the reactant is **3c** and the corresponding energy is displayed with black letters.

S5-2. Halide Effect (X = Cl and I)

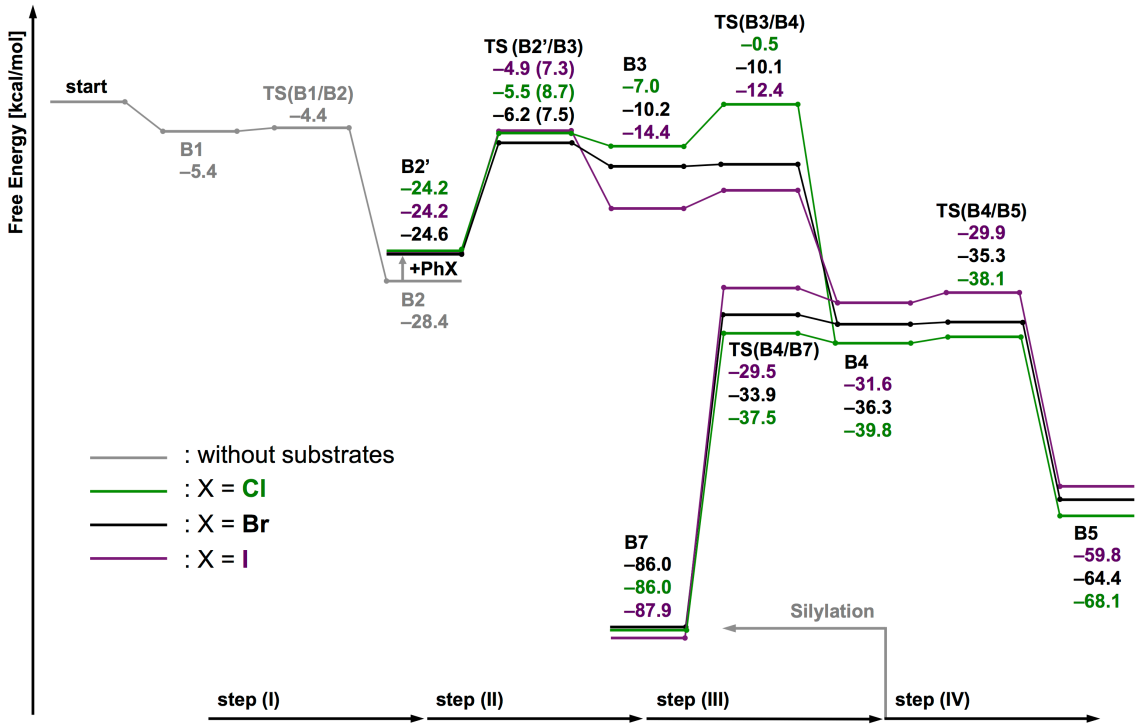

Figure S5-2. Reaction Pathways Leading to the B/Si Products with Different Substrates Ph-X (X = Cl and I)

The use of "**start**" corresponds to the reactant (i.e., **1**, **2a**, **3b**, **3d**, and **3e** which were separately optimized), B*n* to an intermediate complex (local minimum), and TS(B*n*/B*m*) to the transition state connecting B*n* and B*m*. Gibbs free energy values (303.15 K, 1.0 atm) at the M06-L/6-311+G(2d,p) level relative to the "**start**" position are shown in kcal/mol. (For I atom, the Stuttgard ECP46MDF effective core potential and corresponding basis set were applied.) From the "**start**" position to B2, the substrates (**3b**, **3d**, and **3e**) do not explicitly participate in the reaction. From B2' to B5/B7, the green line shows that the reactant is **3d** and the corresponding energy is displayed with green letters. On the other hand, the purple line shows that the reactant is **3e** and the corresponding energy is displayed with purple letters. Single-point energies based on M06/6-311+G(3df,2p) calculations with the C-PCM-THF solvent plus Gibbs free energy corrections in gas phase (303.15 K, 1.0 atm) at the M06-L/6-311+G(2d,p) level are exhibited in parentheses at TS(B2'/B3).

S5-3. Base Effect (LiOMe, NaOMe, KO^{t}Bu, LiO^{t}Bu)

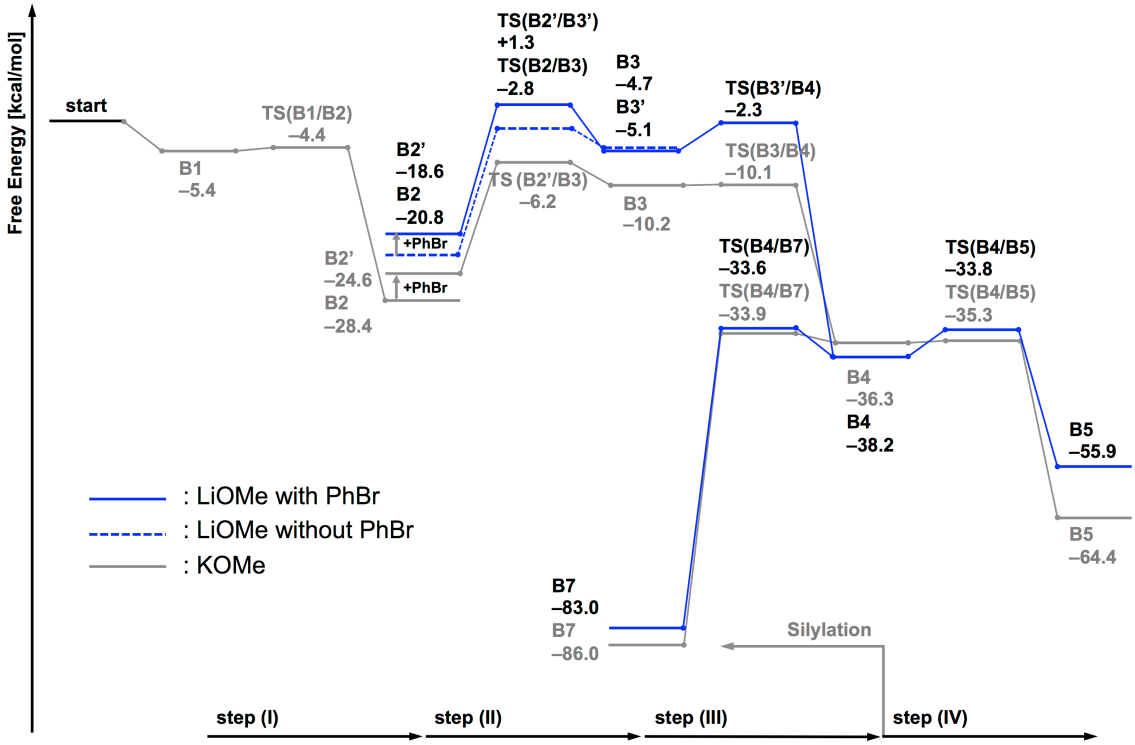

Figure S5-3-1. Reaction Pathways Leading to the B/Si Products with LiOMe

The use of "**start**" corresponds to the reactant (i.e., **1**, **2a**, **2b**, and **3b** which were separately optimized), B*n* to an intermediate complex (local minimum), and TS(B*n*/B*m*) to the transition state connecting B*n* and B*m*. Gibbs free energy values (303.15 K, 1.0 atm) at the M06-L/6-311+G(2d,p) level relative to the "**start**" position are shown in kcal/mol. From the "**start**" position to B2, although PhBr (**3b**) does not explicitly participate in the reaction with **2a** (KOMe), energy profiles for both B2' to B3' and B2 to B3 with and without **3b** are shown by solid- and dashed-line, respectively. From B2 to B5/B7, the blue line and black letters show the profile for **2b** (LiOMe) and the gray line and letters for **2a** (KOMe).

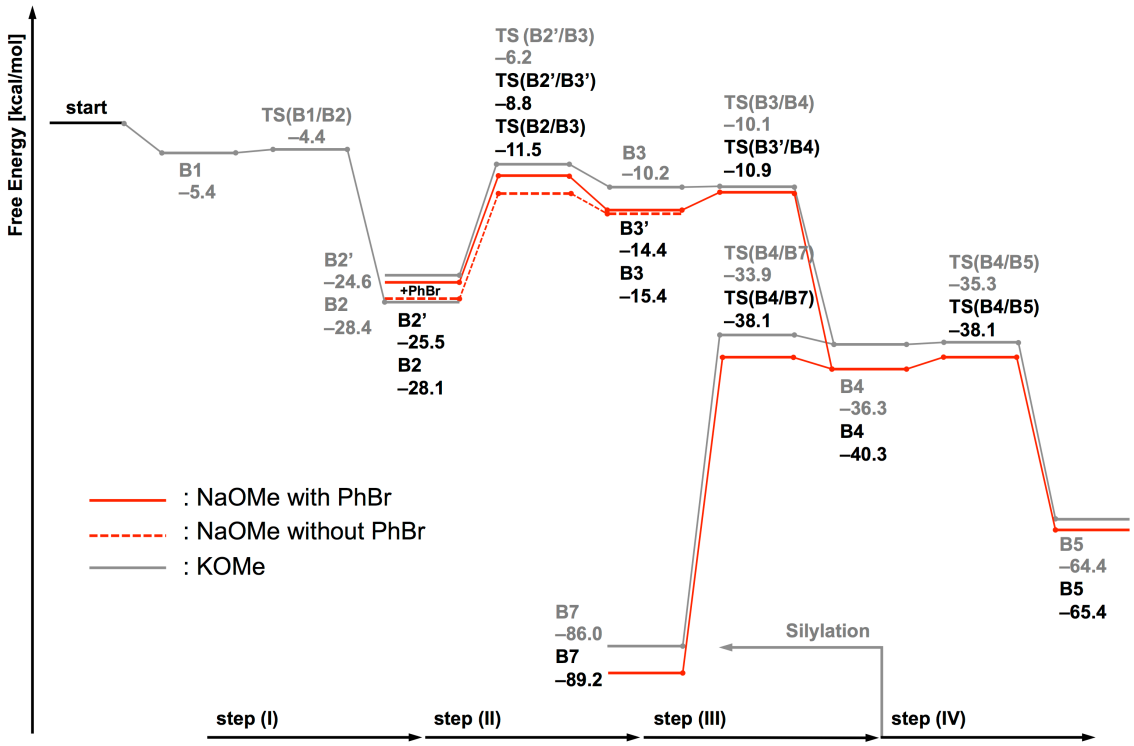

Figure S5-3-2. Reaction Pathways Leading to the B/Si Products with NaOMe

The use of "**start**" corresponds to the reactant (i.e., **1**, **2a**, **2c**, and **3b** which were separately optimized), B*n* to an intermediate complex (local minimum), and TS(B*n*/B*m*) to the transition state connecting B*n* and B*m*. Gibbs free energy values (303.15 K, 1.0 atm) at the M06-L/6-311+G(2d,p) level relative to the "**start**" position are shown in kcal/mol. From the "**start**" position to B3, although PhBr (**3b**) does not explicitly participate in the reaction with **2a** (KOMe), energy profiles for both B2' to B3' and B2 to B3 with and without **3b** are shown by solid- and dashed-line, respectively. From B2 to B5/B7, the red line and black letters show the profile for **2c** (NaOMe) and the gray line and letters for **2a** (KOMe).

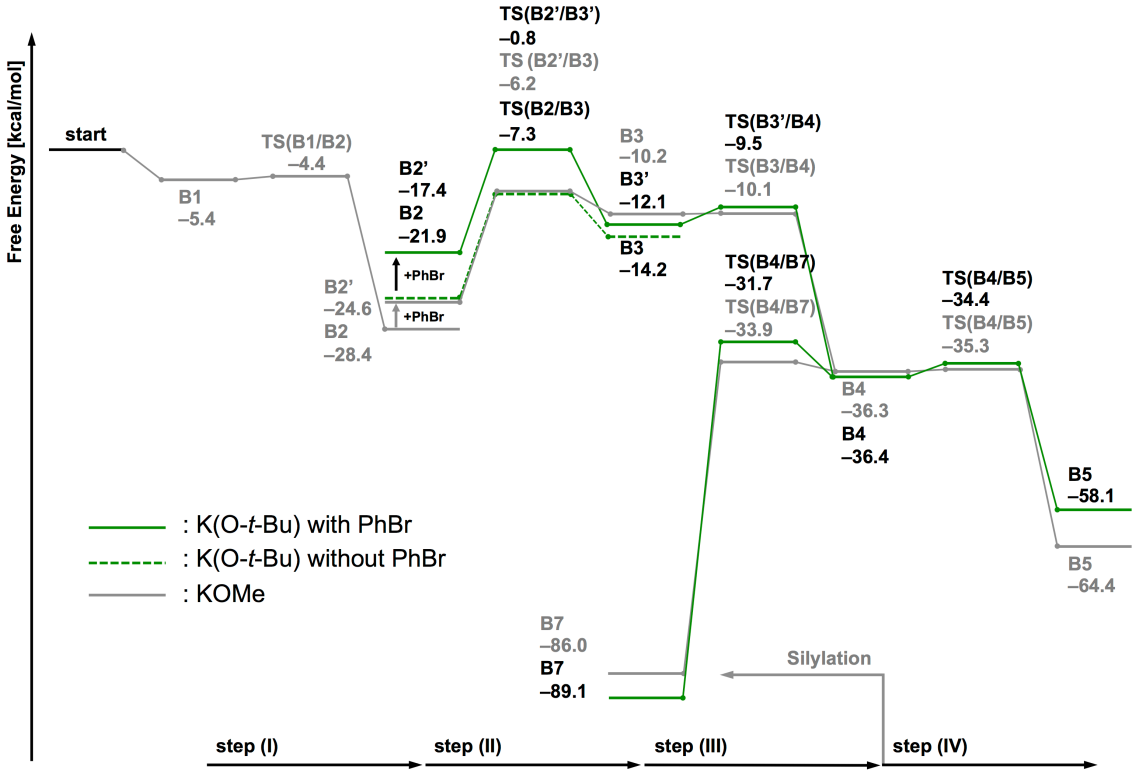

Figure S5-3-3. Reaction Pathways Leading to the B/Si Products with K(O-*t*-Bu)

The use of "**start**" corresponds to the reactant (i.e., **1**, **2a**, **2d**, and **3b** which were separately optimized), B*n* to an intermediate complex (local minimum), and TS(B*n*/B*m*) to the transition state connecting B*n* and B*m*. Gibbs free energy values (303.15 K, 1.0 atm) at the M06-L/6-311+G(2d,p) level relative to the "**start**" position are shown in kcal/mol. From the "**start**" position to B2, although PhBr (**3b**) does not explicitly participate in the reaction with **2a** (KOMe), energy profiles for both B2' to B3' and B2 to B3 with and without **3b** are shown by solid- and dashed-line, respectively. From B2 to B5/B7, the green line and black letters show the profile for **2d** [K(O-*t*-Bu)] and the gray line and letters for **2a** (KOMe).

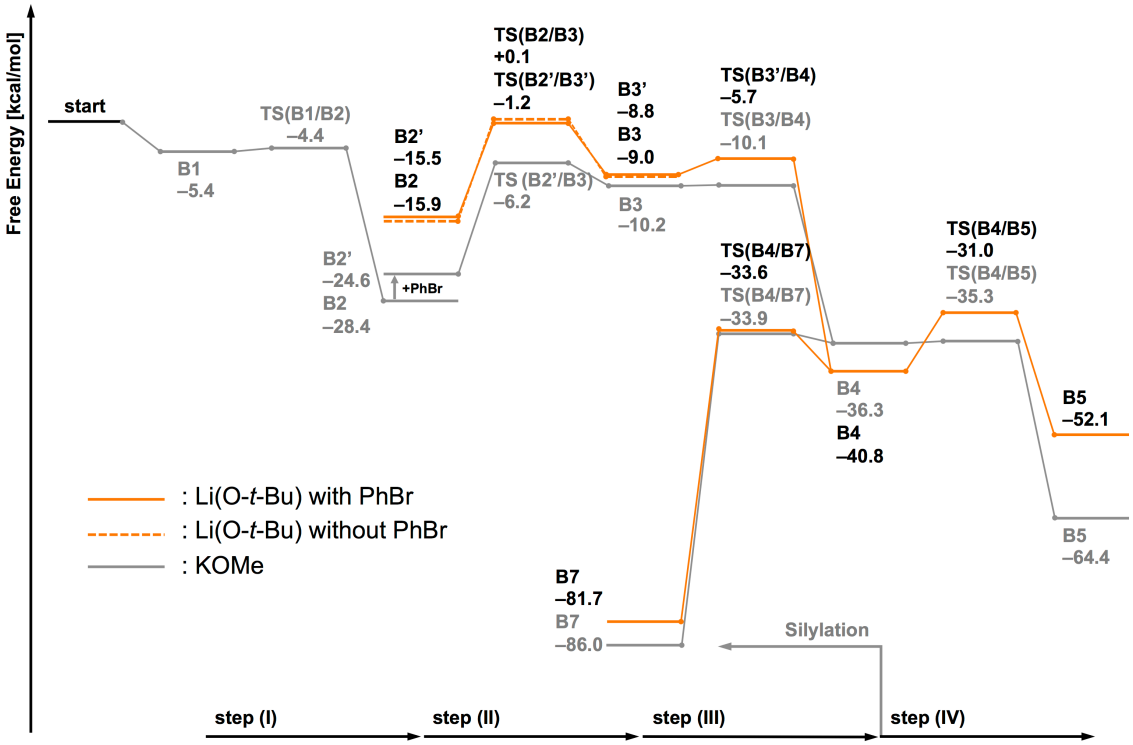

Figure S5-3-4. Reaction Pathways Leading to the B/Si Products with Li(O-*t*-Bu)

The use of "**start**" corresponds to the reactant (i.e., **1**, **2a**, **2e**, and **3b** which were separately optimized), B*n* to an intermediate complex (local minimum), and TS(B*n*/B*m*) to the transition state connecting B*n* and B*m*. Gibbs free energy values (303.15 K, 1.0 atm) at the M06-L/6-311+G(2d,p) level relative to the "**start**" position are shown in kcal/mol. From the "**start**" position to B2, although PhBr (**3b**) does not explicitly participate in the reaction with **2a** (KOMe), energy profiles for both B2' to B3' and B2 to B3 with and without **3b** are shown by solid- and dashed-line, respectively. From B2 to B5/B7, the orange line and black letters show the profile for **2e** [Li(O-*t*-Bu)] and the gray line and letters for **2a** (KOMe).

S5-4. Substitution Effect (R = *p*-F-C_6H_4– and *p*-MeO-C_6H_4–)

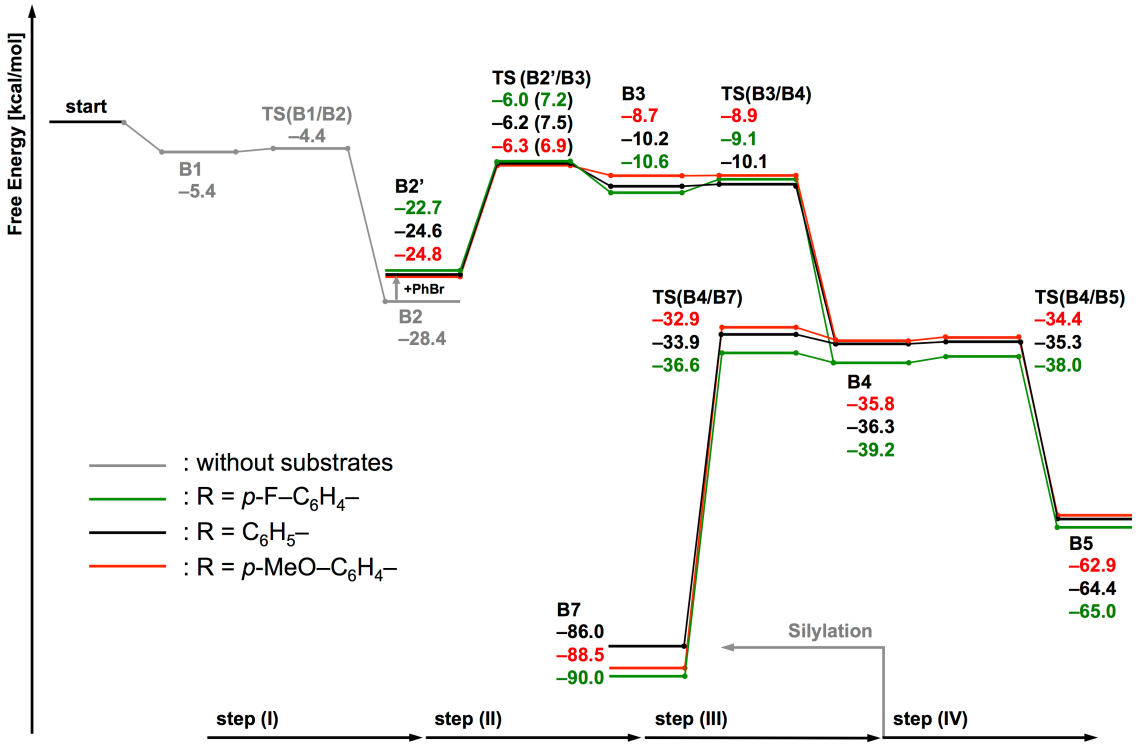

Figure S5-4. Reaction Pathways Leading to the B/Si Products with Different Substrates R–Br (R = *p*-FC_6H_4 and *p*-$MeOC_6H_4$)

The use of "**start**" corresponds to the reactant (i.e., **1**, **2a**, **3b**, **3f**, and **3g** which were separately optimized), B*n* to an intermediate complex (local minimum), and TS(B*n*/B*m*) to the transition state connecting B*n* and B*m*. Gibbs free energy values (303.15 K, 1.0 atm) at the M06-L/6-311+G(2d,p) level relative to the "**start**" position are shown in kcal/mol. From the "**start**" position to B2, the substrates (**3b**, **3f**, and **3g**) do not explicitly participate in the reaction. From B2' to B5/B7, the red line shows that the reactant is **3f** and the corresponding energy is displayed with red letters. On the other hand, the green line shows that the reactant is **3g** and the corresponding energy is displayed with green letters. Single-point energies based on M06/6-311+G(3df,2p) calculations with the C-PCM-THF solvent plus Gibbs free energy corrections in gas phase (303.15 K, 1.0 atm) at the M06-L/6-311+G(2d,p) level are exhibited in parentheses at TS(B2'/B3).

S6. Free Energy Values along Coordination / Decoordination Coordinates

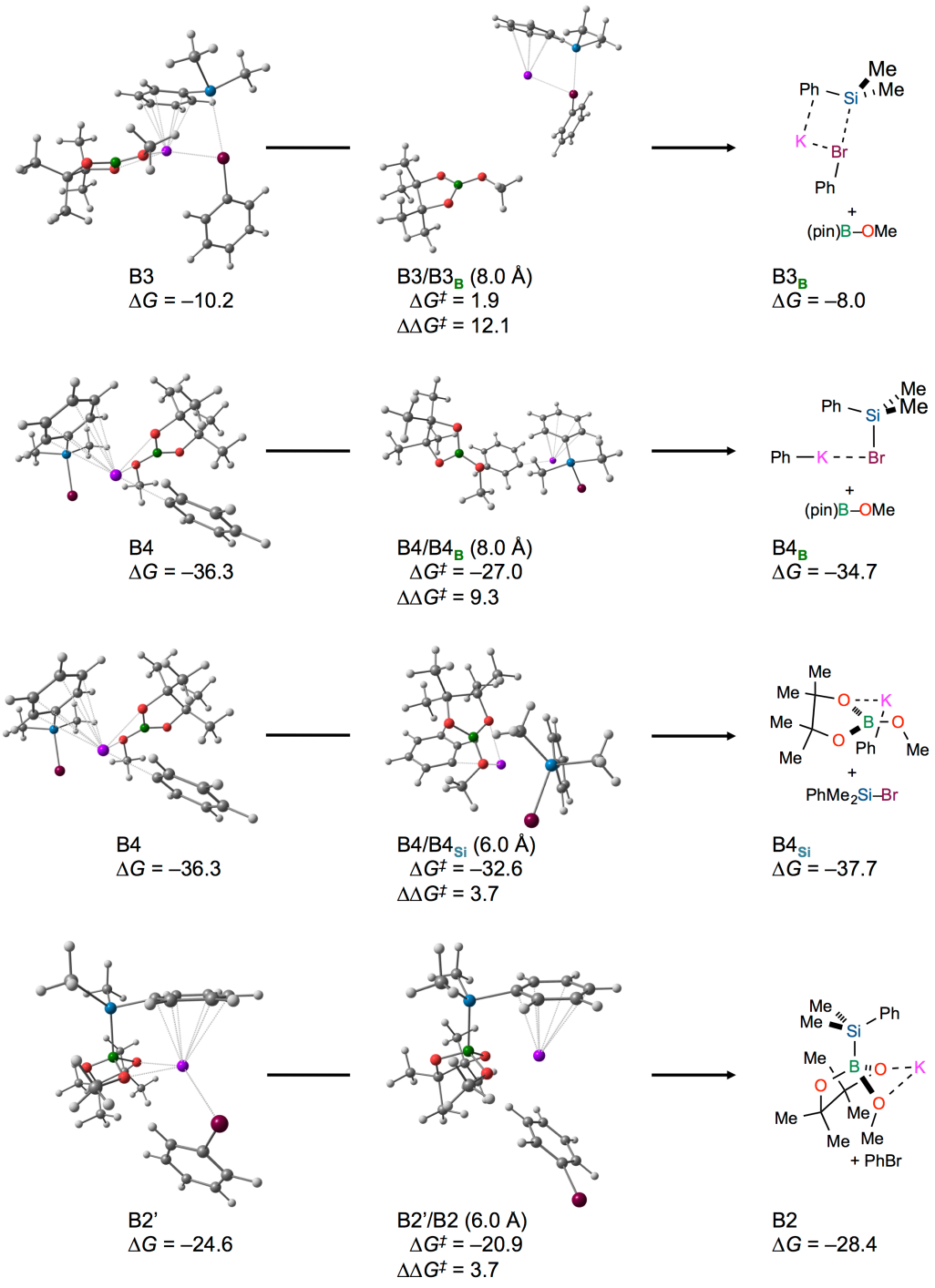

Figure S6-1. Free Energies at a Point along Dissociation Coordinates of (pin)B–OMe from B3', (pin)B–OMe from B4, $PhMe_2Si$–Br from B4, and PhBr from B2'

In the former two cases, the distance $R_{K–B}$ between the K atom and the B atom was chosen as the reaction coordinate. In the latter two cases, the distance $R_{K–Br}$ between the K atom and the Br atom was chosen as the reaction coordinate. Along the reaction coordinate, free energy value was computed by constrained optimization fixing the chosen distance, at $R_{K–B}$ = 8.0 Å for the former two cases and at $R_{K–Br}$ = 6.0 Å for the latter two cases, and normal-mode analysis for the projected Hessian. Gibbs free energy values (303.15 K, 1.0 atm) at the M06-L/6-311+G(2d,p) level relative to the "**start**" position (i.e., **1**, **2a**, and, **3b** which were separately optimized) are shown in kcal/mol. Free energy values at $R_{K–B}$ = 8.0 Å for the dissociation of (pin)B–OMe from B3 and B4, 1.9 and –27.0 kcal/mol, respectively, are much higher than the free energies of the corresponding TSs for forward steps, –10.1 and –35.3 kcal/mol, shown in Figure 3. Free energy value at $R_{K–Br}$ = 6.0 Å for the dissociation of $PhMe_2Si$–Br from B4 –32.6 kcal/mol is also higher than the free energy of the corresponding TS for forward step –33.9 kcal/mol shown in Figure 3. Free energy value at $R_{K–Br}$ = 6.0 Å for the dissociation of PhBr from B2' –20.9 kcal/mol is lower than the free energy of the corresponding TS for forward step –6.2 kcal/mol shown in Figure 3, and attachment / detachment of PhBr thus occurs rapidly before the TS(B2'/B3).

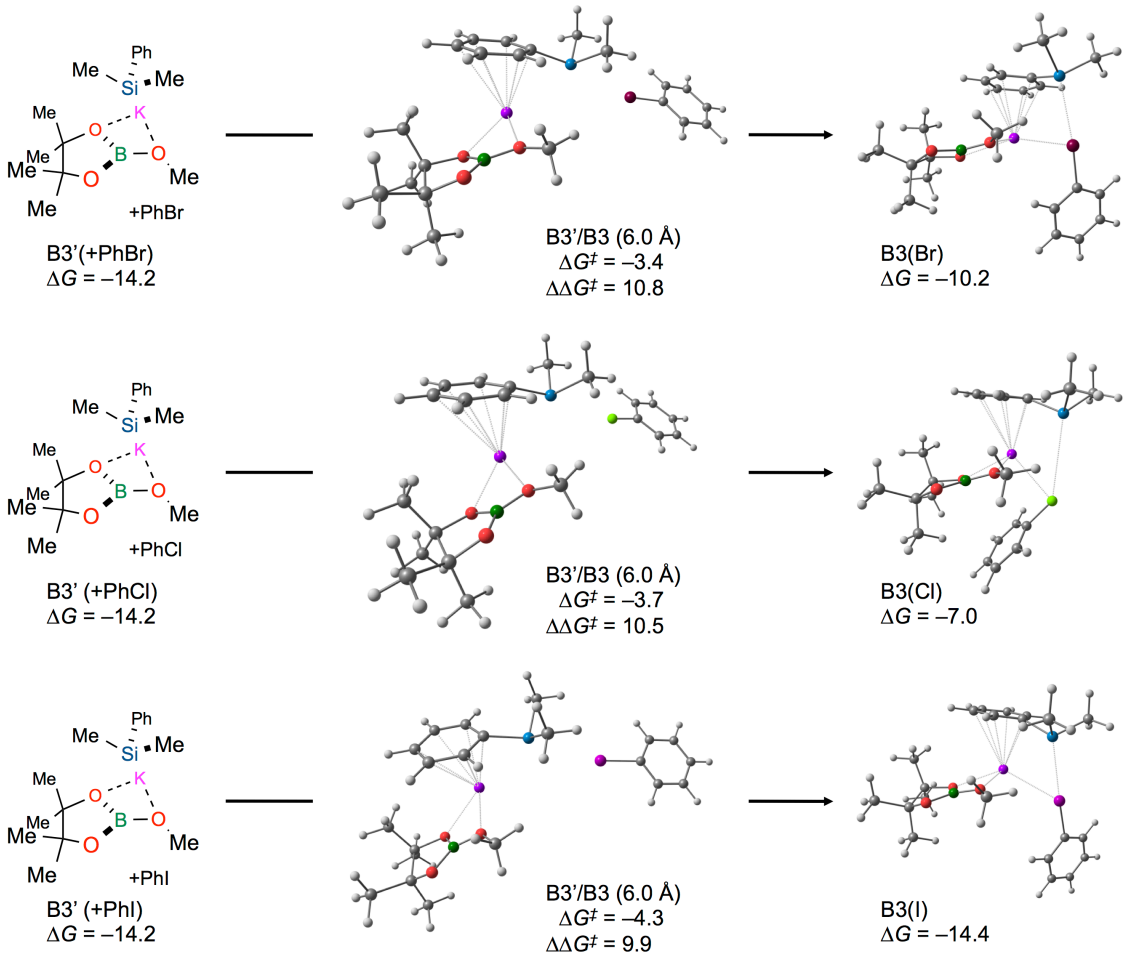

Figure S6-2. Free Energies at a Point along Coordination Coordinates of Ph–X (X = Br, Cl, and I) to B3

The distance $R_{K–X}$ between the K atom and the X atom in Ph–X was chosen as the reaction coordinate. Along the reaction coordinate, free energy value was computed by constrained optimization fixing the chosen distance at $R_{K–X}$ = 6.0 Å and normal-mode analysis for the projected Hessian. Gibbs free energy values (303.15 K, 1.0 atm) at the M06-L/6-311+G(2d,p) level relative to the "**start**" position (i.e., **1**, **2a**, **3b**, **3d**, and **3e** which were separately optimized) are shown in kcal/mol. (For I atom, the Stuttgard ECP46MDF effective core potential and corresponding basis set were applied.) These free energy values of TS(B3'/B3) for X = Br, Cl, I are –3.4, –3.7, and –4.3 kcal/mol, respectively. These are higher than those of TS(B2'/B3) for X = Br, Cl, I (–6.2, –5.5, and –4.9 kcal/mol shown in Figure S5-2, respectively). This suggests that the path through TS(B2'/B3) with participation of the substrate (**3b**, **3d**, or **3e**) is preferred than the path with adsorption of them at B3'.

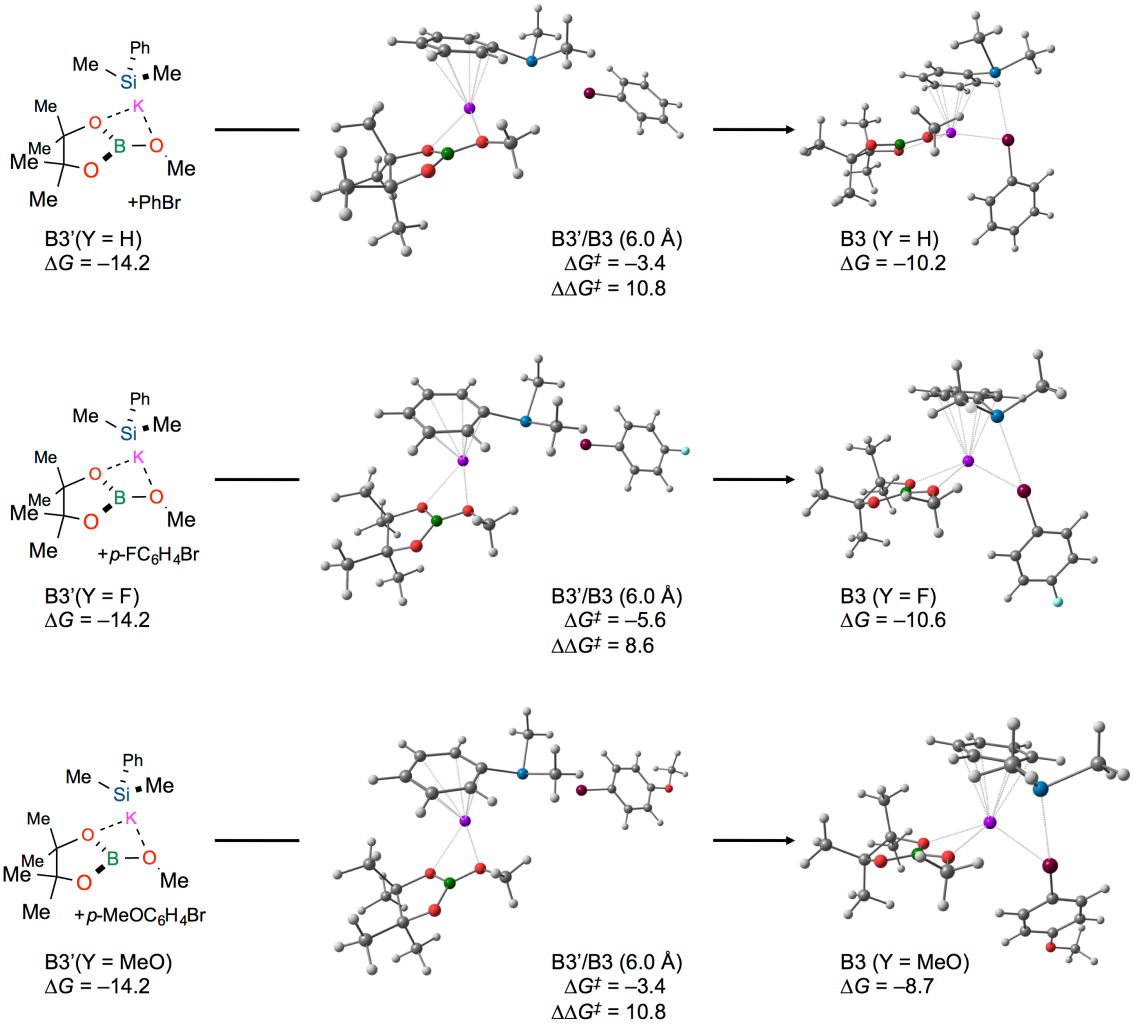

Figure S6-3. Free Energies at a Point along Coordination Coordinates of *p*-Y–C_6H_4–Br (Y = H, F, and MeO) to B3

The distance $R_{K\text{-}Br}$ between the K atom and the Br atom in *p*-Y–C_6H_4–Br was chosen as the reaction coordinate. Along the reaction coordinate, free energy value was computed by constrained optimization fixing the chosen distance at $R_{K\text{–}Br}$ = 6.0 Å and normal-mode analysis for the projected Hessian. Gibbs free energy values (303.15 K, 1.0 atm) at the M06-L/6-311+G(2d,p) level relative to the "**start**" position (i.e., **1**, **2a**, **3b**, **3f**, and **3g** which were separately optimized) are shown in kcal/mol. The free energy values of TS(B3'/B3) for Y = H, F, and MeO are –3.4, –5.6, and –3.4 kcal/mol, respectively. These are higher than those of TS(B2'/B3) for Y = H, F, and MeO (–6.2, –6.0, and –6.3 kcal/mol shown in Figure S5-4, respectively). This suggests that the path through TS(B2'/B3) with participation of the substrate (**3b**, **3f**, or **3g**) is preferred than the path with adsorption of them at B3'.

S7. Natural Population Analysis

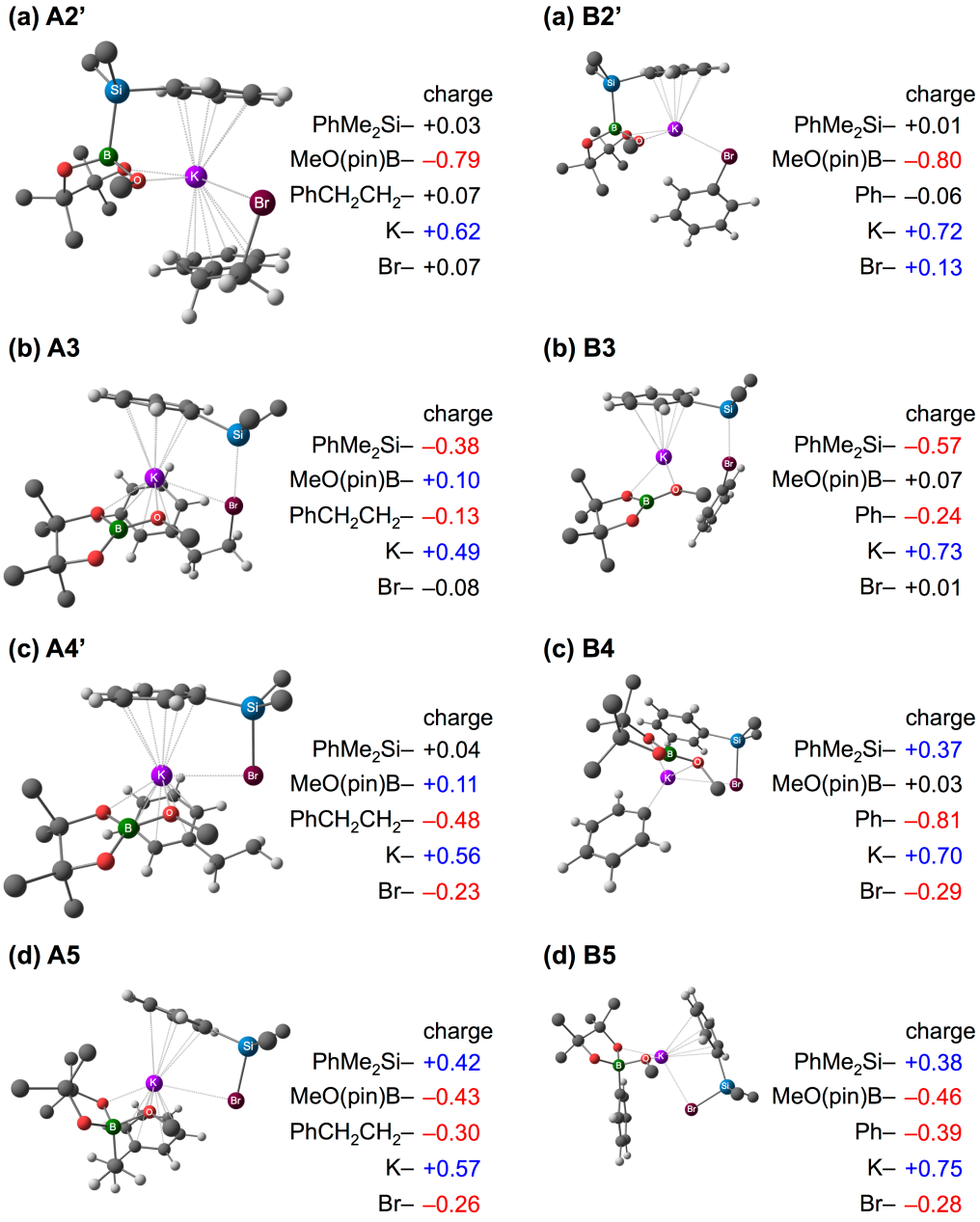

Figure S7. Ball-and-stick Representation of the Charge Distribution in the Intermediates Formed from A2' to A5 and B2' to B5

These charge distribution properties were derived using NPA at the M06-L/6-311+G(2d,p) level. The hydrogen atoms on the methyl groups have been omitted for clarity. Significant positive charges in the charge values have been indicated in blue, whereas negative charges have been indicated in red.

Chapter 4

Key Mechanistic Details of Palladium(II) Catalyzed C–H Functionalization/Intramolecular C–S Bond Formation in Thiobenzanilide

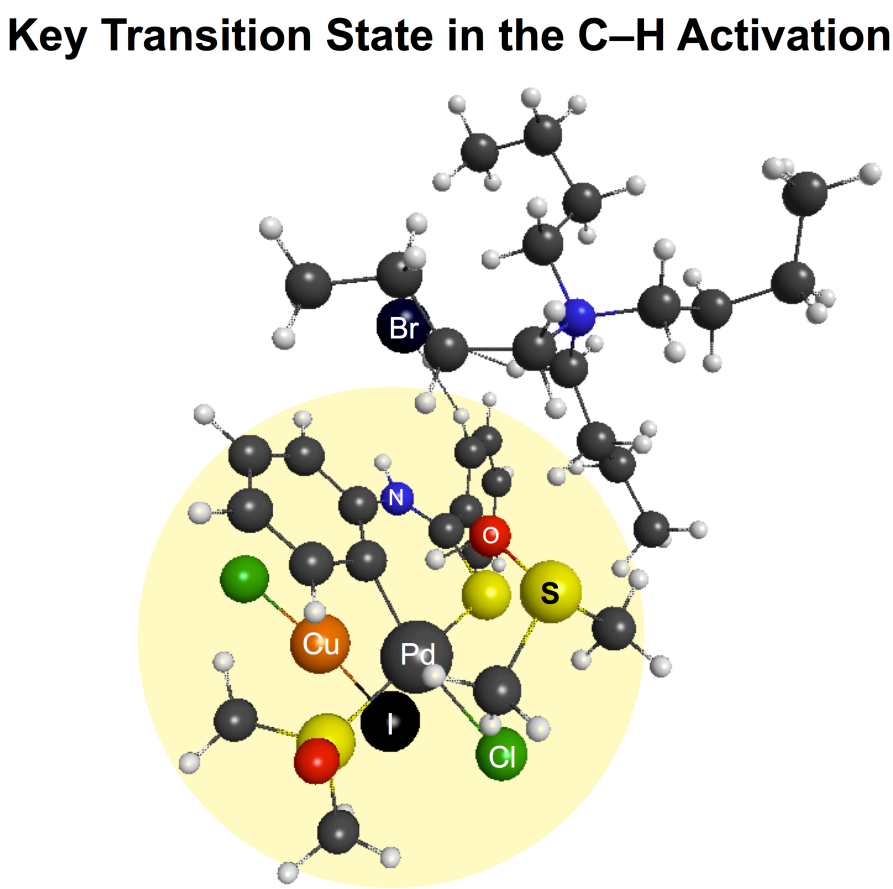

ABSTRACT

The AFIR method was applied to the intramolecular C–S cyclization of thiobenzanilide by using $PdCl_2$/CuI catalyst and Bu_4NBr salt in DMSO/NMP solvent. I found that addition of CuI to the $PdCl_2$, Bu_4NBr, DMSO/NMP and substrate mixture: (a) facilitates C–H bond activation by DMSO and C–S bond formation initiated by Bu_4NBr coordination to N–H bond of substrate, and (b) re-oxidizes Pd-center and re-generates the catalyst.

Introduction

Transition metal catalyzed C–H functionalization/C–S bond formation in an aim for synthesis of N– and S–containing heterocyclic compounds (highly desirable for various pharmatheptic and materials applications) is challenging.[1] Among these compounds, benzothiazole derivatives are important in the field of pharmaceutical compound for exhibiting excellent bioactivity.[2] Hence, many organic chemists have studied the synthetic methods of these molecules.[3-6] Recently, Doi and co-workers have reported the intramolecular C–S cyclization of substituted thiobenzanilides using $PdCl_2$/CuI catalyst and Bu_4NBr salt in DMSO/NMP solvent (scheme 1).[4] This reaction affords the cyclization products in a moderate or good yield and has high functional group compatibilities. That is, the substrates involving the electron withdrawing group (i.e. CO_2Et or CN) group on the phenyl group can be smoothly converted. It was just suggested that this reaction could be proceeded as the mechanism of similar reactions;[4] the details of this reaction is not well understood in spite of the availability. Hence, the mechanistic investigation with theoretical calculation is required for the deep comprehension.

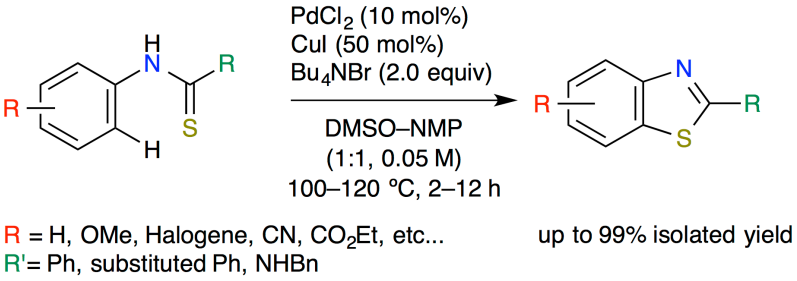

Scheme 1. Palladium(II)-Catalyzed C–H Functionalization/Intramolecular C–S Cyclization

Jacobsen's method and Hugershoff's method, which include oxidative cyclization process, are widely accepted to synthesize the benzothiazole derivatives from thiobenzanilide.[5] These two methods have a week point: low functional group compatibility. For example, it can be difficult to keep alcohoxycarbonyl or cyano group owing to the oxidation condition in Jacobsen's method. Moreover, the stoichiometric or excess amount of toxic-reagents (i.e. Br_2 and metals) are inconveniently demanded for these methods. Thus, the catalytic intramolecular cyclization reaction of 2-halophenylthiobenzamides using Cu(I) or Pd(0) system has developed.[6] It should be appreciated that a halogen atom has to be introduced on the phenyl group by transformation reaction. Under these backgrounds, the Doi's method is superior

because this reaction can directly activate a C–H bond by the catalytic amount of palladium(II)/copper(I) system.[4]

The C–H functionalization/C–S bond formation reaction reported by Doi et al. is a new method: a catalytic C–H activation reaction for the synthesis of substituted thiobenzanilides. However, the mechanism of this reaction has not yet been elucidated. The key factor, based on the screening in the combination of reagents, is the addition of Bu_4NBr salt. It is considerably exhibited that the enhancement effect in the palladium(II)/re-oxidant system. CuI is more suitable re-oxidant than Cu(II) salt [i.e. CuX_2 (X = F, Cl, Br), $Cu(OAc)_2$, $Cu(OTf)_2$, and $Cu(acac)_2$]. In regard to a palladium source, $PdCl_2$, $PdCl_2(cod)$, and $PdBr_2$ have a comparable catalytic ability. Furthermore, when NMP was used as a co-solvent (1:1 ration), the yield was clearly improved in the optimized condition. Since extensive studies on this reaction mechanism have not been reported, further comprehensive theoretical studies are required to provide a deeper understanding of the reaction mechanism.

It is not easy to explain the products resulting from the C–H functionalization/C–S intramolecular cyclization according to our current understanding of organometallic chemistry. It may not be possible to apply our existing theoretical understanding of C–H activation by transition metals[7] to this reaction. With this in mind, further studies are necessary to enhance our theoretical understanding and explaining this transformation adequately. The artificial force induced reaction method is an automated reaction path search method that can be used as a powerful tool in theoretical studies toward the elucidation of reaction mechanisms.[8,9] It can be difficult to apply conventional calculation methods to mechanistic analyses involving novel or poorly defined reaction mechanisms because it may be necessary to consider multiple reaction pathways. Moreover, this approach requires a large number of trial-and-error calculations to consider the sequential identification of the intermediates and transition states (TSs) involved in the assumed mechanism. The AFIR method allows for the identification of working reaction pathways including unexpected ones from the many different possibilities without the need to estimate any of the TS structures.

Herein, I report the results of a detailed density functional theory (DFT) study on the present reaction. The results of this systematic theoretical investigation have explained the key role of each reagent: (a) facilitates C–H bond activation by DMSO and C–S bond formation initiated by Bu_4NBr coordination to N–H bond of substrate, and (b) re-oxidizes Pd-center and re-generates the catalyst.

Results & Discussion

All of the structures described in this paper were optimized at the B3LYP[10]+D3[11] level with 6-31G(d,p) basis set for H, C, N, O, S, and Cl atoms, and SDD effective core potential and corresponding basis set for Cu, Br, Pd, and I atoms. It is important to mention that all the energy profiles described in the current study have been discussed in terms of the Gibbs free energy (298.15 K, 1.0 atm) in the gas phase. Furthermore, the free energy corrections used in the current study were estimated using ideal gas, rigid-rotor and harmonic approximations.

Step-I (Effect of Solvent). I firstly focused on confirming the reactive complex involved in palladium(II) chrolide (**1**), dimethyl sulfoxide (DMSO, **2**), and N-methylpyrrolidone (NMP, **3**). The previous study has already found that compound **1** and **2** react each other and produce S-coordinated *trans*-$PdCl_2(DMSO)_2$ **4**.[12] Here, I compared the thermodynamic stability of **4** and O-coordinated *trans*-$PdCl_2(NMP)_2$ **4'** because the present system also contains **3** as co-solvent. It was confirmed that **4** is 19.2 kJ/mol more stable than **4'**. Hence, I systematically explored the reaction pathways involving the reaction of **4** with thiobenzanilide (**5**) using the AFIR method. Further details of this process have been provided below in the Computational Details section.

The current mechanism was obtained by the application of a systematic reaction path search to the step-I by the AFIR method. The range used in the current reaction path search is described below. An approximate upper energy barrier threshold should be specified in AFIR calculations, and the value used in this step was set to 200 kJ/mol. All of the atoms in the methyl and phenyl groups that are not participated in bond rearrangement of the compound **4** and **5** were set as being inactive. A systematic search was then conducted at a low computational level (see Computational Details). Then, all of the pathways were considered at a reliable computational level and the results are discussed below.

Figure 1 shows the free energy diagram obtained in the step-I reaction, which led to the reactive intermediate of C–H or N–H activation. Two elementary reactions were identified during this process, including (I-a) the substitution of sulfur atom on the thiobenzanilide (**5**) to the palladium atom in complex **4** to give complex [$LPdCl_2$(DMSO), L = substrate, **6**] and DMSO (CP2 of Figure 1); (I-b) the conformational change of $LPdCl_2$(DMSO) and DMSO (between CP2 and CP3 of Figure 1). Since there are no high activation barriers, CP3 is easily given through these simple reactions.

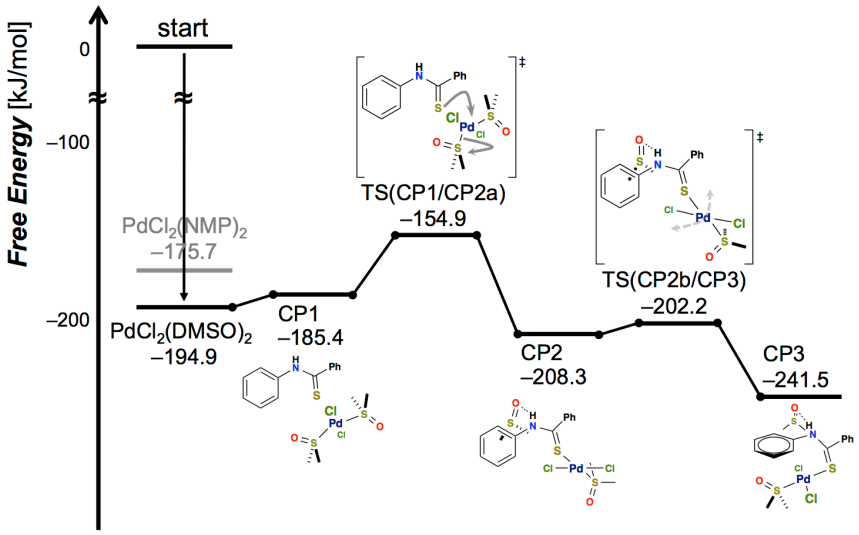

Figure 1. Reaction Pathways Leading to the Reactive Intermediate. The use of "**start**" corresponds to the reactant (i.e., **1**, **2, 3** and **5**, which were separately optimized), CP*n* to an intermediate complex (local minimum), and TS(CP*n*/CP*m*) to the transition state connecting CP*n* and CP*m*. Gibbs free energy values (298.15 K, 1.0 atm) based on B3LYP+D3/6-31G(d,p) & SDD calculations relative to the "**start**" position are shown in kJ/mol. Schematic representations of the optimized structures corresponding to CP*n* or TS(CP*n*/CP*m*) are shown in the current reaction.

It is assumed that the intermediates generated by C–H activation and N–H activation reactions with DMSO **2**, NMP **3**, or Bu_4NBr **7**. Figure 2 shows the stability of these compounds estimated with traditional optimization technique. The generation of the C–H activated intermediate **8** is clearly more stable than the N–H activated intermediate **9** because of coordinative unsaturation. It was also found that these two reactions with Bu_4NBr are unfavorable. Thus, TS structure corresponding to C–H activation in $LPdCl_2(DMSO)$ **6** with DMSO **2** or NMP **3** was found by the AFIR method and two TSs for these C–H cleavage pathways are described in Figure 3. In this AFIR search, an approximate upper energy barrier threshold was set to 750 kJ/mol. The free energies ($\Delta G^{\ddagger}$) relative to the individually optimized reactants ("**start**" in Figure 1) are shown below each TS structure together with the activation free energies ($\Delta\Delta G^{\ddagger}$). The attack of the oxygen on DMSO or NMP through the TSs shown in Figure 3a and 3b would require the formation of unstable TSs with high $\Delta G^{\ddagger}$ values of –55.7 and –44.6 kJ/mol, respectively. It is noted that this tendency is consistent with pKa value[13]. The C–H bond may be cleaved by DMSO, but the activation barrier ($\Delta\Delta G^{\ddagger}$ = 152.7 kJ/mol) for the

pathway was too much higher to proceed. Based on these results, the other reagents are necessary for the C–H activation reaction.

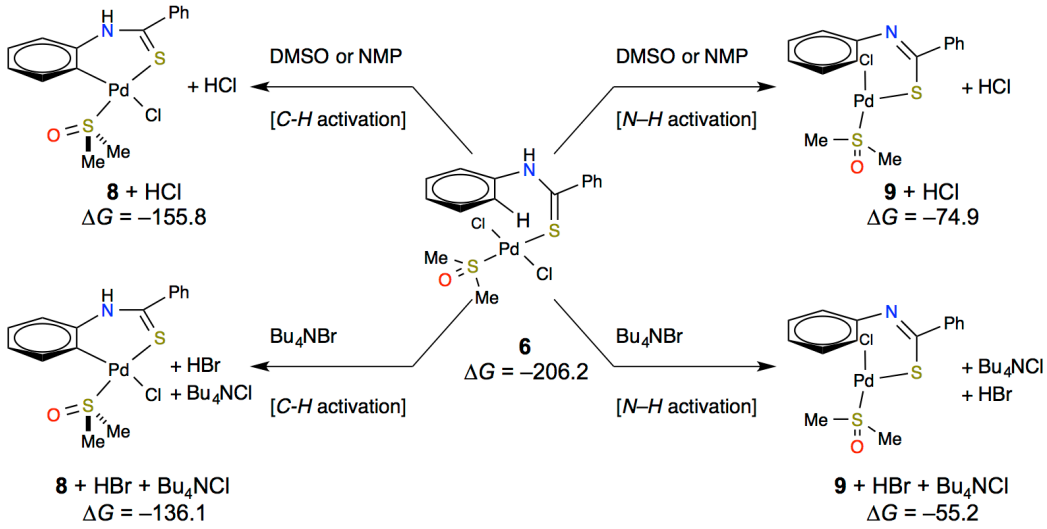

Figure 2. Thermodynamic Stability of C–H or N–H Activated Intermediates. Free Energies (ΔG) Relative to the Reactants (i.e., **1**, **2**, **3**, **5** and **7**) in kJ/mol.

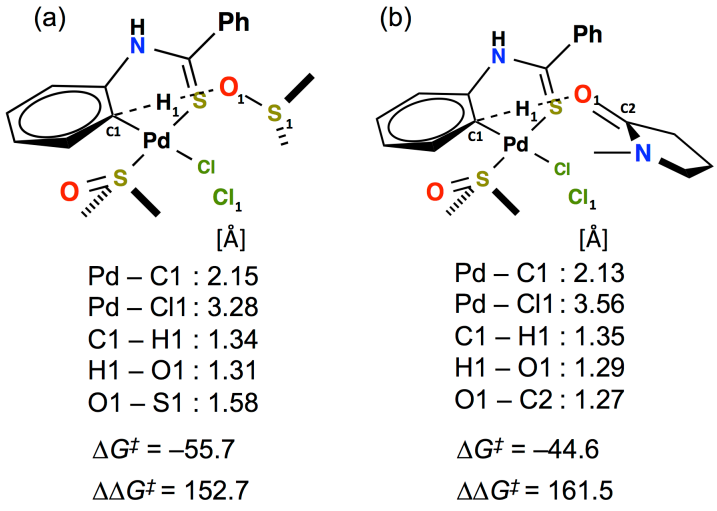

Figure 3. Important Parameter of TS Structures, Free Energies ($\Delta G^{\ddagger}$) Relative to the Reactants (i.e., **1**, **2, 3** and **5**), and Activation Free Energies ($\Delta\Delta G^{\ddagger}$) of the C–H Activation Reaction Pathways. Free energy values based on B3LYP+D3/6-31G(d,p) & SDD calculations have been given in kJ/mol.

Step-II (Effect of CuI). I systematically explored the pathways involved in the reaction of $LPdCl_2(DMSO)$ **6**, DMSO **2**, and copper(I) iodide (**10**) using the AFIR method in same fashion. Figure 4 shows the free energy diagram for leading to cyclization product **11** involved in CP7.

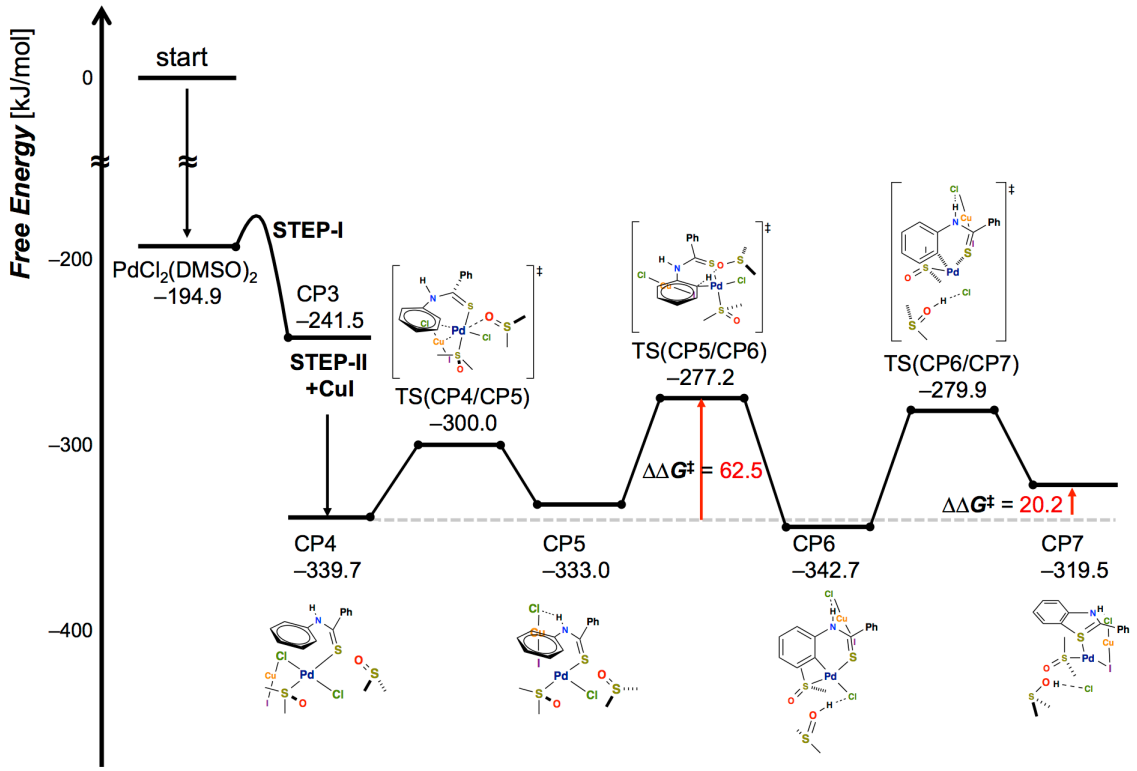

Figure 4. Reaction Pathways Leading to the Cyclization Product. The use of "**start**" corresponds to the reactant (i.e., **1**, **2, 3, 5** and **10**, which were separately optimized), CP*n* to an intermediate complex (local minimum), and TS(CP*n*/CP*m*) to the transition state connecting CP*n* and CP*m*. Gibbs free energy values (298.15 K, 1.0 atm) based on B3LYP+D3/6-31G(d,p) & SDD calculations relative to the "**start**" position are shown in kJ/mol. Schematic representations of the optimized structures corresponding to CP*n* or TS(CP*n*/CP*m*) are shown in the current reaction.

The reasonable reaction pathway was obtained by adding CuI (**10**) to the AFIR search; (II-a) generation of $[CuClI]^-$ (**12**) and palladium(I) complex (**13**) via the cleavage of the Pd–Cl bond (CP5 of Figure 4); (II-b) cleaving the target C–H bond with DMSO giving Pd(II) complex (**14**) involving Pd–C bond (CP6 of Figure 4), (II-c) C–S bond formation by reductive elimination forming the cyclization product **11**, which is coordinated to [(ClCuI)–Pd(DMSO)] complex (CP7 of Figure 4). It is significant that the activation barrier of C–H cleavage becomes lower by adding **10**: the $\Delta\Delta G = \Delta G^{\ddagger}$ [TS(CP5/CP6)]– ΔG (CP4) value is 62.5 kJ/mol. However, the

reaction from CP4 to CP7 is endothermic process. This computational result is consistent with the experiment: this reaction requires existing of Bu_4NBr salt for switching to exothermic process by stabilizing the protonated intermediates.

Step-III (Effect of Bu_4NBr). Conformational analysis of [CP4 + Bu_4NBr (**15**)] system and [CP7 + Bu_4NBr (**15**)] system was performed to confirm the role of **15** by the AFIR method. In this AFIR search, an approximate upper threshold was set to 50 kJ/mol, and TS optimization process was skipped for just finding local minima, and all atoms were set to be active toward bond rearrangement. Figure 5 shows the resulting most stable conformer in free energy. In CP8 composed of CP4 and **15**, H•••Br coordination more strongly stabilizes the palladium intermediate (**6**) than hydrogen bond via DMSO. In CP9, connectivity of intermediate was changed from CP7 by the effect of week artificial force and addition of **15**. That is, the Pd–Cl bond is regenerated and the proton eliminated from reactive phenyl group is shared with another DMSO molecule by a hydrogen bond. The same H•••Br interaction is also observed in CP9. Here, it is strongly suggested that Bu_4NBr (**15**) is demanded for the exothermic process from comparison of thermodynamic stability in these intermediates: $\Delta\Delta G = \Delta G(\text{CP9}) - \Delta G(\text{CP8})$ value is –31.5 kJ/mol.

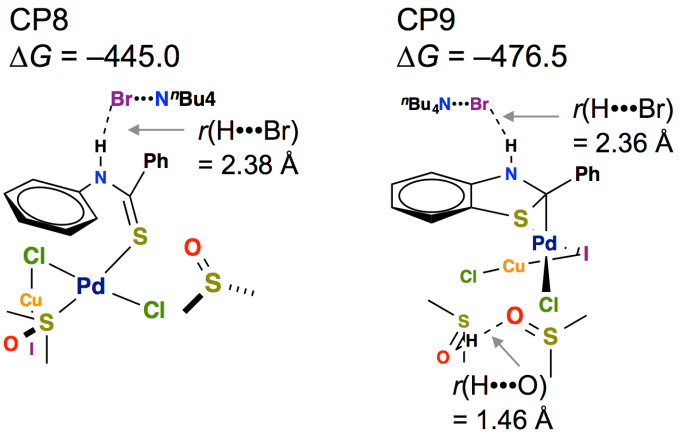

Figure 5. The Most Stable Structures of Intermediate in CP8 (=CP4•••**15**) and CP9 (=CP7•••**15**) system. Free Energies (ΔG) Relative to the Reactants (i.e., **1**, **2**, **3**, **5**, **10** and **15**). Free energy values based on B3LYP+D3/6-31G(d,p) & SDD calculations have been given in kJ/mol.

Conclusion

I applied the AFIR method to explore key mechanistic details of the C–H functionalization/intramolecular C–S cyclization of thiobenzanilide. It is important for activating the target C–H bond on the substrate to participate DMSO solvent, CuI co-catalyst, and Bu_4NBr salt in this system. That is, the chloride atom on the Pd(II) center reacts with CuI and the coordinative unsaturated Pd(I) and $[CuClI]^-$ species are generated. The C–H bond is subsequently cleaved by oxygen atom in DMSO and Pd–C bond is formed. Finally, the C–S bond is generated by reductive elimination reaction. Among these bond rearrangement steps, the bromine anion of Bu_4NBr is coordinated to N–H bond on the substrate. Thus, the palladium intermediates and protonated product are stabilized through this coulomb interaction and the while reaction undergoes as exothermic process in free energy.

Computational Details

By the AFIR method, reaction pathways: (Step-I) among *trans*-$PdCl_2(DMSO)_2$ **4** and thiobenzanilide (**5**): (Step-II) those among $LPdCl_2(DMSO)$ **6**, DMSO **2**, and copper(I) iodide (**10**): (Step-III) [CP4 + Bu_4NBr (**15**)] and [CP7 + Bu_4NBr (**15**)] system were searched at the ONIOM(B3LYP+D3/GENECP:PM6+D3) level, where the atoms in the methyl, buthyl, and phenyl groups that is not participated in bond rearrangement were treated by PM6+D3 and the other reaction-center parts were treated by B3LYP level with 6-31G basis set for H, C, N, O atoms and 6-31G(d) basis set for S, Cl atoms and SDD effective core potential and corresponding basis set for Cu, Br, Pd, I atoms. The AFIR method gives many approximate reaction paths called AFIR paths as minimization paths of a special function called AFIR function.[8] The AFIR paths at the ONIOM level were found to be too crude to be compared to the intrinsic reaction coordinate (IRC) path of the final computational level. Hence, AFIR paths were once refined by a conventional path optimization method, the locally updated plane[14] (LUP) method, at the B3LYP+D3 level with small basis sets (6-31G basis set for H, C, N, O atoms and 6-31G(d) basis set for S, Cl atoms and SDD effective core potential and corresponding basis set for Cu, Br, Pd, I atoms). Since the AFIR path can be a good guess of the minimum energy path, LUP converges quickly and only five LUP iterations were considered. Peaks along the final LUP paths were then optimized to true TSs at the B3LYP+D3 level with lager basis sets; 6-31G(d,p) basis set for H, C, N, O, S, Cl atoms and SDD effective core

potential and corresponding basis set for Cu, Br, Pd, I atoms. Free-energy corrections in gas-phase were estimated at optimized structures assuming the rigid-rotor and harmonic approximations. All DFT calculations were done with Gaussian 09 programs.[15] Using DFT gradients and Hessians, automated searches as well as geometry optimizations were performed by a developmental version of the GRRM program.[16]

References

1. For selected recent reviews on transition metal-catalyzed C–H functionalizations, see: (a) Kakiuchi, F.; Chatani, N. *Adv. Synth.Catal.* **2003**, *345*, 1077–1101. (b) Goj, L. A.; Gunnoe, T. B. *Curr. Org. Chem.* **2005**, *9*, 671–685. (c) Dick, A. R.; Sanford, M. S. *Tetrahedron* **2006**, *62*, 2439– 2463. (d) Yu, J.-Q.; Giri, R.; Chen, X. *Org. Biomol. Chem.* **2006**, *4*, 4041– 4047. (e) Daugulis, O.; Zaitsev, V. G.; Shabashov, D.; Pham, Q.-N.; Lazareva, A. *Synlett* **2006**, 3382–3388. (f) Alberico, D.; Scott, M. E.; Lautens, M. *Chem. Re*V. **2007**, *107*, 174–238. (g) Seregin, I. V.; Gevorgyan, V. *Chem. Soc. Rev.* **2007**, *36*, 1173–1193. (h) Campeau, L. C.; Stuart, D. R.; Fagnou, K. *Aldrichim. Acta* **2007**, *40*, 35–41.
2. For selected recent examples, see: (a) Kok, S. H. L.; Gambari, R.; Chui, C. H.; Yuen, M. C. W.; Lin, E.; Wong, R. S. M.; Lau, F. Y.; Cheng, G. Y. M.; Lam, W. S.; Chan, S. H.; Lam, K. H.; Cheng, C. H.; Lai, P. B. S.; Yu, M. W. Y.; Cheung, F.; Tang, J. C. O.; Chan, A. S. C. *Bioorg. Med. Chem.* **2008**, *16*, 3626. (b) Liu, C.; Lin, J.; Pitt, S.; Zhang, R. F.; Sack, J. S.; Kiefer, S. E.; Kish, K.; Doweyko, A. M.; Zhang, H.; Marathe, P. H.; Trzaskos, J.; Mckinnon, M.; Dodd, J. H.; Barrish, J. C.; Schieven, G. L.; Leftheris, K. *Bioorg. Med. Chem. Lett.* **2008**, *18*, 1874. (c) Henriksen, G.; Hauser, A. I.; Westwell, A. D.; Yousefi, B. H.; Schwaiger, M.; Drzezga, A.; Wester, H.-J. *J. Med. Chem.* **2007**, *50*, 1087.
3. For a general overview of synthetic methods to benzthiazoles, see: (a) Ulrich, H. in *Science of Synthesis: Houben-Weyl Methods of Molecular Transformations*; Schaumann, E., Ed.; Thieme: Stuttgart, 2001; Vol. 11, pp 835–912.
4. Inamoto, K.; Hasegawa, C.; Hiroya, K.; Doi, T. *Org. Lett.* **2008**, *10*, 5147-5150.
5. For selected recent examples, see: (a) Thiel, O. R.; Bernard, C.; King, T.; Dilmeghani-Seran, M.; Bostick, T.; Larsen, R. D.; Faul, M. M. *J. Org. Chem.* **2008**, *73*, 3508. (b) Bose, D. S.; Idrees, M.; Srikanth, B. *Synthesis* **2007**, 819. (c) Wang, M.; Gao, M.; Mock, B. H.; Miller, K. D.; Sledge, G. W.; Hutchins, G. D.; Zheng, Q.-H. *Bioorg.*

Med. Chem. **2006**, *14*, 8599. (d) Bose, D. S.; Idrees, M. *J. Org. Chem.* **2006**, *71*, 8261. (e) Mu, X.-J.; Zou, J.-P.; Zeng, R.-S.; Wu, J.-C. *Tetrahedron Lett.* **2005**, *46*, 4345.

6. (a) Vera, M. D.; Pelletier, J. C. *J. Comb. Chem.* **2007**, *9*, 569. (b) Evindar, G.; Batey, R. A. *J. Org. Chem.* **2006**, *71*, 1802. (c) Joyce, L. L.; Evindar, G.; Batey, R. A. *Chem. Commun.* **2004**, 446. (d) Bened´ı, C.; Bravo, F.; Uriz, P.; Ferna´ndez, E.; Claver, C.; Castillo´n, S. *Tetrahedron Lett.* **2003**, *44*, 6073.
7. For selected recent computational examples in C–H activation reaction, see: (a) Xu, H.; Muto, K.; Yamaguchi, J.; Zhao, C.; Itami, K.; Musaev. D. G. *J. Am. Chem. Soc.* **2014**, *136*, 14834−14844. (b) Musaev. D. G.; Kaledin, A.; Shi, B.-F.; Yu. J.-Q. *J. Am. Chem. Soc.* **2012**, *134*, 1690–1698.
8. (a) Maeda, S.; Morokuma, K. *J. Chem. Phys.* **2010**, *132*, 241102-241104. (b) Maeda, S.; Morokuma, K. *J. Chem. Theory Comput.* **2011**, *7*, 2335-2345. (c) Maeda, S.; Ohno, K.; Morokuma, K. *Phys. Chem. Chem. Phys.* **2013**, *15*, 3683-3701. (d) Maeda, S.; Taketsugu, T.; Morokuma, K. *J. Comput. Chem.* **2014**, *35*, 166-173.
9. For recent examples of computational study of unknown organic synthesis reaction mechanisms by the AFIR method, see: (a) Maeda, S.; Komagawa, S.; Uchiyama, M.; Morokuma, K. *Angew. Chem.,* **2011**, *123*, 670-675; *Angew. Chem., Int. Ed.* **2011**, *50*, 644-649. (b) Hatanaka, M.; Maeda, S.; Morokuma, K. *J. Chem. Theory Comput.* **2013**, *9*, 2882-2886. (c) Hatanaka, M.; Morokuma, K. *J. Am. Chem. Soc.* **2013**, *135*, 13972-13979. (d) Uematsu, R.; Maeda, S.; Taketsugu, T. *Chem. Asian J.* **2014**, *9*, 305-312.
10. Becke, A. D. *J. Chem. Phys.* **1993**, *107*, 8554-8560.
11. Grimme, S.; Antony, J.; Ehrlich, S.; Krieg, H. *J. Chem. Phys.* **2010**, *132*, 154104–154119.
12. Bennett, M. J.; Cotton, F. A.; Weaver, D. L. *Acta. Cryst.* **1967**, *23*, 788–796.
13. (a) Bordwell, F. G.; Branca, J. C.; Johnson, C. R.; Vanier, Noel R. *J. Org. Chem.* **1980**, *45*, 3884. (b) Bordwell, Frederick G; Fried, H. E. *J. Org. Chem.* **1991**, *56*, 4218–4223.
14. Choi, C.; Elber, R. *J. Chem. Phys.* **1991**, *94*, 751–760.
15. Gaussian 09, Revision D.01, Frisch, M. J.; Trucks, G. W.; Schlegel, H. B.; Scuseria, G. E.; Robb, M. A.; Cheeseman, J. R.; Scalmani, G.; Barone, V.; Mennucci, B.; Petersson, G. A.; Nakatsuji, H.; Caricato, M.; Li, X.; Hratchian, H. P.; Izmaylov, A. F.; Bloino, J.; Zheng, G.; Sonnenberg, J. L.; Hada, M.; Ehara, M.; Toyota, K.; Fukuda, R.; Hasegawa, J.; Ishida, M.; Nakajima, T.; Honda, Y.; Kitao, O.; Nakai, H.; Vreven, T.; Montgomery, J. A. Jr.; Peralta, J. E.; Ogliaro, F.; Bearpark, M.; Heyd, J. J.; Brothers, E.; Kudin, K. N.; Staroverov, V. N.; Kobayashi, R.; Normand, J.; Raghavachari, K.; Rendell, A.; Burant, J. C.; Iyengar,

S. S.; Tomasi, J.; Cossi, M.; Rega, N.; Millam, J. M.; Klene, M.; Knox, J. E.; Cross, J. B.; Bakken, V.; Adamo, C.; Jaramillo, J.; Gomperts, R.; Stratmann, R. E.; Yazyev, O.; Austin, A. J.; Cammi, R.; Pomelli, C.; Ochterski, J. W.; Martin, R. L.; Morokuma, K.; Zakrzewski, V. G.; Voth, G. A.; Salvador, P.; Dannenberg, J. J.; Dapprich, S.; Daniels, A. D.; Farkas, Ö.; Foresman, J. B.; Ortiz, J. V.; Cioslowski, J.; Fox, D. J. Gaussian, Inc. , Wallingford CT, 2009.

16. Maeda, S.; Osada, Y.; Morokuma, K.; Ohno, K. GRRM, a developmental version at Hokkaido University.

Chapter 5: General Conclusion

In this study, the three organic synthetic reactions were analyzed by the automated reaction path search method. I employed the AFIR method and the ONIOM method together based on the knowledge of organic chemistry, which could reduce computational cost efficiently. The calculated results were well consistent with the experimental results, indicating that the unknown reaction mechanisms were discovered with the AFIR search.

In chapter 2, I explored reaction pathways among imine, 2-trimethylsiloxyfuran, and water molecules systematically by using the AFIR method to elucidate the mechanism of a recently discovered vinylogous Mannich-type reaction. The search identified five working pathways. Among them, two concertedly produce *anti* and *syn* isomers of the product directly. The other three also converge to the *anti*/*syn* products through stepwise mechanisms. Two of them give an intermediate, which is a regioisomer of the main product. This intermediate can undergo a retro-Mannich reaction to produce a pair of intermediates: an imine and 2-furanol. The remaining pathway directly generates this intermediate pair. The imine can easily react with 2-furanol to afford the product. Thus, all of these stepwise pathways finally converge to achieve the main product and a certain amount of products can revert into a pair of intermediates through the retro-Mannich reaction; *anti*/*syn* selectivity in products is controlled by the thermodynamic stabilities. That is, the *anti*/*syn* ratio calculated by the conformational analysis of products using the ADDF method is consistent with experimental result.

In chapter 3, a theoretical investigation of the base-mediated borylation with silylborane (BBS) reaction has been conducted using the AFIR method. The resulting complete reaction pathway for the BBS method was shown to involve the halogenophilic attack of a silyl anion on the bromine atom of the substrate and the rapid and selective consumption of a resulting carbanion species by a boron electrophile. These calculations provided a rational explanation for the counterintuitive borylation reactivity, as well as accounting for the good functional group compatibility of the reaction and its high reactivity toward sterically hindered substrates. The use of the AFIR method in the current study not only provided a complete reaction pathway but also demonstrated the validity of the proposed reaction mechanism by comprehensively accounting for the other reaction mechanisms. It is hoped that this novel mechanism will allow us to expand our knowledge and understanding of silicon and boron chemistry.

In chapter 4, I applied the AFIR method to explore key mechanistic details of the C–H functionalization/intramolecular C–S cyclization of thiobenzanilide. It is important for

activating the target C–H bond on the substrate to participate DMSO solvent, CuI co-catalyst, and Bu_4NBr salt in this system. That is, the chloride atom on the Pd(II) center reacts with CuI and the coordinative unsaturated Pd(I) and $[CuClI]^-$ species are generated. The C–H bond is subsequently cleaved by oxygen atom in DMSO, and thus Pd–C bond is formed. Finally, the C–S bond is generated by reductive elimination reaction. Among these bond rearrangement steps, the bromine anion of Bu_4NBr is coordinated to N–H bond on the substrate. Thus, the palladium intermediates and protonated product are stabilized through this coulomb interaction and the while reaction undergoes as exothermic process in free energy.

In this study, I challenged to shed light on the reaction mechanism, which is difficult to discuss because of its complexity, by using the automated reaction path search methods. The calculation results of this study led to find the unexpected intermediates in the three reactions and succeed to explain the experimental results. In the future, it is expected to design a new reaction based on these intermediates found in this study. Moreover, when applying the automated reaction path search method toward more complex reaction system, this study can be positioned as a pioneering research.

Acknowledgement

All the studies described in this dissertation were carried out under the supervision of Professor Dr. Tetsuya TAKETSUGU, Department of Chemistry, Faculty of Science, Hokkaido University.

The author would like to express deeply sincere appreciation to Professor Taketsugu for his guidance throughout the course of this work, in the preparation of this thesis, and helpful discussions.

Great acknowledgement is also made to Associate Professor Dr. Satoshi MAEDA for his constant guidance, pertinent and tolerant advice, and helpful discussion.

The author expresses his sincere thanks to Assistant Professor Dr. Masato KOBAYASHI, Assistant Professor Dr. Takeshi IWASA, Assistant Professor Dr. Tomoko AKAMA, and Dr. Yuriko ONO for practical advice and fruitful discussion.

The author wishes to thank sincerely to former Associate Professor Dr. Takeshi NORO, and Associate Professor Dr. Akira NAKAYAMA for their discussions, advice and encouragement.

The author also sincerely thanks to Professor Dr. Keiji TANINO, Professor Dr. Jyn-ya HASEGAWA, and Professor Dr. Hajime ITO for serving his dissertation committee.

The author expresses great thanks to Dr. Eiji YAMAMOTO for the experimental part of the collaboration research in Chapter 3.

The author also expresses deep gratitude to Dr. Djamaladdin G. MUSAEV for his great support of his short-visit in Atlanta, constant guidance, practical advice, and fruitful discussion in Chapter 4.

It is pleasure to express his appreciation to all colleagues, especially Ms. Chihiro SAKA, and Mr. Soshi FUJIKAWA for valuable contribution.

The author is grateful to Dr. Keisuke NIIMI, Mr. Masayuki OKAI, Ms. Chiaki KOIKE, Ms. Aya SATO, and Mr. Yosuke SUMIYA for his/her encouragement.

The author thanks the financial support by “the Research fellowship for young scientists by the Institute for Quantum Chemical Exploration (IQCE)”.

Finally, the author would like to thank sincerely his family, Atsushi, Akemi, Mamiko, and Mikako for their encouragement and understanding.